Intramolecular

interactions in TRPV6, and functional regulation of TRPP channels

by

Xiong Liu

A thesis submitted in partial fulfillment of the requirements for the degree of

Doctor of Philosophy

Department of Physiology

University of Alberta

ABSTRACT

There are 28 members in the mammalian transient receptor potential (TRP) channel superfamily, which are divided into six subfamilies, TRPA/C/M/ML/P/V, and play distinct sensory roles in response to various environmental stimuli. High-resolution structures of various TRP channels show a number of potential contacts between different domains, indicating potential interactions that may be functionally important. In TRPV6, a highly Ca^{2+} selective ion channel, whether these domains physically interact with each other and whether they are of functional importance have not been determined. TRPP3 is a cation channel regulated by Ca^{2+} and activated by calmodulin (CaM) antagonist, calmidazolium (CMZ). How TRPP3 is regulated by CaM is poorly understood. TACAN was recently reported to be a mechano-sensitive ion channel with diverse tissue distribution and was indicated to interact with TRPP2 by a proteomic screening. Whether they physically or functionally interact with each other has yet to be explored.

In Chapter 2, we found that residue R470 in the S4-S5 Linker and W593 in the C-terminal TRP-like domain mediate an intramolecular interaction between the S4-S5 Linker and C-terminus (called L/C interaction). We also found that residue W321 in the N-terminal pre-S1 domain and I597 in the TRP-like domain mediate an intramolecular interaction between the N- and C-terminus (called N/C interaction). These interactions were autoinhibitory for the TRPV6 channel function. We also found that phosphatidylinositol 4,5-bisphosphate (PIP2) interacts with R470 to disrupt these interactions, which activates TRPV6. This study revealed a mechanism of how PIP2 regulates TRPV6, which could represent a shared mechanism by other TRP channels.

In Chapter 3, we found that CaM inhibits TRPP3 in *Xenopus* oocytes and that the two proteins interact with each other through the calcified CaM N-lobe and the TRPP3 C-terminal fragment E566-F621. Furthermore, our data also showed that CaM inhibits TRPP3 mainly through enhancing phosphorylation of TRPP3 at T591 by Ca^{2+}/CaM-dependent protein kinase II (CaMK2). Ca^{2+} entry through TRPP3 increased the formation of the CaM/Ca^{2+} complex that binds to the TRPP3 C-terminus to enhance the TRPP3/CaMK2 interaction thereby promoting the T591 phosphorylation, which inhibits channel function.

In Chapter 4, we found that TACAN is in complex with TRPP2 in different kidney cell lines and that they are co-localized in primary cilia. Using *Xenopus* oocyte expression, we found that TACAN inhibits the channel activity of the TRPP2 gain-of-function (GOF) mutant F604P. Using Chinese hamster ovary (CHO) cell expression, we found that TACAN inhibits both wild-type (WT) TRPP2 and mutant F604P by reducing their single-channel conductance and open probability. We also found that co-expression of TACAN with TRPP2 enhances the cell sensitivity to stretch. Furthermore, our data showed that while both the first and last transmembrane (TM) segments (S1 and S6, respectively) of TACAN are involved in the interaction with the TM domains of TRPP2, only the TACAN S6-involved interaction is functionally relevant. Of note, we also found that the TACAN S6 interacts with the peripheral domain (S1-S4) of TRPP2 and that the TACAN S1 interacts with the pore domain (S5-S6) of TRPP2. This study demonstrated that TACAN is a regulator of TRPP2 channel.

In summary, this thesis is composed of functional characterization of critical PIP2-regulated intramolecular interactions in TRPV6 and studies of how TRPP3 is regulated by CaM

and how TRPP2 is regulated by TACAN. Our work constitutes valuable contributions to understanding the function and regulation of TRPV6, TRPP3 and TRPP2.

PREFACE

This thesis is an original work by Xiong Liu. The frog-associated experiments are under the approval of University of Alberta Animal Care Protocol AUP00000234; Project name is "Molecular Physiology of Polycystins and Fibrocystin, products of the autosomal dominant polycystic kidney disease genes".

Chapter 2 of this thesis is accepted by ***iScience*** as "Autoinhibition of TRPV6 channel and regulation by PIP2"

Ruiqi Cai, Xiong Liu, Rui Zhang, Laura Hofmann,Wang Zheng, Ruhul Md Amin, Lingyun Wang, Qiaolin Hu, Ji-Bin Peng, Marek Michalak, Veit Flockerzi, Declan W Ali, Jingfeng Tang, and Xing-Zhen Chen

Ruiqi Cai and I contributed equally to this paper.

In this paper, I conceived the idea of studying one of the two TRPV6 intramolecular interactions reported, namely the interaction between the S4-S5 Linker and the C-terminus (L/C interaction). Other interaction was between the N- and C-terminus (N/C interaction). In terms of data, I contributed ~90% of mutant's generalization, ~60% of functional characterizations, and ~20% of physical interaction characterizations. I am also involved in manuscript writing and revisions. Of note, Ruiqi Cai wrote the first draft of the manuscript, built the figures, and was involved in revisions. Besides, I designed the zebrafish experiments. Rui Zhang was responsible for performing zebrafish data and Ruiqi Cai was involved in further analysing the data.

Conceptualization, R.C., X.L. and X.-Z.C.; Investigation, R.C., X.L., R.Z., L.H., W.Z., M.R.A., L.W., Q.H.; Supervision, J.-B.P., D.A., V.F., J.T. and X.-Z.C. Writing, R.C. and X.-Z.C.

Chapter 3 of this thesis is a manuscript to be submitted as "Inhibition of TRPP3 by calmodulin through Ca^{2+}/calmodulin-dependent protein kinase II"

Xiong Liu, Ruiqi Cai, Xing-Zhen Chen

In this paper, I conceived the idea to determine the CaM regulation on TRPP3. I designed and conducted all the experiments. Furthermore, I drafted the manuscript and prepared for the revisions.

Conceptualization, X.L. and X.-Z.C.; Investigation, X.L. and R.C. Supervision X.-Z.C.; Writing, X.L. and X.-Z.C.

Chapter 4 of this thesis is a manuscript to be submitted as "TACAN is a novel regulator of TRPP2"

Xiong Liu, Mohammad Fatehi, Rui Zhang, Wentong Long, Yifang Wang, Peter E Light, Jingfeng Tang, Xing-Zhen Chen

In this paper, I conceived the idea to determine the functional and physical interaction between TACAN and TRPP2. I designed and performed most of the experiments. Also, I drafted the manuscript and prepared for the revisions. Of note, Dr. Mohammad Fatehi and Dr. Wentong Long performed the single-channel recordings and helped to generate the corresponding figures. Dr. Rui Zhang and Yifang Wang performed zebrafish related experiments and helped to generate the corresponding figures.

Conceptualization, X.L., and X.-Z.C.; Investigation, X.L., M.F., R.Z., W.L., Y.W.; Supervision, P.R.L., J.T., and X.-Z.C. Writing, X.L., and X.-Z.C.

During my PhD training program, I was involved in several other projects not described here that lead to the following publications:

1) Zheng, W., Cai, R., Hofmann, L., Nesin, V., Hu, Q., Long, W., Fatehi, M., Liu, X., Hussein, S., Kong, T., et al. Direct Binding between Pre-S1 and TRP-like Domains in TRPP Channels Mediates Gating and Functional Regulation by PIP2. Cell Rep 22, 1560-1573. (2018).

I performed *Xenopus* oocytes preparation.

2) Zheng, W., Yang, X., Hu, R., Cai, R., Hofmann, L., Wang, Z., Hu, Q., Liu, X., Bulkley, D., Yu, Y., et al. Hydrophobic pore gates regulate ion permeation in polycystic kidney disease 2 and 2L1 channels. Nat Commun 9, 2302. (2018).

I performed *Xenopus* oocytes extraction and functional characterization of TRPP2 S4-S5 linker mutant. I am responsible for the Fig. 4g indicated in the paper.

3) Lee, J.J., Liu, X., O'Neill, D., Beggs, M.R., Weissgerber, P., Flockerzi, V., Chen, X.Z., Dimke, H., and Alexander, R.T. Activation of the calcium sensing receptor attenuates TRPV6-dependent intestinal calcium absorption. JCI Insight 5. (2019).

I performed all the *Xenopus* oocytes related experiments. I am responsible for Fig. 6A, 6B, 6C, S2 and S3 indicated in the paper.

4) Wang, Z., Ng, C., Liu, X., Wang, Y., Li, B., Kashyap, P., Chaudhry, H.A., Castro, A., Kalontar, E.M., Ilyayev, L., et al. The ion channel function of polycystin-1 in the polycystin-1/polycystin-2 complex. EMBO Rep 20, e48336. (2019).

I performed the radiolabeled calcium uptake experiments. I am responsible for Fig. 3G indicated in the paper.

ACKNOWLEDGEMENTS

I am very lucky to pursue my PhD study in the Department of Physiology in the University of Alberta, Dr. Xing-Zhen Chen's lab for the past years. I would like to thank everyone I interacted during this academic journey. It is you who make Edmonton warm even in wintertime.

First, I would like to thank my supervisor, Dr. Xing-Zhen Chen, for training me to be an independent researcher. I learned so much from our discussions. He encourages me a lot during the first few years and offers me enough freedom to explore my ideas in the latter years. It would be impossible for me to make those achievements without his great training. Furthermore, he is always supportive for my academic career pursuing. And I will never forget the positive control and negative control.

Next, I want to thank my supervisory committee members, Dr. Emmanuelle Cordat and Dr. Harley Kurata. They are always helpful and supportive during my PhD studies. I will miss the big centrifuge machine and PCR machine in Dr. Cordat's lab, and for Dr. Harley Kurata I will never forget that we hugged each other when I passed my candidacy exam.

I also want to thank my previous lab mates, Wang Zheng, Ruiqi Cai, Qiaolin Hu and Paria Edalat for their help and friendship. And we will not fight for the PCR machine, bench space, or electrophysiological equipment anymore.

In addition, I want to thank all helpful staff in the Department of Physiology for their helps. Special thanks go to Debbie and Donna for saving me so many times with the master key.

Finally, I am fortunate to have my wife and my parents for all their love and support. And trust me, we may go somewhere with less snow next time.

TABLE OF CONTENTS

LIST OF FIGURES

LIST OF ABBREVIATIONS

2-APB	2-aminoethoxydiphenyl borate
ADPKD	autosomal dominant polycystic kidney disease
AIP	autocamtide-2 related inhibitory peptide
CaM	calmodulin
CaMBD	CaM binding sites
CaMK2	Ca^{2+}/CaM-dependent protein kinase II
CHO	Chinese hamster ovary
CMZ	calmidazolium
Co-IP	coimmunoprecipitation
Cryo-EM	cryo-electron microscopy
Ctrl	control
DAG	diacyl glycerol
DMSO	dimethyl sulfoxide
Dpf	day(s) post-fertilization
DTT	Dithiothreitol
EGTA	ethylene glycol tetraacetic acid
ER	endoplasmic reticulum
FA	fatty acid
FBS	fetal bovine serum
FL	full length
GOF	gain of function
GST	glutathione S-transferase

IF	immunofluorescence
IP3	inositol 1,4,5 triphosphate
LSD	lysosomal storage disease
MHR	TRPM homology region
MONNA	2-[(4-Methoxy-2-naphthalenyl) amino]-5-nitro-benzoic acid
NCX1	Na^{+}/Ca^{2+} exchanger
NE	nuclear envelope
NFA	niflumic acid
NMDG	N-methyl D-glucamine
NS	not significant
PCD	polycystin domain
PIP2	phosphatidylinositol 4,5-bisphosphate
PLC	phospholipase C
RACK1	receptor for activated protein kinase 1
RT	room temperature
SF	selectivity filter
SHH	sonic hedgehog
TEVC	two-electrode voltage clamp
TMPIT	transmembrane protein induced by TNFα
TRP	transient receptor potential
VSLD	voltage sensor-like domain
WT	wild type

CHAPTER 1

INTRODUCTION

1.1 Transient receptor potential (TRP) superfamily

TRP channels are a superfamily of cation channels located on the plasma membrane, endoplasmic reticulum (ER) membrane or primary cilia of numerous animal cell types to transduce the signals (Dong et al., 2010). In 1969, an unusual phenotype of showing a transient receptor potential to constant light instead of the normal continuous response was discovered in one drosophila melanogaster mutant strain (Cosens and Manning, 1969). This strain was named trp. Cloning of the mutated trp gene led to the first identified member of TRP superfamily and opened the trp era. The TRP superfamily consist of a large group of polymodal ion channels that are mostly conserved from nematodes to humans (Samanta et al., 2018). Based on the sequence similarities, the mammalian TRP channel superfamily is divided into six subfamilies (Nilius and Owsianik, 2011): TRPC (Canonical), TRPV (Vanilloid), TRPM (Melastatin), TRPA (Ankyrin), TRPML (Mucolipin), and TRPP (Polycystic). The first member of mammalian TRP channels, TRP canonical 1 (TRPC1), was identified in 1995 based on the sequence homology to *Drosophila* trp gene (Wes et al., 1995). In 1997, David Julius group found that a non-selective cation channel with structural similarities of TRP ion channels is activated by capsaicin, a vanilloid-like molecule. It was named VR1 (renamed as TRPV1), which is a founding member of the TRPV subfamily (Caterina et al., 1997). The first member of the TRPM subfamily, TRPM1, as a Ca^{2+} permeable ion channel, was first cloned from benign melanomas (Duncan et al., 1998). As the only member of the mammalian TRPA subfamily, TRPA1 was identified as an ankyrin-like transmembrane (TM) protein, with similarities to TRP channels in 1999 (Jaquemar et al., 1999). The first member of TRPML subfamily, TRPML1, was discovered to be important in autosomal-recessive lysosomal storage disease (LSD) (Bassi et al., 2000). For the TRPP subfamily, mutations in the founding members PKD1 (TRPP1) and PKD2 (TRPP2) are related to autosomal dominant polycystic kidney disease (ADPKD) (Mochizuki et al., 1996). There are similarities between PKD1 and PKD2.

However, due to the 11-TM topology of PKD1, it is not considered as a member of TRPP subfamily (Giamarchi et al., 2006). There is also another TRP channel subfamily, which has not been found in mammalian cells so far. TRPN (NOMPC-like) exists only in invertebrates and fish, but not in mammals (Duggan et al., 2000). The members of TRP superfamily are illustrated below (Fig. 1-1). Recently, through bioinformatic analysis of the evolutionary history of TRPM channels, a sister family was proposed to be a novel TRP subfamily with the name of TRP soromelastatin (TRPS) in Cnidaria–Bilateria split (Himmel et al., 2020) (which is not listed here).

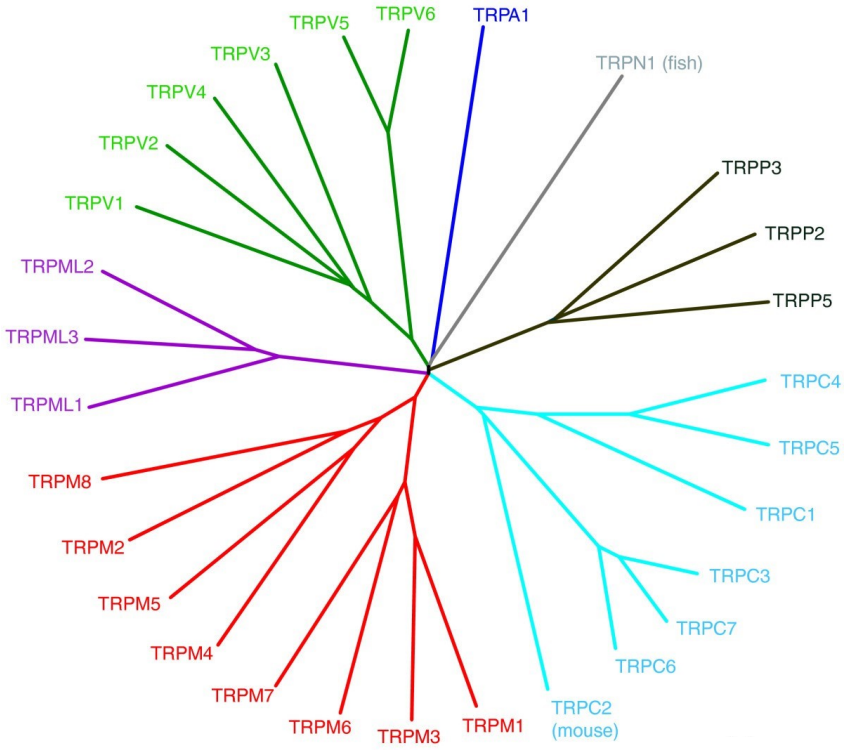

Figure 1-1. Phylogeny of TRP channels. The phylogenic tree shows mammalian TRP channels are divided into 6 subfamilies. TRPN is not available in mammals. Adapted with permission acquired from Nilius et al. *Genome Biol*, 2011 (Nilius and Owsianik, 2011).

1.1.1 Pre-structural characterization of TRP channels

TRP channels are membrane proteins that share similar topological characteristics (Samanta et al., 2018). Overall, they are composed of six TM segments (S1-S6), intracellular N- and C-termini, and an ion conducting pore formed by S5 and S6 (Fig. 1-2). Intracellular domains and extracellular loops differ extensively between subfamilies (Huffer et al., 2020). The large extracellular loop between S1 and S2 has only been found in TRPML and TRPP subfamilies. A variable number of ankyrin repeats are identified in the N-terminus of different TRP subfamilies, such as TRPV, -C and -N. There is a unique TRPM homology region (MHR) located in the N-terminus of TRPM subfamily. In the C-terminus, a highly conserved TRP helix is found in TRPV, -C, -M subfamilies. An EF-hand with Ca^{2+} binding affinity is in TRPP channels, although its functional relevance is under debate (Vien et al., 2020).

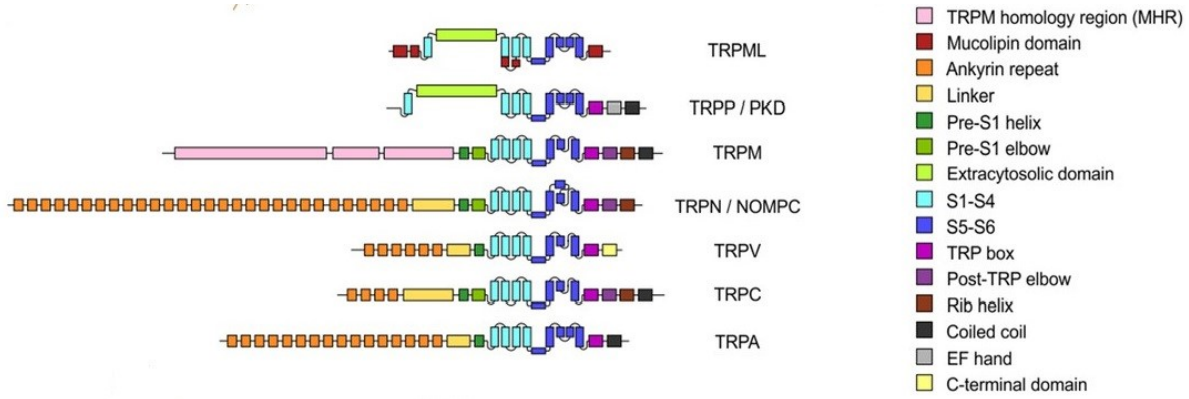

Figure 1-2. Topology of TRP channels. Schematic of domains architecture of TRP channel subunits. TM regions are indicated by perpendicular rectangles. Functional domains are indicated by distinct colors (Huffer et al., 2020). (Permission is not required for this figure to be reused in a thesis)

1.1.2 High structural characterization of TRP channels

Due to the challenge of membrane protein purification into a stable and native protein conformation, 3D structure information of entire TRP channels was limited before 2013 (Nilius and Owsianik, 2011). Fortunately, a structural revolution in the TRP channel field has been initiated by the development of cryo-EM technology with more sensitive detectors and single-particle analysis. In 2013, the first TRP channel structure, TRPV1, was determined at a 3.4 Å overall resolution (Liao et al., 2013). Since then, an exponential increase in the number of structures of TRP channels has been achieved at high resolution (Vangeel and Voets, 2019). So far, except TRPC1, -C2, -C7, -M1, -M3, -M6 and -ML2, 20 members with at least one in each subfamily have been solved at high resolution (Fig. 1-3). These structures further confirmed that TRP channels are homotetramers, with six TM helices in each subunit, and that the central ion permeation pathway is formed by the last two TM domains. Because those structures are determined in the absence or presence of activating ligands or inhibitors, they also provide considerable information on the structural basis of pharmacological regulation and gating mechanisms.

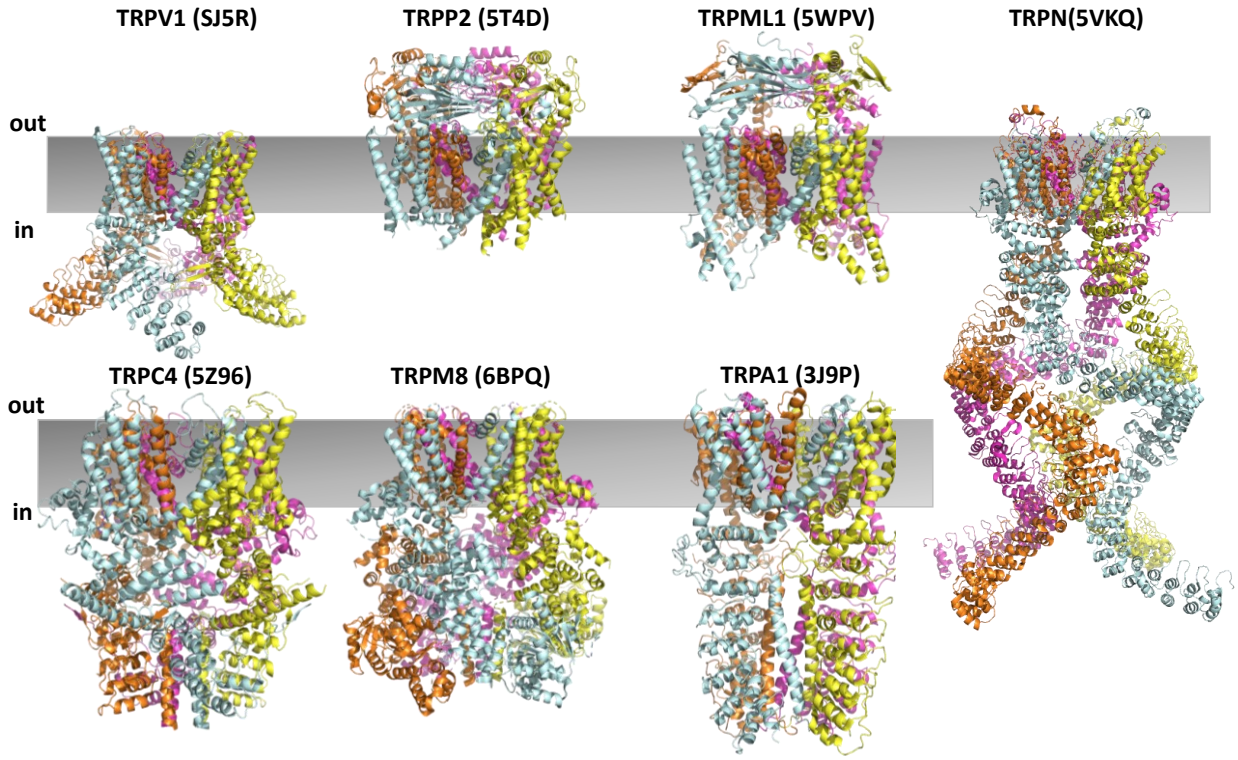

Figure 1-3. Representative structures of TRP channels from different subfamilies. Figure is generated from Pymol modified with distinct color on each subunit within the homotetramer. The plasma membrane and PDB IDs are indicated.

1.1.3 Functional regulations of TRP channels

For the importance and relevance to the studies described in this thesis, intramolecular interaction, Ca^{2+} regulation and oligomerization of TRP channels are presented here.

Intramolecular interactions in TRP channels.

Earlier in 2013, the first high-resolution TRPV1 structure revealed an intramolecular proximity of the pre-S1 and TRP domains (Fig. 1-4). Later solved structures of TRPA1, -V2 and -V6 further confirmed this observation.

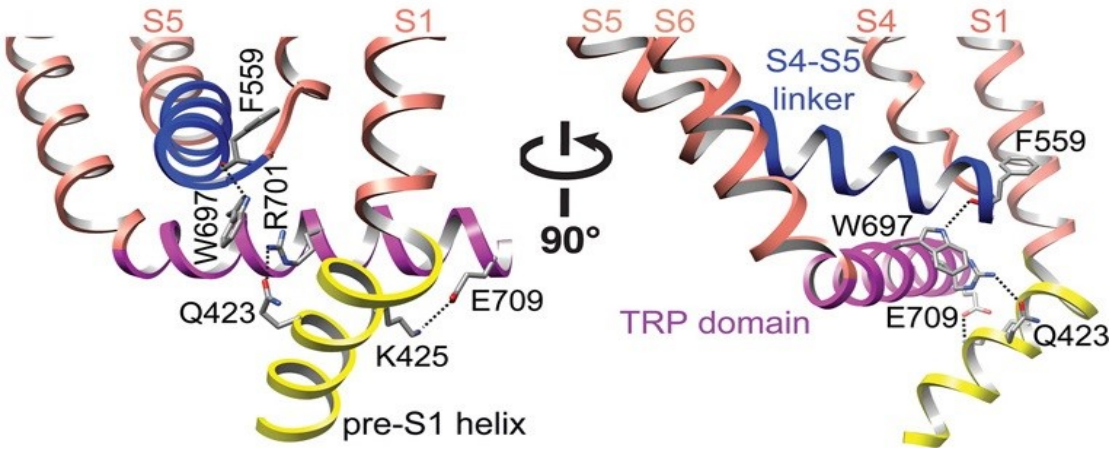

Figure 1-4. Potential interactions in TRPV1 structure. Pre-S1 domain (yellow) and S4-S5 linker stay close to TRP domain (purple). Adapted with permission acquired from Liao et al. *Nature*, 2013 (Liao et al., 2013).

However, whether pre-S1 domain and TRP domain indeed physically interact with each other was unknown at that time. Through a series of studies, our lab identified the functional importance of the interaction between a conserved residue in the pre-S1 of the N-terminus and a cationic residue in the TRP domain of the C-terminus (named N/C interaction) (Zheng et al., 2018a). And this N/C interaction is highly conserved among TRPP2, -P3, -V1 and -M8. Furthermore, we also found that PIP2 inhibits TRPP2, -P3 by disrupting this intramolecular interaction. The detailed mechanism is illustrated below (Fig. 1-5). Whether N/C interaction is conserved in other TRP channels is not clearly known.

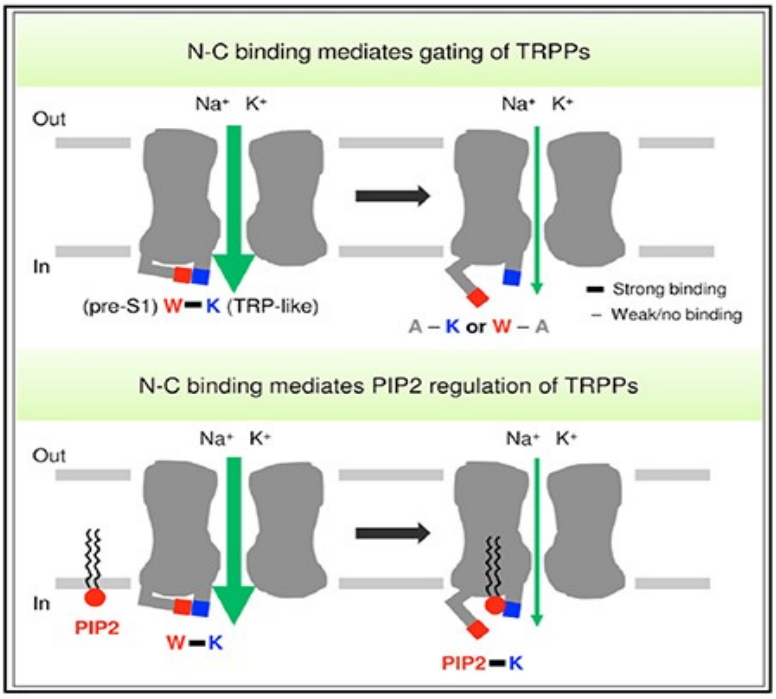

Figure 1-5. Schematic model showing the association between N/C interaction and PIP2 regulation on TRPP channels. N/C interaction is mediated by aromatic W (Tryptophan) residue in pre-S1 and a cationic K (Lysine) residue in the TRP-like domain. TRPP channels are inhibited by PIP2 by disrupting the N/C interaction (Zheng et al., 2018a). (As the author of this article, permission is not required for this figure to be reused in a thesis.)

Ca^{2+} and TRP channels

TRP channels exhibit a wide range of Ca^{2+} selectivity (Owsianik et al., 2006). Basically, extracellular Ca^{2+} concentration is around 1-2 mM, while intracellular Ca^{2+} is close to 100 nM. Furthermore, as the Ca^{2+} store pool, concentration in the ER can be as high as 800 μM (Samtleben et al., 2013). As the Ca^{2+} permeable channels, most TRP channels are Ca^{2+} permeable cation channels with no prominent selectivity between cations. Two epithelia TRP channels, TRPV5 and -V6, are highly Ca^{2+} selective with P_{Ca}/P_{Na} values more than 100 (Yue et al., 2001; Vennekens et al., 2000). For TRPM4 and -M5, they demonstrate negligible Ca^{2+} permeability (P_{Ca}/P_{Na} <0.001), and are regarded as Ca^{2+} non-permeable (Launay et al., 2002; Prawitt et al., 2003). There is ongoing debate on the ion selectivity of TRPP2, which was first reported to be Ca^{2+} permeable (Hanaoka et al., 2000) but was later shown to be blocked by Ca^{2+} (Cai et al., 2004). Recently, we found that heteromeric channels comprising PKD1 in complex with TRPP2 show highly increased Ca^{2+} permeability compared with TRPP2 homotetramer (Wang et al., 2019). This finding strongly indicates that the Ca^{2+} selectivity needs to be considered together with other factors, such as the assembling subunit, physical or chemical stimuli.

Altered Ca^{2+} homeostasis acts as a stressor, leading to the cell damage (Cerella et al., 2010). Cytosolic Ca^{2+} overload over-stimulates many enzymes related to the degradation of supramolecular assemblies, proteins or lipids degrading. Ca^{2+} overload in the mitochondria negatively impacts the cell metabolism level. Also, intracellular Ca^{2+} depletion, which is leaked by ER could progress into apoptosis (Kass and Orrenius, 1999). In contrast, some specific cells related to the immune system are able to initiate the survival pathways (Simon, 2003). Due to the physiological role of Ca^{2+} in cell adaptation, survival and death, TRP channels are tightly

involved in Ca^{2+} signaling in response to physiological changes. And cytosolic Ca^{2+} signals also shape the activities of TRP channels (Vangeel and Voets, 2019). The impact of Ca^{2+} on TRP channels can be diverse, leading to either activation or inhibition, by direct or indirect mechanisms (Vangeel and Voets, 2019). Overall, there are three general mechanisms. The first one is that Ca^{2+} influx into the cell activates phospholipase C (PLC) to decrease PIP2 level, which is sensed by TRP channels (Rohacs, 2014). In the second mode, Ca^{2+} binds directly to TRP channels to modulate the channel function. For instance, the Ca^{2+} binding sites forming by S2-S3 regions in TRPM2, -M4, -M8 and -A1 have been reported (Huang et al., 2018; Autzen et al., 2018; Diver et al., 2019; Zhao et al., 2020). And Ca^{2+} is also reported to bind at the pore domain of TRPP3 to block the channel directly (DeCaen et al., 2016). The third mode involves Ca^{2+} sensing protein, such as CaM (Vangeel and Voets, 2019). CaM consists of two global domains, each of which obtains two Ca^{2+} binding sites. Multiple CaM binding sites have been found in TRP channels (Chin and Means, 2000). Conformational changes induced by Ca^{2+} binding on CaM modulate TRP channels. TRPV1 is reported to interact with CaM in a Ca^{2+}-dependent manner and this interaction is important for Ca^{2+} dependent TRPV1 inhibition (Rosenbaum et al., 2004). Recently, structures of TRPV5/CaM and TRPV6/CaM complexes were identified. Both structures showed that CaM binds at the lower gate of the channel and blocks the ion permeation directly (Hughes et al., 2018; Singh et al., 2018a) (Fig. 1-6). Whether this obstruction mechanism is conserved in other TRP channels or whether there could be other CaM regulation mechanisms involved remains largely unknown.

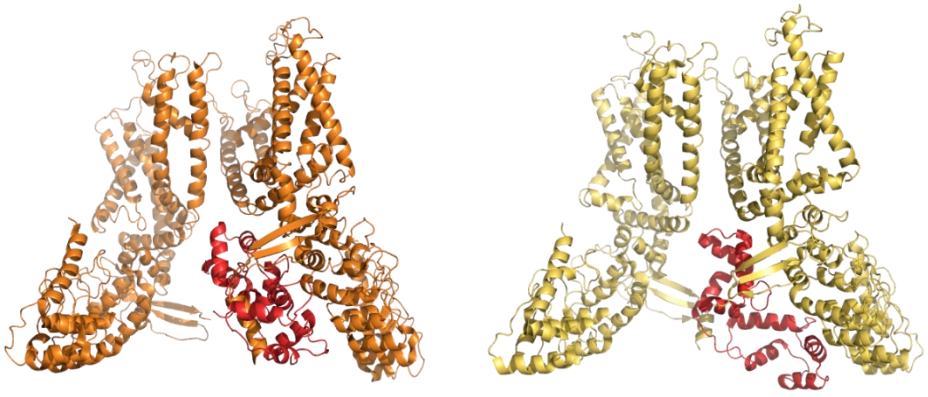

Figure 1-6. Structures of TRPV5/CaM and TRPV6/CaM complexes. TRPV5 (in orange)/CaM (in red) (left panel) and TRPV6 (in yellow)/CaM (in red) (right panel) structure complexes are indicated. To be simplified, only 2 subunits of the homotetramer are shown. Figures are generated by Pymol with distinct color on each segment. PDB ID: 6DMU (TRPV5/CaM); 6E2F (TRPV6/CaM).

Assembly of TRP channels.

Although TRP channels normally function as homotetramers, heteromerization has also been widely reported (Cheng et al., 2010). Channel complexes can be formed by subunits from the same or different subfamily, or even G protein-coupled receptors (GPCRs). In TRPV subfamily, TRPV5 and TRPV6 can form a functional heterotetrametric ion channel with diverse ratios, each with distinct channel properties (Hoenderop et al., 2003). Heterotetramerization of TRP subunits demonstrates one way to produce diverse functions of this superfamily. The molecular mechanism governing the TRP channel subunits assembly lies in the ankyrin repeat domains, TRP domain, coiled -coil domain on intracellular N- or C-termini. However, these principles have been deduced from the functional characterization or biochemical studies. Recent cryo-EM structures indicated that the intracellular N- or C-terminus is not essential for the channel assembly. For instance, cryo-EM structures of homotetrameric TRPP2 and TRPP3 were formed by a short version of corresponding protein without coiled-coil domains (Shen et al., 2016) (Su et al., 2018b). Consistent with this, recently solved PKD1/TRPP2 structures also demonstrated that the coiled-coil domain is not essential for hetero-oligomerization (Su et al., 2018a).

1.1.4 TRP channels and human diseases

Mutations in TRP channel genes have been linked to a wide range of diseases in humans (called TRP channelopathies) (Nilius and Szallasi, 2014). Numerous TRP channelopathies are well established, such as autosomal dominant polycystic kidney disease (TRPP2) (Kim and Park, 2016), Charcot-Marie-Tooth disease type 2C (TRPV4) (Landouré et al., 2010), autosomal dominant familial episodic pain (TRPA1) (Kremeyer et al., 2010). Details are indicated below

(Fig. 1-7). One of the best characterized physiological roles of TRP channels is the involvement of pain sensation. TRP channels have been found to be involved in numerous pain modalities, including neuropathic pain, inflammatory pain and pain related to pathological conditions, such as cancer (Jardín et al., 2017). The involvement of TRPV1 in pain sensation has been thoroughly characterized, including inflammatory pain, visceral pain and neuropathic pain. TRPV1 is activated in response to mediators contained in the inflammatory milieus after injury or infection (Tominaga et al., 1998). The activity and trafficking of TRPV1 are regulated by a variety of proinflammatory mediators such as bradykinin, histamine and chemokines (Zhang et al., 2008). TRPV1-lacking mice and those treated with TRPV1 antagonists lose the ability to develop carrageenan-induced thermal hyperalgesia, indicating that TRPV1 is required for inflammatory sensitization (Davis et al., 2000; Tékus et al., 2010). TRPV1 is expressed in visceral afferent neurons which are immunoreactive for several proinflammatory neuropeptides (Tan et al., 2008) (Tan et al., 2009). TRPV1 is proposed to play a key role in visceral mechanosensation and pain, although it is not a mechanosensor. The hypersensitivity of pelvic afferents is induced by TRPV1 activation in response to colorectal distension (van den Wijngaard et al., 2009). TRPV1 is upregulated in response to spinal nerve ligation in neuropathic pain models (Xiao et al., 2013). And the knock-down of TRPV1 in the mice model suppresses mechanical hypersensitivity (Christoph et al., 2008). Besides TRPV1, other two TRP channels, TRPA1 and TRPM8, have also emerged as critical sensors in pain processing (Bourinet et al., 2014). TRPA1 is expressed in a subpopulation of nociceptors of the dorsal root, nodose, and trigeminal ganglia together with TRPV1 in both humans and rodents (Nagata et al., 2005). TRPA1 deficient mice with intraplanar injection of bradykinin failed to produce thermal or mechanical hypersensitivity (Bautista et al., 2006). TRPM8, as the primary mammalian sensor of cold, plays important a role in thermo-

sensation. It can also have analgesic effects neuropathic pain (Knowlton et al., 2011). Functional roles for TRP channels in organismal development, physiological function or pathologies continue to be identified. Recently, TRPC5 was identified as a cold sensor in the teeth in human inflammatory conditions (Bernal et al., 2021).

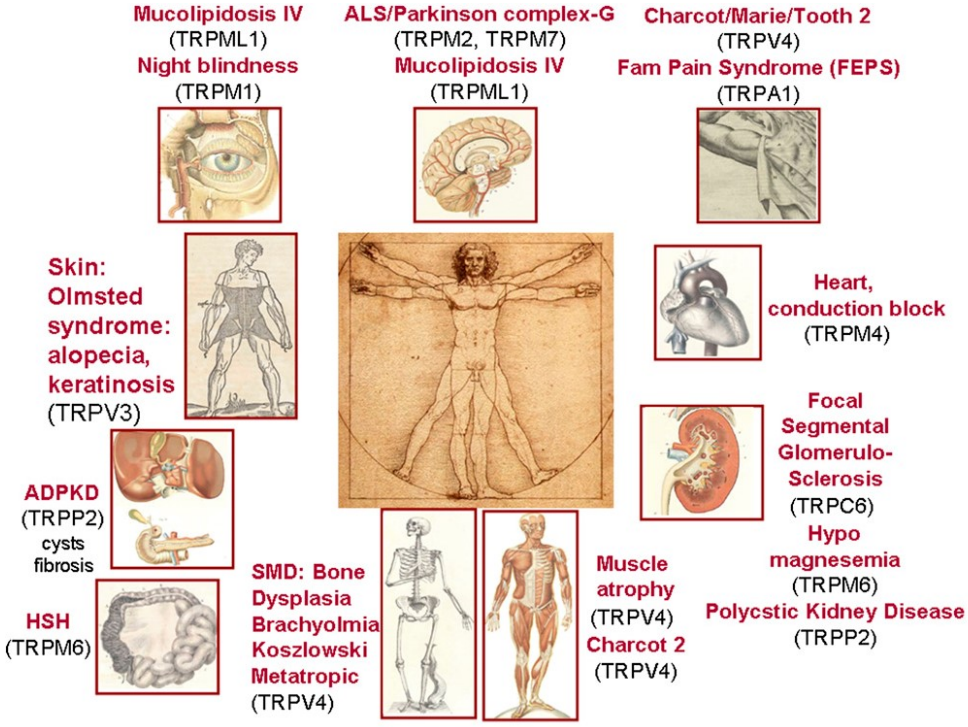

Figure 1-7. TRP channelopathies. The spectrum of human diseases associated to mutant TRP channels. Adapted with permission acquired from Nilius et al. *Pharmacol Rev*, 2014 (Nilius and Szallasi, 2014).

1.2 TRPV6

TRPV6 belongs to the vanilloid subfamily, and it was firstly cloned in 1999 (Peng et al., 1999). Due to a gene duplication, TRPV6 has a close homologue, TRPV5, which shares 75% of amino acid identity and similar functional properties. Unlike other TRP channels, which are non-selective, TRPV6, together with TRPV5, is highly Ca^{2+} selective, with a Ca^{2+}/Na^{+} ratio grater than 130 (Yue et al., 2001). TRPV5 is mainly expressed in the kidney, but TRPV6 is predominantly expressed in small intestine, and presents in other organs, such as testis, prostate, ovary, breast and liver (Peng et al., 2018). In this way, TRPV5 mainly functions in maintaining urinary Ca^{2+} excretion, while TRPV6 plays important roles in intestinal Ca^{2+} absorption and other physiological processes, due to the its wide tissue distribution (Peng et al., 2018). As shown in Fig. 1-8, at the cellular level, TRPV5 and TRPV6 are responsible for the active epithelial Ca^{2+} transport (van Abel et al., 2005). Under the regulation of calciotropic hormones, Ca^{2+} entering through TRPV5 and TRPV6 homo- or hetero-tetrameric channels binds to calbindin-D. After Ca^{2+}- calbindin-D diffuses to the basolateral membrane, Ca^{2+} is extruded through ATP-dependent Ca^{2+}-ATPase or Na^{+}/Ca^{2+} exchanger. In this way, TRPV5 and TRPV6 play central roles in maintaining Ca^{2+} balance together with the passive entry of Ca^{2+} across the luminal or apical membrane.

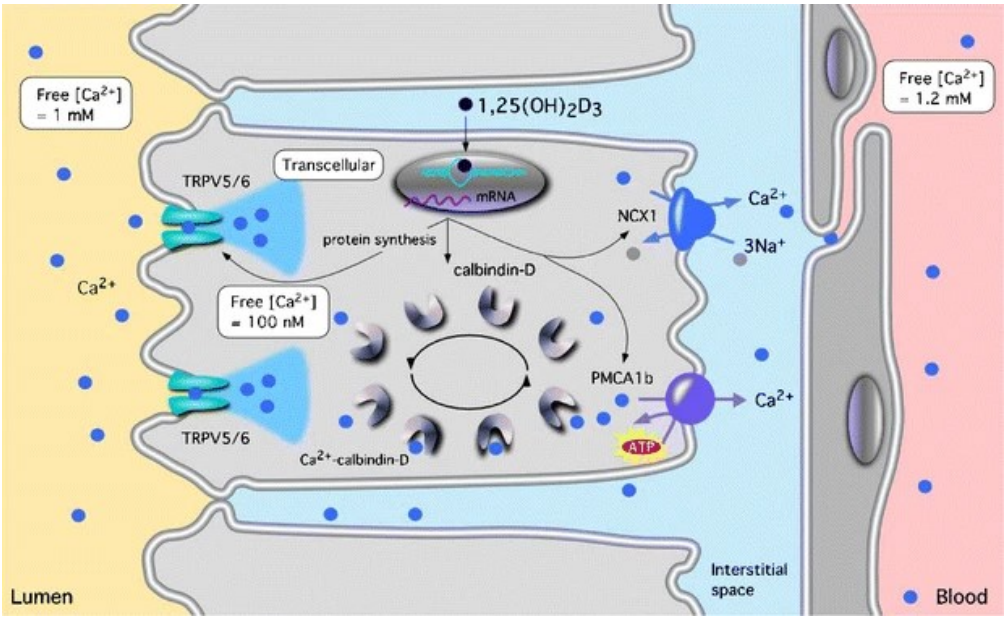

Figure 1-8. The process of epithelial Ca^{2+} transport. Ca^{2+} is transported from the luminal space to the extracellular compartment. Adapted with permission acquired from van Abel et al. *Naunyn-Schmiedebergs Archiv*, 2005 (van Abel et al., 2005).

1.2.1 Functional characterization of TRPV6

As a highly Ca^{2+} selective ion channel, heterogeneous expression of TRPV6 in *Xenopus* oocytes robustly increases the radiotracer $^{45}Ca^{2+}$ uptake (Peng et al., 1999). Besides this macroscopic characterization, microscopic characterization on TRPV6 by patch-clamp further demonstrates its highly selective for Ca^{2+} (Nilius et al., 2000). Calcium, as the most abundant metal element in the human body, is tightly controlled, due to its essential role in different signal transduction pathways (Shah et al., 2006). Ca^{2+}-dependent feedback control mechanisms are involved in TRPV6 regulation to fulfil this goal. The intracellular loop between S2 and S3 is important for fast inactivation of TRPV6 (Nilius et al., 2002). Functional experiments have suggested that slow inactivation is associated with Ca^{2+}-CaM interacting with the C-terminus of TRPV6 (Niemeyer et al., 2001), although it is not consistent with the current TRPV6/CaM structure (Fig. 1-6). Another regulatory mechanism involves PIP2. Decreased PIP2 levels correlate with decreased TRPV6 activity (Peng et al., 2018). It is proposed that Ca^{2+} influx stimulates phospholipase C (PLC), which in turn hydrolyzes PIP2, leading to the inactivation of channel activity, since PIP2 is essential for the function of TRPV6 (Thyagarajan et al., 2008). However, PIP2 binding sites in TRPV6 are still not clearly known. One positively charged residue (R575) between S4 and S5 in TRPV1 has been proven to be important for the high-affinity binding of PIP2 (Poblete et al., 2015). TRPV6 G488R, which is built through site-directed mutagenesis on the corresponding residue (R575) in TRPV1, demonstrates high PIP2 binding affinity and abolished the inactivation regulation by Ca^{2+}, indicating the critical role of PIP2 on TRPV6 (Velisetty et al., 2016).

1.2.2 Structural characterization of TRPV6

In 2016, Sobolevsky group solved the first high-resolution structure of rat TRPV6 by X-ray crystallography (Saotome et al., 2016). The overall structure is similar to other TRP channels with 4 subunits co-assembling to form a functional channel. Further, This structure provided the first structural evidence that high Ca^{2+} selectivity results from aspartate side chains in the selectivity filter. However, failure to resolve the structure of the intracellular S4-S5 linker hindered insights into how the S1-S4 is coupled with the pore domain. Later in 2018, the same group solved human TRPV6 structures in open and closed conformation with more detailed information on the loop (McGoldrick et al., 2018). A local α to π helical transition in S6 was proposed to open the channel. In the following years, TRPV6 in complex with 2-aminoethoxydiphenyl borate (2-APB), CaM or other inhibitors was also solved, providing alternative mechanisms of how TRPV6 is inhibited (Singh et al., 2018b; Singh et al., 2018a; Bhardwaj et al., 2020). 2-APB is demonstrated to competitively interact with TRPV6 against a stimulatory lipid. CaM is shown to block the pore domain through a cation-π interaction, which is further supported by the TRPV5/CaM structure (Fig. 1-6).

1.2.3 TRPV6 and cancer

TRPV6 is widely distributed in human tissues, indicating its multiple roles in physiology (Peng et al., 2018). Due to the critical role of calcium in the generation, development, and maintenance of cancer phenotypes, TRPV6 is highly related to different epithelial origin cancers (Lehen'kyi et al., 2012). Although the exact role of TRPV6 in cancer cell proliferation is not well understood, TRPV6 is still classified as an onco-channel (Huber, 2013). The evidence is that altered abundance of TRPV6 mRNA is identified in several cancer cell lines or tissues (Fig. 1-9)

(Stewart, 2020). TRPV6 mRNA is up-regulated in colorectal cancer lines (Peng et al., 2000), prostate cancer lines (Peng et al., 2001) and breast cancer cell lines (Bolanz et al., 2008). For some cancers, such as early-stage cervical squamous cell carcinoma, TRPV6 has been reported down-regulated (Sun et al., 2016). Due to its critical role in regulating intracellular Ca^{2+} concentration and downstream signaling pathway, TRPV6 has become a target in the treatment of these cancers (Stewart, 2020). A peptide based TRPV6 inhibitor (SOR-13) has been shown to reduce cell growth rate and has been tested in phase I human trials (Fu et al., 2017).

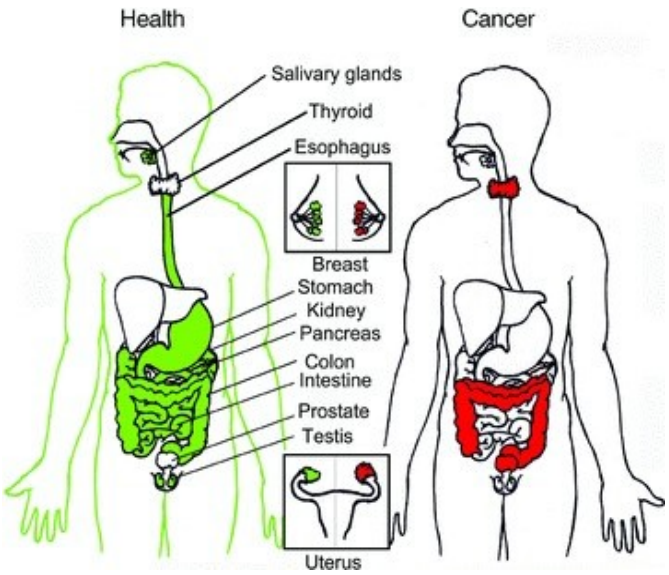

Figure 1-9. Patterns of mRNA expression of TRPV6. TRPV6 expression in health (left panel, green) and up-regulated expression in cancer (right panel, red). Adapted with permission acquired from Lehen'kyi et al. *J Physio,* 2012 (Lehen'kyi et al., 2012).

1.3 TRPP3

TRPP3 (also called PKD2L1), which is composed of 805 amino acids, was first identified as a TRPP2 homologue with 71% similarity (Shen et al., 2016). Unlike TRPP2, TRPP3 is not involved in ADPKD.

1.3.1 Functional characterization of TRPP3

TRPP3 was first cloned in 1999 and it formed a functional ion channel when expressed in *Xenopus* oocytes (Chen et al., 1999). TRPP3 is activated by extracellular Ca^{2+} and conducts cations with no preference. The Ca^{2+} induced activation is followed by a long-term inactivation with unknown mechanisms. Oocytes expressing TRPP3 and pre-injected with the Ca^{2+} chelator, ethylene glycol tetraacetic acid (EGTA) pre-injection, have no response to extracellular Ca^{2+}, indicating that it could be the intracellular Ca^{2+} that is essential for TRPP3 activation. There is an EF-hand with Ca^{2+} binding affinity localized in TRPP3 C-terminus. However, TRPP3 truncation without EF-hand exhibits similar channel activity as the WT channels, suggesting that it is not involved in the Ca^{2+}-dependent activation (Li et al., 2002). It remains unclear how Ca^{2+} activates TRPP3 directly or through other Ca^{2+} related signaling pathways. Calmidazolium (CMZ), a CaM antagonist, activates TRPP3 channel with an unknown mechanism (DeCaen et al., 2013) (Park et al., 2018). Whether TRPP3 is under the regulation of CaM has been poorly studied.

TRPP3 forms a heteromeric channel complex with PKD1L3, a homologue of PKD1 protein, which can be activated by acids leading to an off-response manner (activation is initiated only when extracellular acid is removed) (Inada et al., 2008). It was proposed that TRPP3/PKD1L3 complex acts as the sour taste receptor (Ishimaru et al., 2006). However, later studies demonstrated that TRPP3 or PKD1L3 knock-out mice show no sour deficit (Busin et al.,

1986) (Nelson et al., 2010). And our lab also showed that TRPP3 alone is activated by acid (Hussein et al., 2015), indicating that the off-response is PKD1L3 independent. So far, the exact mechanism of the off-response remains unknown.

1.3.2 Structural characterization of TRPP3

TRPP3 structure has been solved by two groups independently (Su et al., 2018b) (Hulse et al., 2018). The overall structure demonstrates many of the hallmarks of TRP channels, such as the homotetramer with a domain-swapped voltage sensing-like domain. Like other group 2 TRP channels, a large extracellular loop is localized between S1 and S2. TRPP3 is reported to respond to mechanical force, but whether it is mechanically-gated is under debate (Ranade et al., 2015). Currently, it is not clear how TRPP3 is activated. Although Ca^{2+} activates TRPP3 in *Xenopus* oocytes, mammalian cells with TRPP3 expression demonstrate no activation on extracellular Ca^{2+}. Recent report shows that TRPP3 is activated and then inactivated over longer time scales due to pore-block by intracellular Ca^{2+}. But the underlying mechanism of Ca^{2+}-dependent activation of TRPP3 is still unknown. It is proposed that an unknown ligand binds to the extracellular domain and initiates the gating process (Hulse et al., 2018; Su et al., 2018b).

1.3.3 TRPP3 in human diseases

The physiological role of TRPP3 is not thoroughly understood. Unlike TRPP2, mutation in TRPP3 is not related to ADPKD. So far, there are no human diseases linked directly to TRPP3 mutation. One report demonstrated that deficiency of TRPP3 is related to pathological cardiac hypertrophy, due to an indirect effect leading to Na^{+}/Ca^{2+} exchanger (NCX1) overexpression (Lu et al., 2018). Because TRPP3 is localized in the primary cilia, TRPP3 is associated with the Ca^{2+}

concentration in the primary cilia and hence is involved in hedgehog signaling, a signaling pathway involved in protein translation from the cell body to the primary cilia. Mice with TRPP3 knocked out show a mild intestinal malrotation phenotype, which is related to sonic hedgehog (SHH) pathway defects (Delling et al., 2013). To date, the exact physiological role of TRPP3 is still not clearly known.

1.4 TRPP2

TRPP2, also called PKD2, is a transmembrane protein with 968 amino acids. It is a non-selective cation channel and can form a complex with PKD1 to be important in ADPKD.

1.4.1 Functional characterization of TRPP2

TRPP2 is a nonselective ion channel with wide subcellular localization, including endoplasmic reticulum (ER) membrane, plasma membrane and primary cilia (Luo et al., 2003). TRPP2 seems to have different biophysical proprieties depending on the cell-type and binding partners, which leads to distinct function in different subcellular compartment (Liu et al., 2018). It is proposed that TRPP2 could function as a calcium release channel in the ER and modulates apoptosis (Wegierski et al., 2009). TRPP2 can also form a complex with TRPV4 on the primary cilia where it may mediate the flow-induced Ca^{2+} influx (Köttgen et al., 2008). And TRPP2 can also form a mechano-sensitive ion channel with PKD1 in the primary cilia, however, it has been challenged by the report that the currents from primary cilia patch-clamping is PKD1 independent (Liu et al., 2018). Although the involvement of PKD1 and TRPP2 in the ADPKD is widely accepted, the detailed mechanisms of how those mutations lead to the disease is largely unknown (Douguet et al., 2019). Numerous functional characterizations of TRPP2 are from

single channel recordings. Recently a gain of function (GOF) form of TRPP2, F604P, expressed in *Xenopus* oocytes was reported to enable detectable currents on the plasma membrane (Arif Pavel et al., 2016). Directed patch-clamp from the primary cilia also enabled the functional characterization of TRPP2 (Liu et al., 2018). These functional readouts generated a better of TRPP2 function.

1.4.2 Structural characterization of TRPP2

TRPP2 structure was solved by cryo-EM by several groups (Fig. 1-10) (Shen et al., 2016; Grieben et al., 2017; Wilkes et al., 2017). Four TRPP2 subunits form a homotetramer with each containing a pore domain, a selectivity filter (SF), and a voltage sensing-like domain (VSLD). Asp643 in the SF is associated with the binding of extracellular Ca^{2+} and inhibition of TRPP2 ion permeation. Although there is another Ca^{2+} binding domain, EF-hand, which was proposed to be important for the Ca^{2+} dependent regulation on TRPP2 (Kuo et al., 2014), it is strongly challenged by a recent study showing that the EF-hand is not related to the function of TRPP2 (Vien et al., 2020). A hydrophobic gate residue, Leu677, is located at the intracellular side of S6. TRPP2 contains a large extracellular domain called the polycystin domain (PCD), which is involved in channel assembly. Glycosylation on PCD also plays a critical role in stabilizing and trafficking of TRPP2 (Hofherr et al., 2014). Furthermore, the PCD is also highlighted by the clinical data showing that it is a hot spot for pathogenic mutations (Shen et al., 2016).

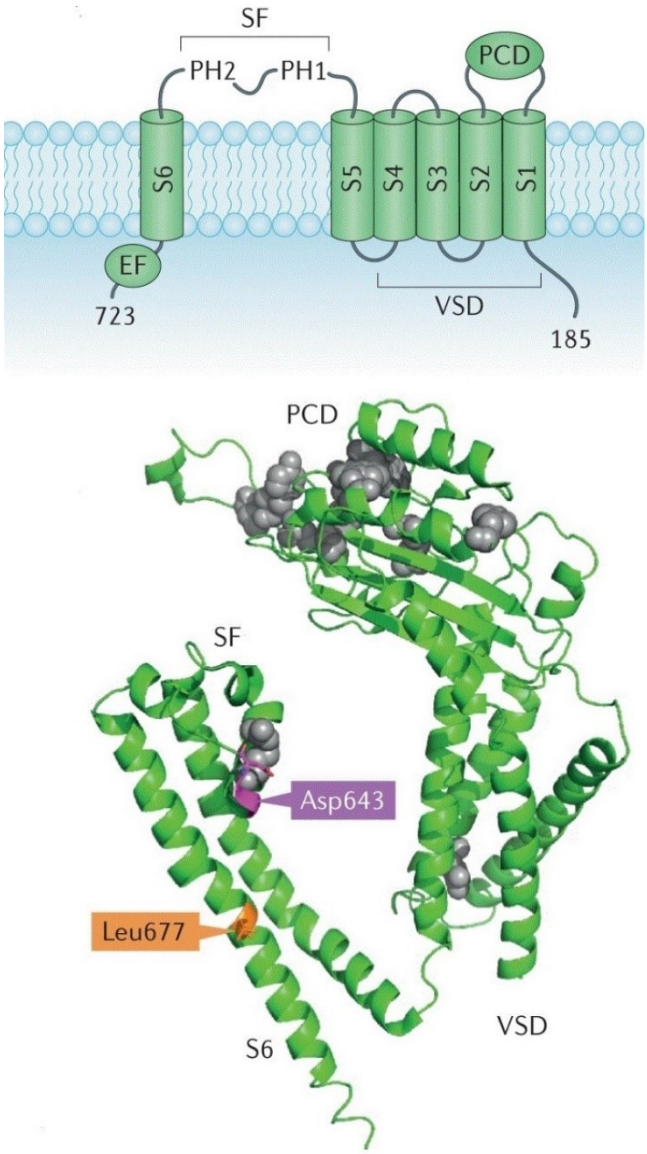

Figure 1-10. TRPP2 structure. Upper panel: topological model of TRPP2; Lower panel: structure of TRPP2. Critical residues are indicated. Pathogenic substitution mutations are indicated by grey spheres. Adapted with permission acquired from Douguet et al. *Nat Rev Nephrol.,* 2019 (Douguet et al., 2019)

1.4.3 TRPP2 and ADPKD

Autosomal dominant polycystic kidney disease (ADPKD) is an inherited systemic disorder affecting 0.2% of the adult population (Douguet et al., 2019). It is characterized by the accumulation of fluid-filled cyst formation in both kidneys. The disease leads to a gradual decline in renal function, with complications affecting other organs including liver and pancreas.

The genetic basis of ADPKD is clearly known, such as the mutated genes involved. 85% of ADPKD is due to the mutations in the *PKD1* gene, which encodes the protein polycystin-1 (also called PC1, PKD1 and TRPP1). And 15% of the disease is caused by mutations in the *PKD2* gene, encoding polycystin-2 (also called PC2, PKD2 and TRPP2) (Cornec-Le Gall et al., 2019). However, the physiological function of polycystins is poorly understood (Douguet et al., 2019). TRPP1 is a large glycoprotein with a large extracellular N-terminus, 11 TM regions and a short intracellular C-terminus. The last 6 TMs share sequence similarities with TRP channels. There has been a recent explosion in our understanding of the role of PKD1 in the channel, although with controversies. PKD1/TRPP2 Cryo-EM structure shows that three positively charged residues of PKD1 face towards the ion conducting path, indicating that PKD1 acts as a dominant negative subunit. It is also proposed that the channel activity is irrelevant to ADPKD (Su et al., 2018a). Through the co-expression of PKD1 and TRPP2 GOF mutant and radio-labeled $^{45}Ca^{2+}$ uptake assay in *Xenopus* oocytes, we and our collaborator found that PKD1 modifies the ion selectivity of the channel complex (Wang et al., 2019). Another group reported that the extracellular N-terminus of PKD1 acts as an activation ligand of PKD1/TRPP2 complex (Ha et al., 2020). More work is required to identify the potential therapeutic strategy towards ADPKD based on our current limited knowledge.

1.5 TACAN

1.5.1 Functional characterization of TACAN

Touch and pain sensations are critical for our interactions with the environment (Ranade et al., 2015). TMEM120A was initially named as TMPIT for transmembrane protein induced by TNFα, because it appeared in a transcriptome list of genes up-regulated by TNFα in endothelial cells (Pinto et al., 2014). Then it was found to be localized in the nuclear envelope (NE) and involved in adipogenesis (Batrakou et al., 2015). Recently, it was reported to contribute to sensation of mechanical pain (Beaulieu-Laroche et al., 2020). Unlike Piezo1 or Piezo2, which have a low activation threshold, TACAN has a relative high threshold. Heterogeneous expression of TACAN in different mammalian cell lines significantly increased the mechano response (Kefauver et al., 2020). Reconstituted TACAN in the lipid bilayers also exhibited nonselective channel activity (Beaulieu-Laroche et al., 2020). However, more recent structures of TACAN suggest that it is not itself a pore-forming ion channel protein (Niu et al., 2021; Rong et al., 2021; Xue et al., 2021).

1.5.2 Structural characterization of TACAN

TACAN structure has recently been solved by three groups independently (Niu et al., 2021; Rong et al., 2021; Xue et al., 2021), although these reports have not yet been peer-reviewed. Overall, all the structures are similar. TACAN forms a homodimeric complex, with each monomer containing 6 TM segments (S1-S6). The dimer is stabilized by the interaction between the TM domain and interaction between the coiled-coil domain in the N-terminus. Instead of a classic known channel structure, TACAN structure shares high similarity with a long-chain fatty acid (FA) elongase (ELOVL7). In addition, TACAN is co-purified with the

coenzyme-A molecule (CoASH), reasoning TACAN could be a coenzyme-A dependent enzyme. More experiments are needed to clarify the physiological role of TACAN.

1.6 Objective, hypothesis, and rationale

1.61 Objective

The main purpose of this study is to understand the functional role of intramolecular interactions in TRPV6, and functional regulation of TRPP3 and TRPP2 ion channels. For this, my specific objectives are 1) to explore intramolecular interactions (namely interaction between S4-S5 Linker and C-terminus, L/C interaction; interaction between N-terminus and C-terminus, N/C interaction) in TRPV6 and how PIP2 activates this channel; 2) to characterize how CaM regulates TRPP3 and whether CaMK2 is involved in the regulation; 3) to investigate the functional and physical interactions between TACAN and TRPP2.

1.62 Hypothesis

We hypothesize 1) that the L/C (S4-S5 linker/C-terminus) and N/C (N-terminus/C-terminus) interactions are mediated by functional critical residues, and that PIP2 binding to positively charged amino acids is related to modulate the L/C and N/C interactions and TRPV6 channel function; 2) that TRPP3 is negatively regulated by CaM, and that there is physical interaction between CaM and TRPP3, which is Ca^{2+} dependent, and that CaMK2 associated phosphorylation is the main cause of the CaM's inhibition on TRPP3; 3) TACAN is functionally and physically associated with TRPP2.

1.63 Rationale

TRP channels are a superfamily of ion channels working as cellular sensors as well as signal integrators. Understanding the functional regulation mechanisms of TRP channels is

critical for the development of novel TRP channel specific drugs and improves our appreciation of the physiological and pathological functions of TRP channels.

In our earlier work (Zheng et al., 2018a), we verified that the N/C interaction exists in TRPP2, P3, V1, and M8. We identified critical residues located in the N-terminus and C-terminus which are involved in the interaction in these four TRP channels. We also identified that PIP2 disruption or enhancement of the N/C interaction is associated with the inhibition on these channels. Current TRPV6 structures demonstrated close proximities of Pre-S1, S4-S5 linker and TRP domains (McGoldrick et al., 2018). PIP2 was reported to activate TRPV6 with an unknown mechanism (Velisetty et al., 2016). Whether PIP2 regulation on TRPV6 is linked to intramolecular interaction in a similar fashion as shown for TRPP channels is unclear. Our expertise with *Xenopus* oocytes for expression and functional characterization of different TRP channels through two-electrode voltage clamp has been valuable for previous functional investigation of TRPV6 (Zheng et al., 2018b).

CMZ activation was used by several groups to characterize TRPP3 channel function (DeCaen et al., 2013; Park et al., 2018). Although CMZ is an antagonist of CaM, CaM's effect on TRPP3 is never thoroughly explored. Compared with TRPP3 expressed in mammalian cells, TRPP3 efficiently traffics to the plasma membrane when expressed in *Xenopus* oocytes and it demonstrates well-documented calcium activated channel activity. Our lab has used *Xenopus* oocytes to functionally characterize TRPP3 for many years. It is appropriate to explore CaM's effect on TRPP3 in this system.

The previously unknown functional transmembrane protein, TMEM120A (also named TACAN), has been identified to contribute to mechanical pain sensation. Diverse tissue distribution indicates it may have a variety of physiological roles. Earlier in 2009, a potential

biochemical interaction between TACAN and TRPP2 was indicated by a proteomic screening (Sharif-Naeini et al., 2009). However, the functional interactions between TACAN and TRPP2 have never been explored due to the lack of a reliable recording on TRPP2 (Arif Pavel et al., 2016). Our lab has used the robust current from TRPP2 F604P GOF mutant as a readout to successfully identify the functional critical intramolecular interactions and gate residues in the past few years (Zheng et al., 2018a; Zheng et al., 2018c). It is suitable for us to determine the impact of TACAN on TRPP2 F604P at the whole-cell level. Meanwhile, our collaborators can also determine the influence of TACAN on TRPP2 through patch-clamp at the single-channel level. And our well-established molecular techniques enable us to explore the physical interaction between TACAN and TRPP2.

CHAPTER 2

RESULTS #1

Autoinhibition of TRPV6 channel and regulation by PIP2

2.1 ABSTRACT

Transient receptor potential vanilloid 6 (TRPV6), a calcium-selective channel possessing six transmembrane domains (S1-S6) and intracellular N-/C-termini, plays crucial roles in calcium absorption in epithelia and bone and is involved in human diseases including vitamin-D deficiency, osteoporosis and cancer. The TRPV6 function and regulation remain poorly understood. Here we show that the TRPV6 intramolecular S4-S5 linker to C-terminal TRP helix (L/C) and N-terminal pre-S1 helix to TRP helix (N/C) interactions, mediated by Arg470:Trp593 and Trp321:Ile597 bonding, respectively, are autoinhibitory and are required for maintaining TRPV6 at basal states. Disruption of either interaction by mutations or blocking peptides activates TRPV6. The N/C interaction depends on the L/C interaction but not vice versa. Three cationic residues in S5 or C-terminus are involved in binding PIP2 to suppress both interactions thereby activating TRPV6. This study reveals 'PIP2-intramolecular interactions' as a regulatory mechanism for both activation and auto-inhibition of TRPV6. Future comparisons with other TRP channels may help elucidating similar mechanisms of regulation.

2.2 INTRODUCTION

Mammalian transient receptor potential (TRP) superfamily of ion channels contains 28 members divided into six subfamilies known as TRP canonical (TRPC), vanilloid (TRPV), polycystin (TRPP), melastatin (TRPM), ankyrin (TRPA) and mucolipin (TRPML) (Gees et al., 2010). TRP proteins share tetrameric assembly and membrane topology, i.e., six transmembrane domains (S1-S6) and intracellular N- and C-termini (Liao et al., 2013; Saotome et al., 2016). As a member of the TRPV subfamily TRPV6 is a cation channel highly selective to calcium (Ca) with a permeability (P) ratio $P_{Ca}/P_{Na} = 130$ (Yue et al., 2001). It is expressed in several human tissues such as small intestine, kidney, placenta and testis (Peng et al., 1999). Physiologically, TRPV6 plays crucial roles in Ca homeostasis of small intestine and kidney and in Ca-dependent sperm maturation (Bianco et al., 2007; van Goor et al., 2017). A TRPV6 loss-of-function mutation in male mice leads to severely impaired sperm motility and fertility (Weissgerber et al., 2011; Weissgerber et al., 2012). TRPV6 is also essential in responding to fluid shear stress during microvilli development (Miura et al., 2015). Malfunction of TRPV6 is associated with a variety of human diseases including vitamin D-deficiency rickets, kidney stone disease and osteoporosis (van Abel et al., 2003; Suzuki et al., 2008; Lieben et al., 2010). Elevated expression of or mutations in TRPV6 is found in cancer including breast, prostate, non-small cell lung, kidney and skin cancer, making it a potential target for clinical interventions (Peters et al., 2012; Peng et al., 2000; Forbes et al., 2008; Stewart, 2020).

TRPV6 structures determined by X-ray crystallography and cryo-electron microscopy (EM) revealed proximity of the C-terminal TRP helix with the N-terminal pre-S1 and intracellular S4-S5 linker (McGoldrick et al., 2018; Saotome et al., 2016). Similar physical arrangements were also seen in other TRP members with resolved structures, while TRPP

channels have a TRP-like helix (Su et al., 2018a; Liao et al., 2013; Lopez-Romero et al., 2019). However, whether and how these domains interact with each other, and the functional implications of these interactions are poorly understood.

Predominantly anchored to the inner plasma membrane, phosphatidylinositol 4,5-bisphosphate (PIP2, or PI(4,5)P2) accounts for more than 99% of double-phosphorylated PIs in mammalian cells, with PI(3,4)P2 and PI(3,5)P2 accounting for the rest (Vanhaesebroeck et al., 2001). Phospholipase C hydrolyzes PIP2 into second messengers inositol 1,4,5-trisphosphate and diacylglycerol. PIP2 is known to modulate ion channels through electrostatic force between its negatively charged inositol head and a pocket formed by cationic residues in a channel protein. For instance, cationic residues in TRPP3, -M4, -M8 and -V1 have been identified to be part of the PIP2 binding pocket (Zheng et al., 2018a; Nilius et al., 2008). PIP2 may exert an inhibitory or stimulatory effect on a TRP channel. For example, PIP2 stimulates the function of TRPV5, -V6, -M4, -M5, -M7 and -M8 while it inhibits TRPP2 and -P3 (Zheng et al., 2018a; Samanta et al., 2018; Ma et al., 2005). The effect of PIP2 on TRPV1 may be stimulatory or inhibitory, depending on experiment conditions (Lukacs et al., 2007). Based on a rabbit TRPV5 cryo-EM structure resolved with the analogue diC_8-PIP2 present in the nanodisc, it was suggested that PIP2 would bind to residues in the N-terminus, S4-S5 linker and TRP domain (Hughes et al., 2018).

In the present study, we characterized intramolecular interactions among the S4-S5 linker, TRP and pre-S1 helices of TRPV6 by means of co-immunoprecipitation (co-IP), *in vitro* pull-down and co-immunofluorescence (co-IF). We examined how they modulate TRPV6 channel function by the two-electrode voltage clamp electrophysiology in *Xenopus* oocytes and Ca imaging in mammalian cells. We also identified TRPV6 residues involved in these interactions

or PIP2 binding and determined how PIP2 modulates TRPV6 intramolecular interactions through which it activates TRPV6.

2.3 METHODS

Plasmids, mutations, antibodies and chemical reagents

Human TRPV6 cDNA was subcloned into *Xenopus* expression vector pBSMXT-MCS. For expression in HEK293 cells, human TRPV6 cDNA was subcloned into the mammalian expression vector pMAX-GFP. Quick Change Lightning Site-Directed Mutagenesis kit (Agilent Technologies, La Jolla, CA) was used to generate mutations, which were all verified by sequencing. Antibody against TRPV6 was custom made in house, as previously described (Fecher-Trost et al., 2013). Antibodies against β-actin, GST, His, HA and Flag were purchased from Santa Cruz Biotechnology (Santa Cruz, CA). Secondary anti-mouse, -rabbit and -goat antibodies were purchased from GE Healthcare (Waukesha, WI). Wortmannin and NFA were purchased from Millipore Sigma Canada (Oakville, ON) and diC_8-PIP2 from Echelon Biosciences (Salt Lake City, UT).

List of mutants used in this chapter

TRPV6	
F468A	R589Q
R470A	R628Q
F472A	R632Q
F478A	K484Q/R589Q/R632Q
W593A	R470F
R594A	W593F
W321A	W593Y
I597A	R320Q/K322Q/R323Q
W321I	R409Q
I597W	R414Q
W321I/I597W	R584Q
W321E	R594Q

W321E/I597W	K606Q
I597E	R607Q
W321R/I597E	R610Q
ΔN	R615Q
ΔN/I597E	R621Q
ΔN/I597W	R636Q
ΔN/I597R	R641Q
W593A/I597A	R643Q
W321A/R470A	R646Q
W321A/W593A	R654Q
R470A/I597A	K661Q
K484Q	K666Q
R588Q	Q473A

Xenopus oocyte expression

Capped RNAs encoding TRPV6 and peptides were synthesized by an *in vitro* transcription T3 or T7 mMESSAGE mMACHINE kit (Ambion, Austin, TX) and injected (25-50 ng per oocyte) into *Xenopus* oocytes prepared as described (Zheng et al., 2018c). Oocytes injected with equal volumes of water served as control. After injection, oocytes were incubated at 18℃ for 1-2 days before experiments. The present study was approved by the Ethical Committee for Animal Experiments of the University of Alberta and was carried out in accordance with the Guidelines for Research with Experimental Animals of the University of Alberta and the Guide for the Care and Use of Laboratory Animals (NIH Guide) revised in 1996.

Two-electrode voltage clamp electrophysiology

The two-electrode voltage clamp electrophysiology experiments in *Xenopus* oocytes were performed as we described previously (Zheng et al., 2016b). Briefly, the electrodes (Capillary pipettes, Warner Instruments, Hamden, CT) that impale an oocyte were filled with 3 M KCl for a tip resistance of 0.3-2 MΩ. Unless otherwise indicated, an NMDG-containing extracellular solution was used (in mM): 100 NMDG, 2 KCl, 0.2 $MgCl_2$ and 10 HEPES (pH 7.5) with or without 5 mM $CaCl_2$ with the presence of 1 mM NFA, and oocytes were clamped at -50 mV. The Na-containing solution was formed by replacing NMDG with Na. On-site injection of diC_8-PIP2 was performed by a third electrode after the initial measurements. The second measurements were performed 10 min after the injection (Zheng et al., 2018a). Unless described otherwise, measurements were performed when a complete oocyte was voltage clamped and held at -50 mV. Whole-cell currents and membrane potentials were recorded at room temperature and analyzed using a Geneclamp 500B amplifier and Digidata 1322A AD/DA converter (Molecular Devices, Union City, CA) together with the pClamp 9 software (Axon Instruments, Union City, CA). Current and voltage signals were digitized at 200 μs/sample and filtered at 2 kHz through a Bessel filter. SigmaPlot 13 (Systat Software, San Jose, CA) and GraphPad Prism 8 (GraphPad Software, San Diego, CA) were used for data plotting.

Surface protein biotinylation

Oocytes were washed three times in ice-cold PBS solution, *Xenopus* oocytes were incubated with 0.5 mg/ml sulfo-NHS-SS-Biotin (Pierce, Rockford, IL) for 30 min at room temperature. Non-reacted biotin was quenched using 1 M NH_4Cl. Oocytes were then washed with ice-cold PBS solution and harvested in ice-cold CelLytic M lysis buffer (Sigma)

supplemented with Halt^{TM} protease inhibitor cocktail (Thermo Scientific, Waltham, MA). With gentle shaking, lysates were incubated at 4℃ overnight upon addition of 100 μL streptavidin (Pierce). The surface protein absorbed by streptavidin was resuspended in SDS loading buffer and subjected to SDS-PAGE.

Whole oocyte immunofluorescence

Immunofluorescence assays using whole *Xenopus* oocytes were performed as described (Zheng et al., 2018a). After PBS wash, 15 min fixation in 4% paraformaldehyde and 3-time washes in PBS plus 50 mM NH_4Cl, oocytes were permeabilized with 0.1% Triton X-100 for 4 min. PBS plus 3% skim milk was used to block oocytes for 30 min. Oocytes were then incubated at 4℃ overnight with indicated primary antibodies (with Flag tag for NP, CP and their mutants and HA tag for LP and its mutant), followed by incubation with secondary Alexa-488-conjugated donkey anti-rabbit or Cy3-conjugated goat anti-mouse antibodies (Jackson Immuno Research Laboratories, West Grove, PA) for 30 min. Oocytes were then mounted in Vectashield (Vector Labs, Burlington, ON) and examined on an AIVI spinning disc confocal microscope (Cell Imaging Facility, Faculty of Medicine and Dentistry, University of Alberta).

Co-IP and *in vitro* pull-down

Co-IP experiments were performed as we previously described (Zheng et al., 2018a). Briefly, a group of 20-30 oocytes were washed with PBS and solubilized in ice-cold CelLytic-M lysis buffer (Sigma) supplemented with Halt^{TM} protease inhibitor cocktail. After centrifugation at 16,100 Relative Centrifugal Force (RCF) for 15 min, supernatants were collected and precleaned for 1 hour (hr) with 50% protein G-Sepharose (GE Healthcare), followed by incubation with

antibodies at 4℃ for 4 hr. The mixture upon the addition of 100 μL of 50% protein G-Sepharose was incubated at 4℃ overnight with gentle shaking. The immune complexes conjugated to protein G-Sepharose were washed five times with Nonidet P-40 lysis buffer (1% Nonidet P-40, 150 mM NaCl, 50 mM Tris, pH 7.5) and eluted by SDS loading buffer. Precipitated proteins were loaded to SDS-PAGE gel and transferred to a PVDF membrane (Bio-Rad, Hercules, CA), and then analyzed by WB.

GST- or His-tagged human TRPV6 peptides were purified from *E. coli* and incubated at the same amount (2 μg) and solubilized in the CelLytic-M lysis buffer (Sigma). The mixture was incubated at 4℃ for 4 hr with gentle shaking, followed by overnight incubation after addition of 10 μl 50% Ni-NTA agarose beads (Qiagen, Hilden, Germany). The beads were then washed three times with PBS buffer supplemented with 1% Nonidet P-40, and the remaining proteins were eluted using SDS loading buffer and resolved by SDS-PAGE and transferred to PVDF membrane (Bio-Rad). His and GST antibodies were used to immunoblot the membrane.

Dot-blot assay

Lysates of TRPV6-expressing oocytes or purified peptides were spotted onto a nitrocellulose membrane and then let the membrane dry. To enhance the retention of proteins on the membrane. The membrane was immersed in PBS containing 0.5% (v/v) glutaraldehyde for 5 min and moved to a fresh PBS/glutaraldehyde solution for 10 min, followed by placement in PBS containing 50 mM glycine to stop cross-linking reaction. Membrane was then washed once with PBS buffer. Water soluble PIP2 analogue diC8 PIP2 were further loaded on the corresponding position. Membrane was washed again by PBS buffer and analyzed by WB.

Ratiometric Ca imaging

HEK293 cells plated on PLL-coated glass coverslips in the incubation medium were loaded with 5 μM Fura-2-AM in the dark and incubated at 37°C for 30 min. Cells were then washed with bath solution (in mM): 1 $MgCl_2$, 2 $CaCl_2$, 4 KCl, 140 NaCl, 10 HEPES, 10 glucose, pH adjusted to 7.2 with NaOH. $CaCl_2$ was replaced by $MgCl_2$ to form a nominal Ca-free solution. An inverted microscope (Axiovert S100, Zeiss, Oberkochen, Germany) equipped with a monochromator (Polychrome V, TILL-Photonics Graefelfing, Germany) and a 20× Fluar objective (Zeiss) was used for all measurements. Fura-2 was alternately excited at 340 nm and 380 nm for 30 ms every 2 s and the emitted fluorescence (>510 nm) was recorded with a cooled charge-coupled device (CCD) camera (TILL Imago, TILL-Photonics). F340 and F380 pictures were used to calculate the ratiometric images after background correction, i.e. subtraction by the fluorescence intensity in a cell-free area corresponding to 340 and 380 nm excitation, respectively. Single cells were marked as regions of interest and the F340/F380 ratio was plotted versus time. Monochromator, camera, acquisition and analysis were controlled by TILLvisION software (TILL-Photonics).

Determination of death of HEK293 cells and oocytes

HEK293 cells were suspended in the PBS solution two days post transfection. Cells were stained with 0.08% trypan blue (Gibco, Waltham, MA). The cell death percentage was calculated as the number of stained cells divided by the total number of cells measured by a hemocytometer under microscopy. Oocytes were collected three days after mRNA injection. The oocyte death percentage was determined as the number of unhealthy oocytes divided by the total number of

oocytes. 12-24 h more incubation time are needed to detect the cell death compared with oocytes subjected to electrophysiological recordings and co-IP experiments.

Knockdown of zebrafish Trpv5/6 by CRISPR-Cas9

Single guide RNAs (sgRNAs: CGGTGTCCTCCTGAAATCAT and CCTGAAATCATGCCACCCGC) targeting the second coding exon of zebrafish Trpv5/6 (ENSDART00000127453.3) was designed and synthesized as previously described (Zhang et al., 2019). The Cas9 protein was purchased from NEB (Ipswich, MA). Mixture of sgRNA and Cas9 was injected into one-cell stage zebrafish embryos (sgRNA 150 pg/embryo and Cas9 300 ng/embryo). The effect of injected CRISPR-Cas9 was confirmed by sequencing (Sangon, Shanghai, China) and quantitative PCR (Q-PCR) using SYBR qPCR master mix (Vazyme, Nanjing, China).

Total RNA was extracted using Trizol reagent (Invitrogen, Carlsbad, CA) according to the manufacturer's instructions and extracted with RNeasy Min Elute Clean up kit (Tiangen, Beijing, China). Reverse transcription reaction was performed using 1 μg of total RNA with cDNA synthesis kit (Vazyme). The mRNA expression level was determined by Q-PCR and Q-PCR Detection System (Applied Biosystems, Foster City, CA). Primers used were as below: Trpv5/6-F: CCATCCTGCACCTGTTGGTTTT, Trpv5/6-R: CATCCCTTGCAGCGAGTTTGAA. β-actin-F: 5'-CTCCCCTTGTTCACAATAACCTACTAATACACAGC; β-actin-R: TTCTGTCCCATGCCAACCATCACTC. Gene expression was normalized to β-actin. Genomic DNA was isolated from an individual 2 dpf embryo, as previously described (Zhang et al., 2019). Genotyping was performed by PCR amplification of the region of interest using the

primers Trpv5/6-F: CCCTTTAACCTATTGGGTTTTACAG, Trpv5/6-R: CATATTCAATCTAATAAGAACAATCAATGC. Mutations were confirmed by sequencing.

Staining protocol was performed as previously reported (Vanoevelen et al., 2011; Walker and Kimmel, 2007). Briefly, zebrafish embryos at 7 dpf were fixed in 4% formaldehyde (Sigma) with shaking at room temperature for 2 hr. Embryos were then dehydrated in 50% ethanol and stained with Alcian blue 8GX (Sigma) in 70% ethanol with 80 mM $MgCl_2$. After bleaching using 1% H_2O_2 and 1% KOH, embryos were washed in sodium tetraborate solution and digested with trypsin for 1 hr. Embryos were then stained using Alizarin red S (Sigma) in 1% KOH and stored in 70% glycerol at 4℃. Pictures were taken using Nikon SMZ18 (Tokyo, Japan). The notochord tip area was selected and the corresponding intensity quantified using ImageJ. Zebrafish experiments were carried out in compliance with the protocol specifically approved for the use of laboratory animals of the Hubei University of Technology.

Statistical analysis

All statistical data in this study are expressed as mean ± SEM (standard error of the mean) from N measurements. Statistical significance was determined by two-sided paired or unpaired Student's t-test. One-way ANOVA test was also used for multiple comparisons. *, ** and *** indicate $p < 0.05$, 0.01 and 0.001, respectively; ns indicates statistically not significant.

2.4 RESULTS

Functionally critical residues in the S4-S5 linker and TRP helix of TRPV6

Pathogenic mutations have been found in the S4-S5 linker of several TRP channels such as TRPV4, -A1, -M4 and -ML1 (Dai et al., 2010; Goldin et al., 2004; Kremeyer et al., 2010; Stallmeyer et al., 2012). However, the mechanism of how the linker exercises its functional importance is largely unclear. Based on the proximity of the TRPV6 S4-S5 linker to the C-terminal TRP helix (McGoldrick et al., 2018) we examined the functional relevance of the residues that may be involved in the physical arrangement. For this we first substituted all aromatic and charged residues with alanine in this region of human TRPV6 and examined the channel function of the resulting mutants using the two-electrode voltage clamp in *Xenopus* oocytes in extracellular solutions containing 1 mM niflumic acid (NFA) to block the endogenous Ca-activated Cl channels (Peng et al., 1999; Huang et al., 2013; Wang et al., 2019), similarly as we recently did for TRPP2 with or without co-expression of PKD1 in oocytes (Wang et al., 2019). Under this condition, steady-state currents elicited by extracellular Ca (5 mM) relative to the solution containing impermeable N-methyl D-glucamine (NMDG) served as a TRPV6 function readout. We found that each of the mutations R470A and F478A in the S4-S5 linker (Fig. 2-1A) substantially increases Ca-induced steady-state currents without affecting the plasma membrane expression in expressing oocytes (Fig. 2-1B, C and D). Because fragment 593-WRAQI-597 within the TRP helix is located proximal to the S4-S5 linker under cryo-EM conditions (Fig. 2-1E), we tested the function of TRPV6 mutants W593A and R594A and found that mutant W593A, but not R594A, exhibits substantially activated channel function compared with WT TRPV6 given the unaffected surface membrane expression by these mutations (Fig. 2-1B and C). We further generated R470F, W593F and W593Y mutants and found that they have

similar or reduced function compared with WT channel (Fig. 2-1F and G), which presumably means the presence of an interaction between sites 470 (or 478) and 593, possibly of a π-π or π-cation interaction. Consistently, Na currents, serving as another function readout of TRPV6, mediated by mutants R470A and W593A increased 4.3 and 3.5-fold (Fig. 2-1H). In summary, we found that residues R470 and F478 in the linker and W593 in the TRP helix are required to maintain TRPV6 channel at its basal function (i.e., prevent it from activation), suggesting their involvement in the linker/TRP helix association.

Interaction between the S4-S5 linker and TRP helix

We next examined the S4-S5 linker to TRP helix (referred to as L/C) interaction by co-IP assays using the linker-containing peptide LP (amino-acid (aa) V465-F493) and full-length (FL) TRPV6 co-expressed in oocytes. We found that LP indeed associates with TRPV6 and that the association is substantially reduced in the presence of the R470A mutation in LP or the W593A mutation in TRPV6 (Fig. 2-1I) but remains unaffected by the F478A mutation in LP (Fig. 2-J). These data indicate that R470 and W593 mediate the LP/TRPV6 interaction, presumably through forming a R470:W593 cation-π bond. We also documented the L/C interaction by examining colocalization of LP or C-terminal TRP helix-containing peptide CP (aa W583-V602) with FL TRPV6 using co-IF with whole oocytes. FL TRPV6, but not peptide LP or CP, was localized on the surface membrane of oocytes when expressed alone, as expected (Fig. 2-1K). Both LP and CP were localized on the surface membrane when co-expressed with WT TRPV6. LP failed to be on the surface membrane when it contains mutation R470A or when there is mutation W593A in TRPV6, but mutation F478A in LP had no effect, suggesting that TRPV6 recruits LP to the surface membrane through their binding mediated by the R470:W593 pair. Interestingly, both

mutations W593A in CP and R470A in S4-S5 linker, which is assumed to disrupt the L/C interaction, failed to affect the surface membrane targeting of CP (Fig. 2-1K, last two columns), suggesting the possibility that CP can bind with TRPV6 through another site, which will be examined in the next section.

We further documented the L/C interaction by *in vitro* pull-down experiments using purified (from *E. coli*) glutathione S-transferase (GST)-tagged LP and His-tagged C-terminal peptide CP1 (aa M578-L677) that contains the TRP helix, to further characterize the interaction. We found that the two peptides directly bind with each other and that the binding is significantly reduced by the R470A mutation in LP or the W593A mutation in CP1 (Fig. 2-1L). Our data together suggested that the S4-S5 linker directly binds with the TRP helix possibly through the R470:W593 pair, which is required to maintain TRPV6 channel function at its basal levels and prevent channel activation (Fig. 2-1B and C).

We next utilized a blocking peptide strategy to further document the functional importance of the R470:W593-mediated L/C interaction. For this we co-expressed LP or CP with FL TRPV6 in oocytes and reasoned that over-expressed LP or CP would disrupt the intramolecular L/C binding within the TRPV6 protein and thus activate TRPV6. Indeed, LP and CP significantly increased TRPV6 channel function (Fig. 2-1M) without affecting its surface expression (Fig. 2-N). Mutant peptide LP-R470A did not stimulate TRPV6 function (Fig. 2-1M) as expected because of lack of physical binding between them (Fig. 2-1I and L), whereas CP-W593A continued to activate TRPV6 channel (Fig. 2-1M), which is consistent with its co-localization with TRPV6 (Fig. 2-1K). It is noted that a blocking peptide may induce functionally important structural changes in addition to disrupting the L/C binding, which requires further investigations. Also, there might be other residues in the S4-S5 linker and TRP helix that are

involved in the L/C interaction, but they do not seem to be as essential as the R470-W593 pair of which the involvement has been verified by several pieces of data. In summary, our data using the blocking peptide strategy further supported the autoinhibitory role of R470:W593-mediated intramolecular L/C interaction in TRPV6.

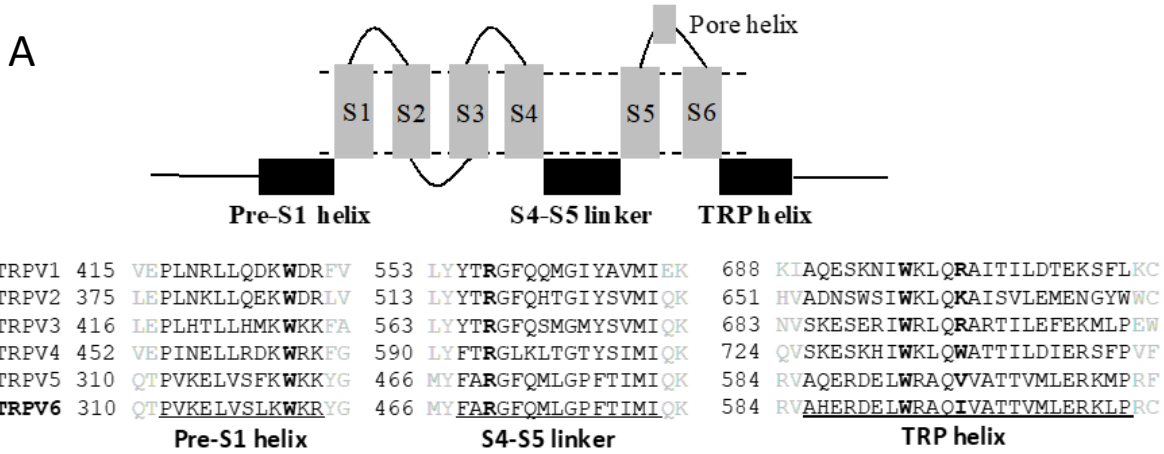
A
Pore helix
S1
S2
S3
S4
S5
S6
Pre-S1 helix
S4-S5 linker
TRP helix
rTRPV1 415 VEPLNRLLQDKWDRFV 553 LYYTRGFQQMGIYAVMIEK 688 KIAQESKNIWKLQRAITILDTEKSFLKC
rTRPV2 375 LEPLNKLLQEKWDRLV 513 LYYTRGFQHTGIYSVMIQK 651 HVADNSWSIWKLQKAISVLEMENGYWWC
hTRPV3 416 LEPLHTLLHMKWKKFA 563 LYYTRGFQSMGMYSVMIQK 683 NVSKESERIWRLQRARTILEFEKMLPEW
rTRPV4 452 VEPINELLRDKWRKFG 590 LYFTRGLKLTGTYSIMIQK 724 QVSKESKHIWKLQWATTILDIERSFPVF
RTRPV5 310 QTPVKELVSFKWKKYG 466 MYFARGFQMLGPFTIMIQK 584 RVAQERDELWRAQVVATTVMLERKMPRF
hTRPV6 310 QTPVKELVSLKWKRYG 466 MYFARGFQMLGPFTIMIQK 584 RVAHERDELWRAQIVATTVMLERKLPRC
Pre-S1 helix
S4-S5 linker
TRP helix

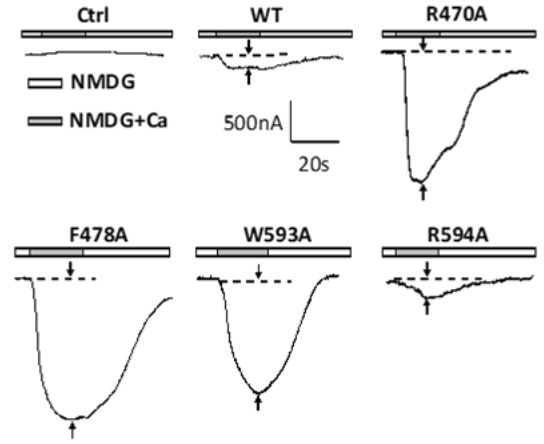
B
Ctrl
WT
R470A
NMDG
NMDG+Ca
500nA
20s
F478A
W593A
R594A

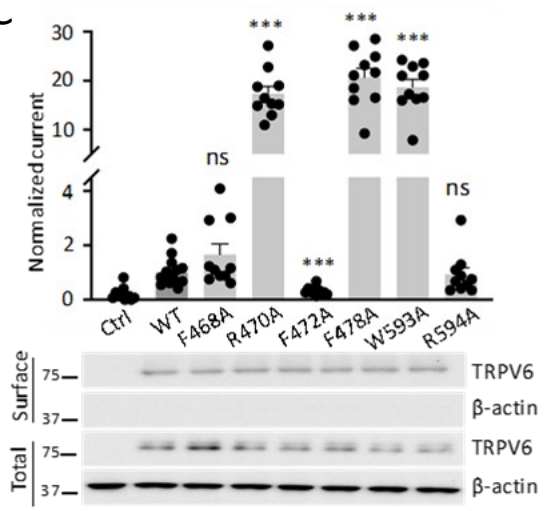
C
Normalized current
30
20
10
4
2
0
***
ns
Ctrl
WT
F468A
R470A
F472A
F478A
W593A
R594A
Surface
Total
75
37
TRPV6
β-actin

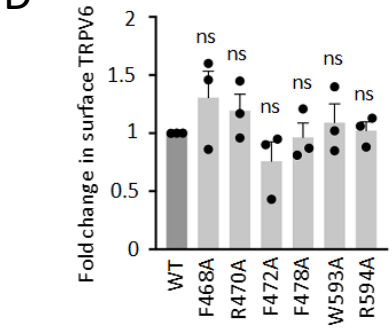
D
Fold change in surface TRPV6
2
1.5
1
0.5
0
ns
WT
F468A
R470A
F472A
F478A
W593A
R594A

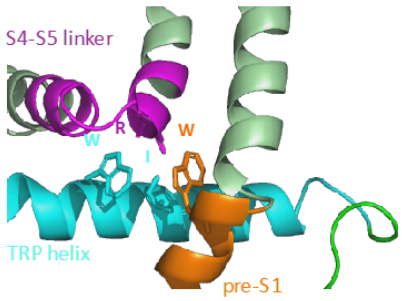
E
S4-S5 linker
TRP helix
pre-S1
R
W
W
I

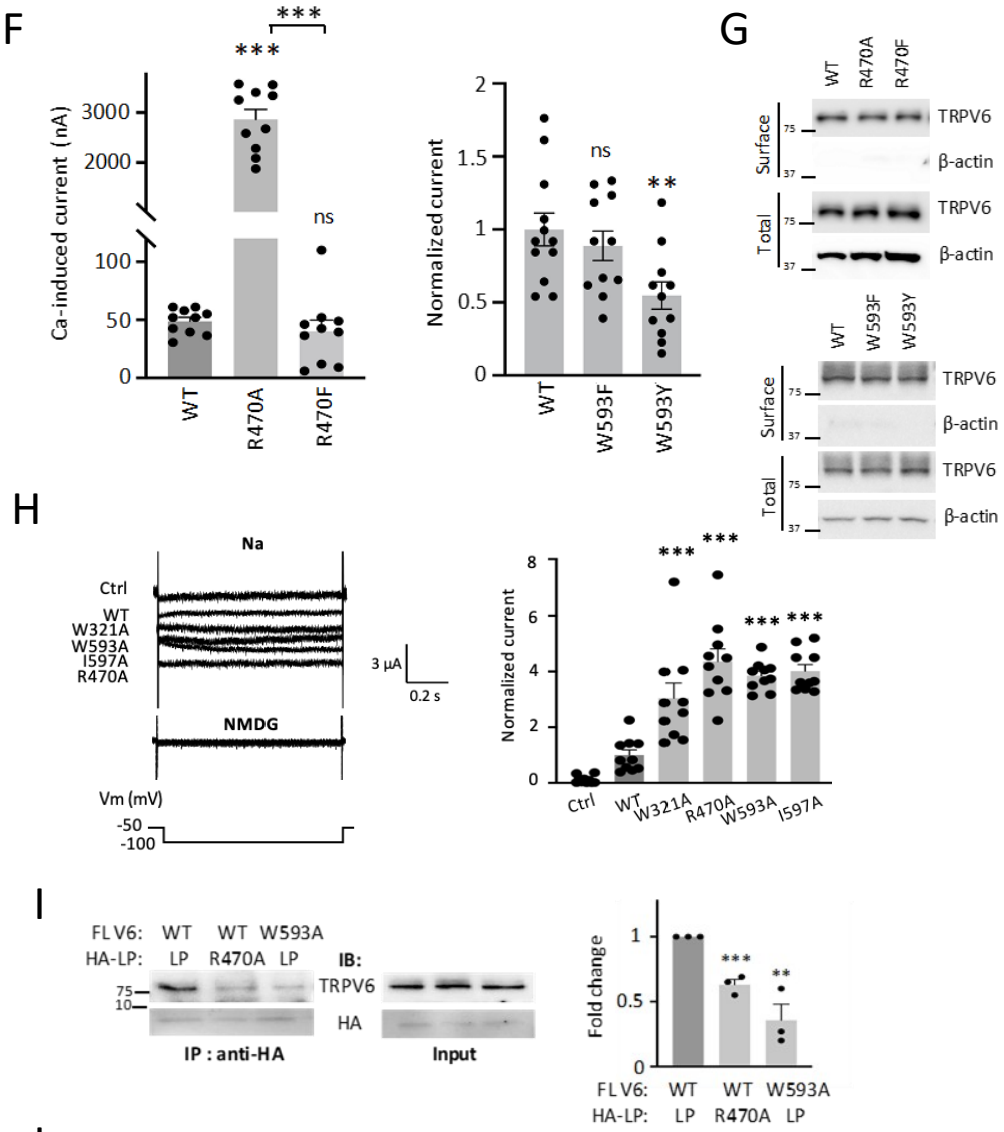
F
***
***
ns
Ca-induced current (nA)
3000
2000
100
50
0
WT
R470A
R470F
Normalized current
2
1.5
1
0.5
0
ns
**
WT
W593F
W593Y
G
WT
R470A
R470F
Surface
Total
TRPV6
β-actin
75
37
WT
W593F
W593Y
H
Na
Ctrl
WT
W321A
W593A
I597A
R470A
3 μA
0.2 s
NMDG
Vm (mV)
-50
-100
Normalized current
8
6
4
2
0
***
***
***
***
Ctrl
WT
W321A
R470A
W593A
I597A
I
FLV6: WT WT W593A
HA-LP: LP R470A LP
IB:
TRPV6
HA
75
10
IP : anti-HA
Input
Fold change
1
0.5
0
***
**
FLV6: WT WT W593A
HA-LP: LP R470A LP
J
FL V6: WT WT
HA-LP: WT F478A
IB:
TRPV6
HA-LP
75
10
IP : anti-HA
Input

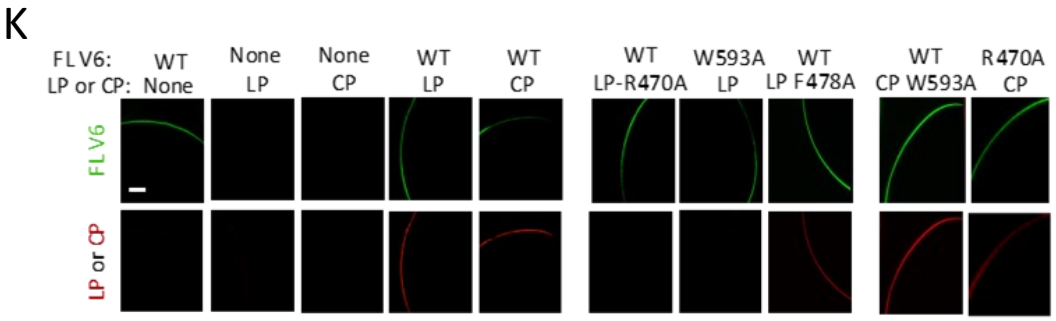
K
FLV6: WT None LP None CP WT LP WT CP WT LP-R470A W593A LP WT LP F478A WT CP W593A R470A CP
LP or CP:
FLV6
LP or CP

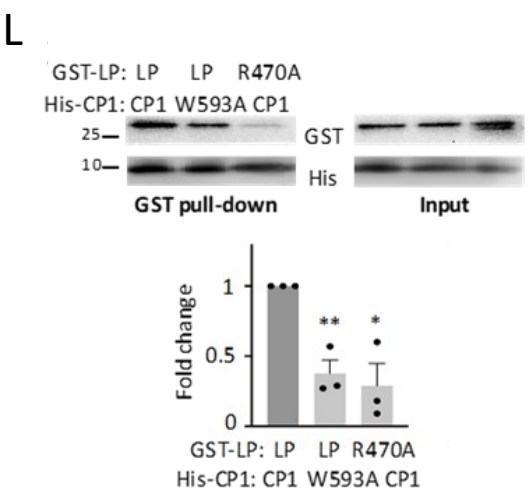
L
GST-LP: LP LP R470A
His-CP1: CP1 W593A CP1
25
10
GST
His
GST pull-down
Input
Fold change
1
0.5
0
**
*
GST-LP: LP LP R470A
His-CP1: CP1 W593A CP1

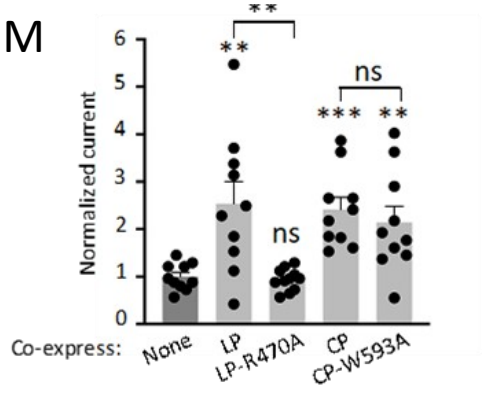
M
Normalized current
6
5
4
3
2
1
0
**
**
ns
***
**
ns
Co-express: None LP LP-R470A CP CP-W593A

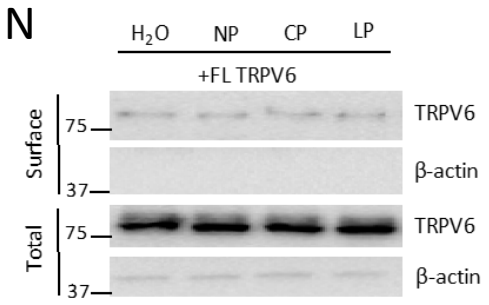
N
H2O NP CP LP
+FL TRPV6
Surface
Total
75
37
75
37
TRPV6
β-actin
TRPV6
β-actin

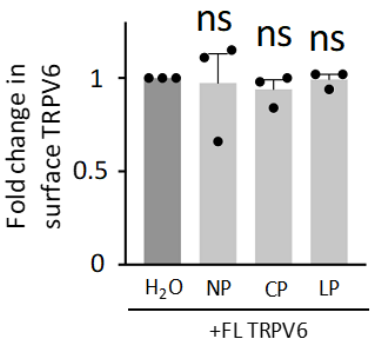
Fold change in surface TRPV6
1
0.5
0
ns
ns
ns
H2O NP CP LP
+FL TRPV6

Figure 2-1. Roles of residues in the TRPV6 S4-S5 linker and TRP helix in the channel function, L/C interaction and L/C co-localization. A. Upper panel: membrane topology of TRPV channels with indicated key domains. Dashed lines indicate the lipid membrane. Lower panel: sequences of the TRPV pre-S1, S4-S5 linker and TRP helices. The four residues involved in intramolecular interactions are in bold. **B.** Representative whole-cell current traces obtained from *Xenopus* oocytes expressing human TRPV6 or a mutant (as indicated), measured by two-electrode voltage clamp. Oocytes were clamped at -50 mV and perfused with a NMDG-containing solution (100 mM NMDG, 2 mM KCl, 0.2mM MgCl2, 10 mM HEPES at pH 7.5) with (NMDG+Ca) or without (NMDG) 5 mM CaCl2, in with the presence of 1 mM NFA throughout. Ca^{2+}-induced currents were measured as a time point indicated by arrows. Ctrl, water injected oocytes. **C.** Upper panel: normalized Ca^{2+}-activated currents obtained as in panel A. Data were averaged from N = 10-14oocytes from three batches. ***p < 0.001 and ns (not significant) in comparison with WT, by Student's t-test. Currents were normalized to the mean current for WT TRPV6. Statistical significance was examined using Student's t-test. Lower panel: representative surface and total expression of WT and mutant TRPV6 by biotinylation, with β-actin as loading controls. Protein markers (in kDa) were labeled. **D.** Data from three independent surface biotinylation experiments were quantified, normalized and averaged. ns, not significant compared with WT. **E.** Structural data (PDB: 6BO8) showing proximity of TRPV6 pre-S1 and S4-S5 linker to TRP helix, generated using PyMOL. The four key residues are shown. **F.** Bar graphs showing the channel function of WT or mutant TRPV6. Normalized Ca-induced currents obtained at -50 mV from expressing oocytes. **p < 0.01; ***p < 0.001, by Student's t-test. **G.** Representative images showing the surface and total expression of indicated proteins. Data were averages from 10-12 oocytes from three batches. Data are presented as mean ± SEM. **H.** Left panel, representative membrane currents obtained using a jump protocol, as indicated, in the presence of the extracellular solution Na or NMDG. Dashed lines indicate the zero-current level. Right panel, averaged plateau current amplitudes at -100 mV obtained under the same experimental conditions as in the left panel (n = 10 from three batches). ***p < 0.001, by Student's t-test. Data are presented as mean ± SEM. **I.** Left panel: representative co-IP data from FL TRPV6 and

HA-tagged TRPV6 LP with or without an indicated mutation. Right panel: data from three independent co-IP experiments were quantified, normalized and averaged. **$p < 0.01$, compared with dark grey group. **J.** Representative co-IP data showing interaction of HA-tagged LP with FL TRPV6 co-expressed in oocytes, with or without mutation F478A in LP. **K.** Representative images showing co-localization of LP or CP with FL TRPV6 by co-IF using oocytes expressing FL TRPV6 or a peptide, with or without a mutation. Scale bar, 50 μm. **L.** Upper panel: representative data from a His pull-down assay showing binding between (E. coli) purified GST-tagged human TRPV6 S4-S5 linker peptide (GST-LP) and His-CP1 with or without an indicated mutation. Lower panel: data from three independent in vitro binding experiments were quantified, normalized and averaged. *$p < 0.05$, compared with dark grey group. **M.** Representative Ca^{2+}-induced currents in oocytes expressing FL TRPV6 with or without indicated peptide. Data were normalized and averaged from 10-11 oocytes from three batches. **N.** Left panel: representative data in oocytes showing effects of peptides NP, CP, LP on the surface and total expression of WT TRPV6, revealed by biotinylation. Right panel: data from three independent experiments were quantified, normalized and averaged. ns, not significant compared with dark grey group. Data are presented as mean ± SE

Interaction between the pre-S1 and TRP helices

Given the proximity between W321 and I597 in the intracellular Pre-S1 and TRP helices, respectively, revealed by TRPV6 structures (Fig. 2-1E) (McGoldrick et al., 2018; Saotome et al., 2016), we first tested the functional roles of W321 and I597 and found that mutants W321A and I597A both exhibit substantial channel activation (Fig. 2-2A-C). In agreement with Ca activation, we determined the Na currents of these two mutants (Fig. 2-1H). Both mutants showed a significantly larger Na current (3.0-4.0 folds) compared with WT. Further, we also employed human embryonic kidney (HEK) cells in combination with Fura-2 Ca fluorimetry as a readout of the Ca influx to examine the functional importance of residues W321 and W593. We found that expression of mutant W321A or W593A results in significantly increased intracellular Ca levels, with or without extracellular Ca, compared with WT TRPV6 (Fig. 2-2D-F), indicating that both are activated mutants, in agreement with our data using oocytes. The increased basal intracellular Ca levels in cells expressing mutant W321A or W593A is presumably due, at least in significant part, to Ca entry during incubation with Ca-containing culture medium. Interestingly, we additionally found that expression of W321A or W593A mutant significantly induces more death both in oocytes and HEK293 cells (Fig. 2-2G-I), similar to a previous study on the TRPV5 gate hinge mutant (van Goor et al., 2017), indicative of the gain-of-function nature of these mutants.

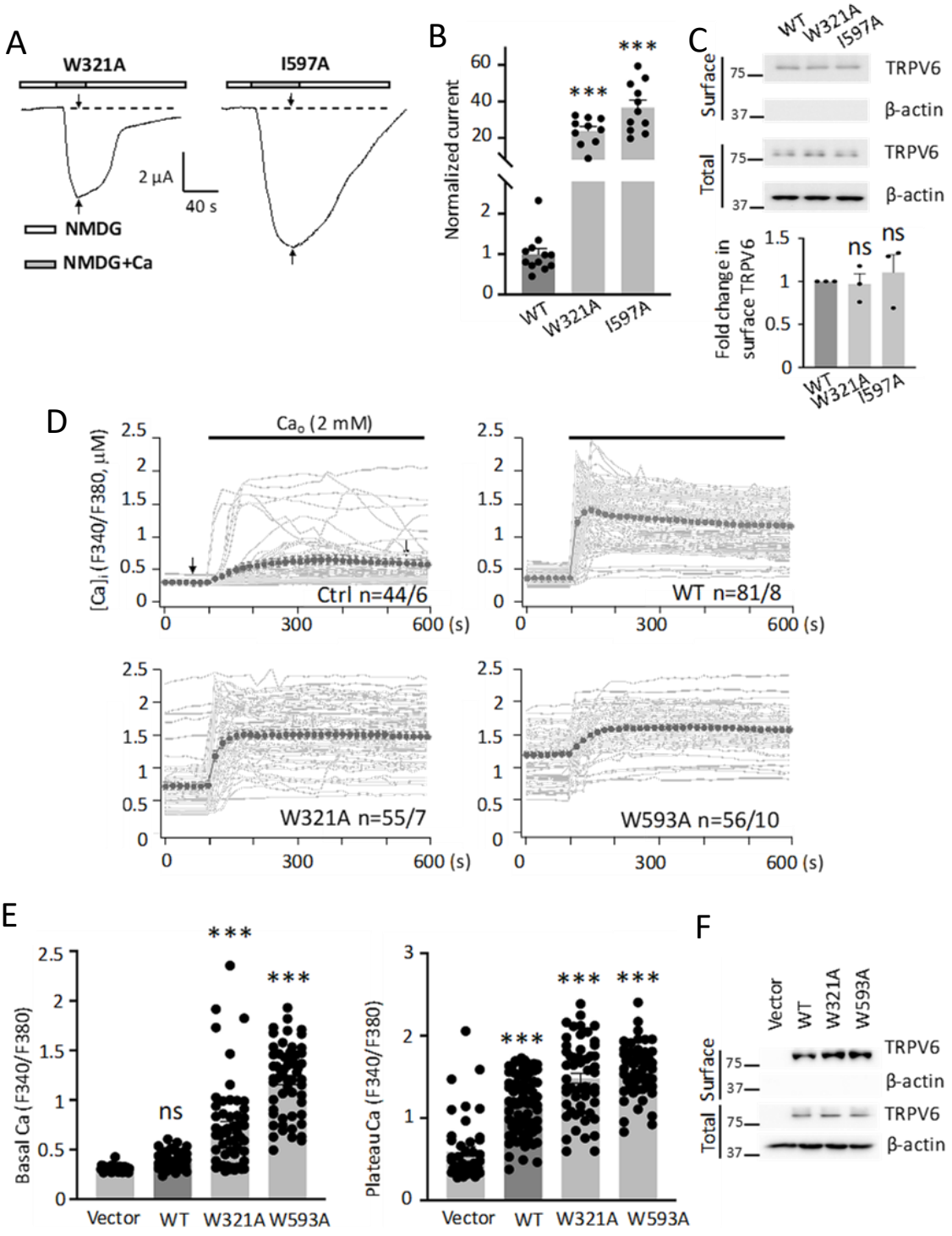
A
W321A
I597A
2 μA
40 s
NMDG
NMDG+Ca
B
Normalized current
***
***
WT
W321A
I597A
C
WT
W321A
I597A
Surface
Total
TRPV6
β-actin
75
37
Fold change in surface TRPV6
ns
ns
D
Ca$_o$ (2 mM)
[Ca]$_i$ (F340/F380, μM)
Ctrl n=44/6
WT n=81/8
W321A n=55/7
W593A n=56/10
0
300
600 (s)
E
Basal Ca (F340/F380)
Plateau Ca (F340/F380)
ns
***
Vector
WT
W321A
W593A
F
Vector
WT
W321A
W593A
Surface
Total
TRPV6
β-actin

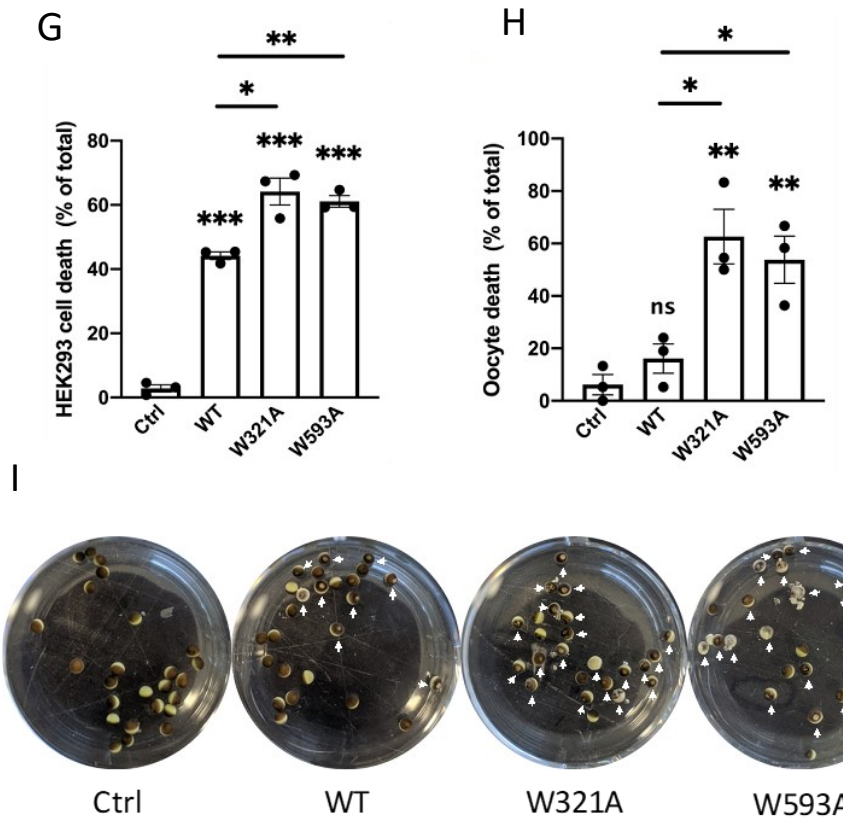
G
H
I
HEK293 cell death (% of total)
Oocyte death (% of total)
Ctrl
WT
W321A
W593A
ns
*
**
***

Figure 2-2. Characterization of functional critical residues in the pre-S1 and TRP helices of TRPV6 in oocytes and HEK293 cells. A. Representative Ca-induced current traces recorded in oocytes expressing a mutant TRPV6, as indicated. **B.** Normalized Ca-activated currents obtained at -50 mV from WT or an indicated mutant TRPV6. Data were averaged from 10-12 oocytes from three batches. **C.** Upper panel: representative data showing the surface and total expression of TRPV6 and mutants measured by biotinylation and WB. Lower panel: data from three independent experiments were quantified, normalized and averaged. ***$p < 0.001$, ns, not significant compared with WT. **D.** Time dependence (0-600 s) of the intracellular Ca concentration ([Ca]i) traces in HEK293 cells expressing human WT or a mutant TRPV6 determined as the F340/F380 ratio by Fura-2 ratiometric Ca imaging, before and after application of 2 mM extracellular Ca (Cao). Averaged traces were obtained from 44-81 cells from 6-10 batches, as indicated. **E.** Averages of basal Ca levels determined from panel D at a time point between 1-100 s (indicated by an arrow) before Ca application. Averages of steady-state Ca levels determined at a time point between 500-600 s (indicated by an arrow) in the presence of Ca. **F.** Representative WB data showing surface and total expression of WT and mutant TRPV6 in HEK cells. **G.** Bar graphs showing death percentage in HEK293 cells expressing WT or mutant channel. **H.** Bar graphs showing death percentage in oocytes expressing WT or mutant channel. **I.** Representative images showing healthy and dead (white arrows) oocytes expressing WT or a mutant channel. Experiments were performed three times from three batches of oocytes. Data are presented as mean ± SEM. ns, not significant; *$p < 0.05$; **$p < 0.01$; ***$p < 0.001$, by Student's t-test.

These data suggest the possibility that the W321:I597 pair forms a bond, plausibly by a van der Waals force, to mediate physical interaction between pre-S1 and TRP helix (referred to as N/C interaction) that is required to prevent TRPV6 channel activation. We reasoned that disrupting and re-establishing the bonding at 321:597 should result in activation and 'rescue' of function, respectively. For this we tested mutants W321I (no bonding by the I:I pair), I597W (W:W bonding) and double mutant W321I-I597W (rescued I:W bonding, vs W:I bonding in WT TRPV6) and indeed found that W361I is an activated mutant while the other two have comparable channel function than WT TRPV6 (Fig. 2-3A and B). The function 'rescue' of mutant W321I-I597W possessing the I:W bonding strongly supported the concept that the W321 directly interacts with I597 rather than indirectly affecting the bonding formed by another pair of residues in pre-S1 and TRP helices. To provide further documentations, we mutated W321 or I597 to anionic glutamic acid to break down the hypothetical bond within the pair and indeed found that both mutants W321E (E:I) and I597E (W:E) exhibit substantial channel activation (Fig. 2-3C and D). Further, introduction of a cationic residue R to the other side of the pair in these two mutants, which generated double mutants W321E-I597R (E:R) and W321R-I597E (R:E), significantly rescued the channel function to its basal levels (Fig. 2-3C and D), possibly through forming a salt bridge. These data together strongly supported the possibility that the W321:I597 pair mediates the N/C binding that is autoinhibitory for TRPV6.

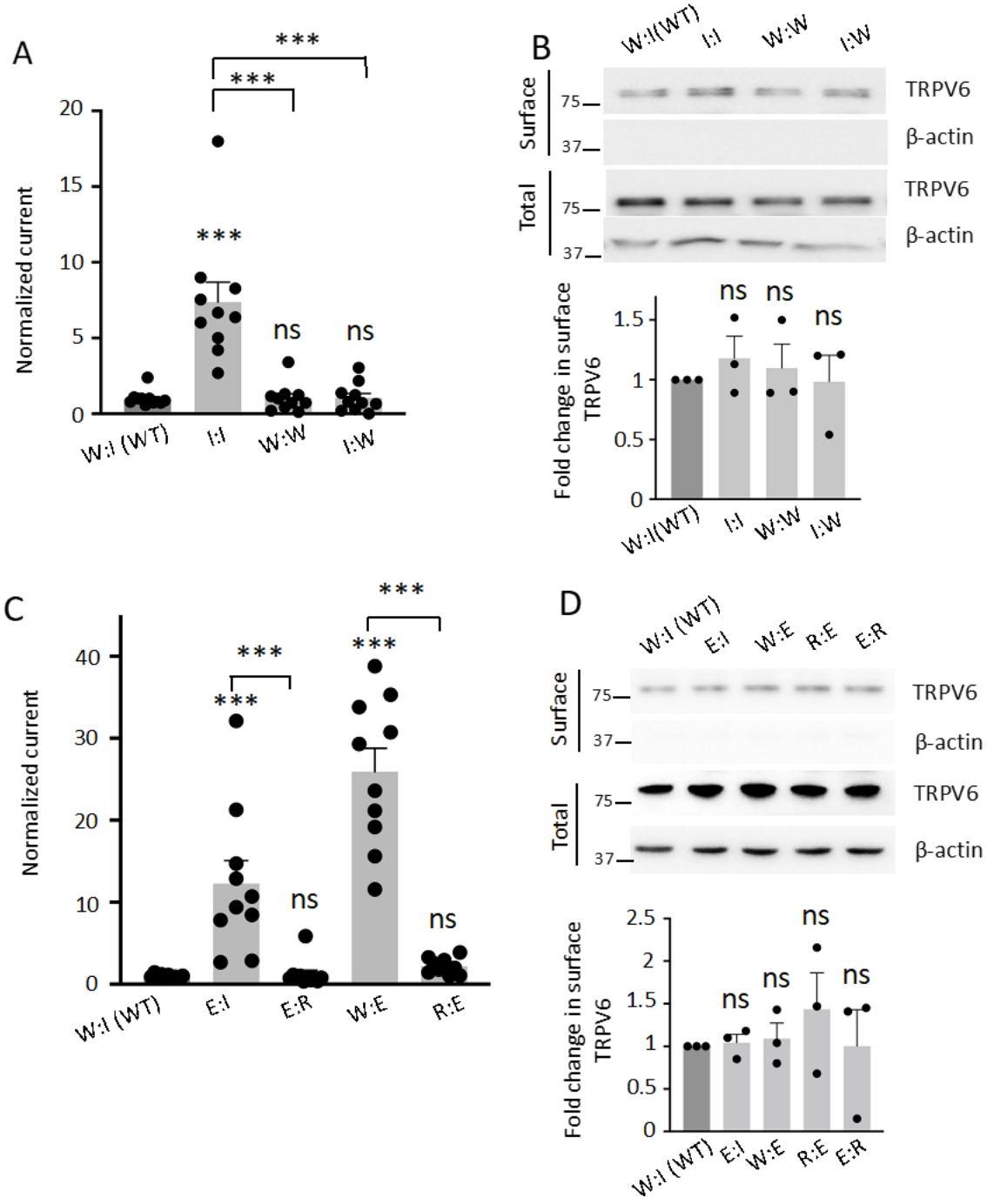
A
Normalized current
***
***
***
ns
ns
W:I (WT)
I:I
W:W
I:W
B
W:I(WT)
I:I
W:W
I:W
Surface
Total
75
37
TRPV6
β-actin
Fold change in surface TRPV6
ns
C
Normalized current
E:I
E:R
W:E
R:E
D
E:I
W:E
R:E
E:R

Figure. 2-3. Functional rescues by mutations at the W361:I637 pair. A. Normalized Ca-activated currents at -50 mV showing functional rescues by the WI: to I:W mutation (W321I-I597W). Data were averaged from 9-11 oocytes from three batches. **B.** Upper panel: representative data from a biotinylation assay showing the surface and total expression of TRPV6 proteins in panel A. Lower panel: data from three independent experiments were quantified, normalized and averaged. ns, not significant compared with WT. **C.** Normalized Ca-activated currents obtained from TRPV6-expressing oocytes. Data were averaged from three batches of oocytes (N = 10-11). **D.** Upper panel: representative biotinylation data on TRPV6 mutants in panel C. Lower panel: data from three independent experiments were quantified, normalized, and averaged.

We next investigated the N/C interaction by co-IP assays and found that TRPV6 N-terminal peptide NP (aa T298-P327) containing the pre-S1 helix and FL TRPV6 are in the same complex in oocytes and that the interaction is disrupted by the W321A mutation in NP or the I597A mutation in TRPV6 (Fig.2-4A), which supports the involvement of the W321:I597 pair in the interaction. By *in vitro* pull-down assays using purified TRPV6 N-terminal peptide NP1 (aa H228-P327) and C-terminal peptide CP1 that contains pre-S1 and TRP helix, respectively, we found that NP1 directly associates with CP1 and that the association is disrupted in the presence of mutation W321A in NP1 or I597A in CP1 (Fig. 2-4B), supporting that W321:I597 mediates direct binding between NP1 and CP1. We also used NP to precipitate the TRPV6 N-terminal truncation mutant (TRPV6-ΔN, aa Y328-I725) that lacks the N/C binding within the molecule, to further document the relationship between the N/C binding strength and channel function and found that the N/C binding strength inversely correlates with the channel activity (Fig. 2-4C and D).

We also investigated the N/C interaction by co-IF experiments using whole oocytes. Peptide NP was co-localized on the surface membrane with WT TRPV6 and this co-localization was disrupted by mutation W321A in NP or I597A in TRPV6 (Fig. 2-4E). These data strongly supported that the W321:I597-mediated NP/TRPV6 interaction retains NP on the surface membrane. We noticed that mutation W321A in TRPV6 or I597A in CP, which presumably disrupts the TRPV6/CP, fails to dissociate CP from the surface membrane (Fig. 2-4E and 2-1D), probably because CP can still bind to the S4-S5 linker within TRPV6. Indeed, double mutation W593A-I597A in CP was then sufficient to bring CP down from the surface membrane. These data together thus nicely supported that the autoinhibitory N/C interaction is mediated by the W321:I597 pair.

We further documented the N/C interaction and its functional roles using a blocking peptide strategy. Similar to LP and CP, expression of NP significantly stimulated the TRPV6 channel activity without altering the surface membrane targeting (Fig. 2-4F and 2-1N), consistent with the assumption that NP acts as a blocking peptide that weakens the intramolecular L/C binding within the TRPV6 molecule. While the W321A mutation in NP abolished its stimulating effect, only double mutation I597A-W593A in CP, but not each of the single mutations, abolished its stimulating effect (Fig. 2-1M and 2-4F). This is presumably because when CP only carries single mutation I597A (or W593A), it can still competitively reduce the TRPV6 intramolecular L/C (or N/C) binding to activate TRPV6 whereas when CP carries the double mutation, it can no longer bind with TRPV6 (and thus no longer has functional effect). Therefore, these data together strongly supported that each of the N/C and L/C interactions is functionally autoinhibitory and that disruption of either interaction leads to channel activation.

We next wanted to examine whether the TRPV6 intramolecular L/C and N/C interactions are independent of each other. Because NP precipitated more mutant TRPV6-W321A than WT channel (Fig. 2-4G), likely due to the absence of the N/C interaction within the TRPV6-W321A protein, we next utilized TRPV6-W321A for assessing the NP/TRPV6 interaction. By co-IP assays we found that either mutation R470A or W593A, which removes the intramolecular L/C interaction within TRPV6-W321A, almost abolishes the NP/TRPV6 (N/C) interaction (Fig. 2-4H), indicating that the L/C interaction is required for the maintenance of the N/C interaction. Similarly, we utilized TRPV6-R470A for the assessment of the LP/TRPV6 interaction. In contrast, none of the W321A and I597A mutations, which disrupts the N/C interaction within TRPV6-R470A, affected the LP/TRPV6 (L/C) interaction (Fig. 2-4I), indicating that the N/C

interaction is not required for the L/C interaction. Thus, it seems that the N/C interaction is downstream of the L/C interaction in a regulatory relay in TRPV6.

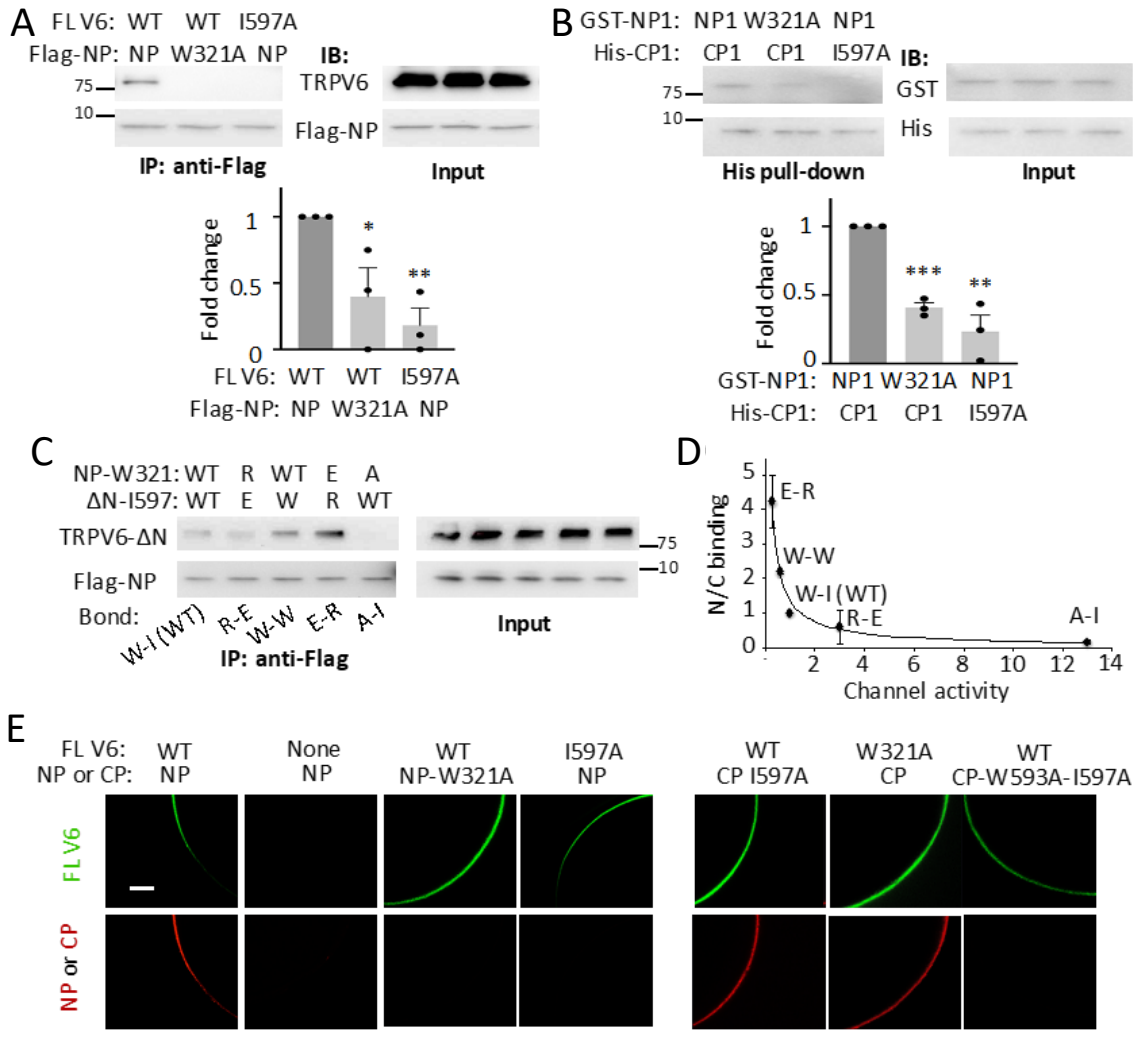
A
FLV6: WT WT I597A
Flag-NP: NP W321A NP
IB:
TRPV6
Flag-NP
IP: anti-Flag
Input
Fold change
FLV6: WT WT I597A
Flag-NP: NP W321A NP
B
GST-NP1: NP1 W321A NP1
His-CP1: CP1 CP1 I597A
IB:
GST
His
His pull-down
Input
Fold change
GST-NP1: NP1 W321A NP1
His-CP1: CP1 CP1 I597A
C
NP-W321: WT R WT E A
ΔN-I597: WT E W R WT
TRPV6-ΔN
Flag-NP
Bond:
W-I (WT)
R-E
W-W
E-R
A-I
IP: anti-Flag
Input
D
N/C binding
E-R
W-W
W-I (WT)
R-E
A-I
Channel activity
E
FL V6: WT None WT I597A WT W321A WT
NP or CP: NP NP NP-W321A NP CP I597A CP CP-W593A-I597A
FLV6
NP or CP

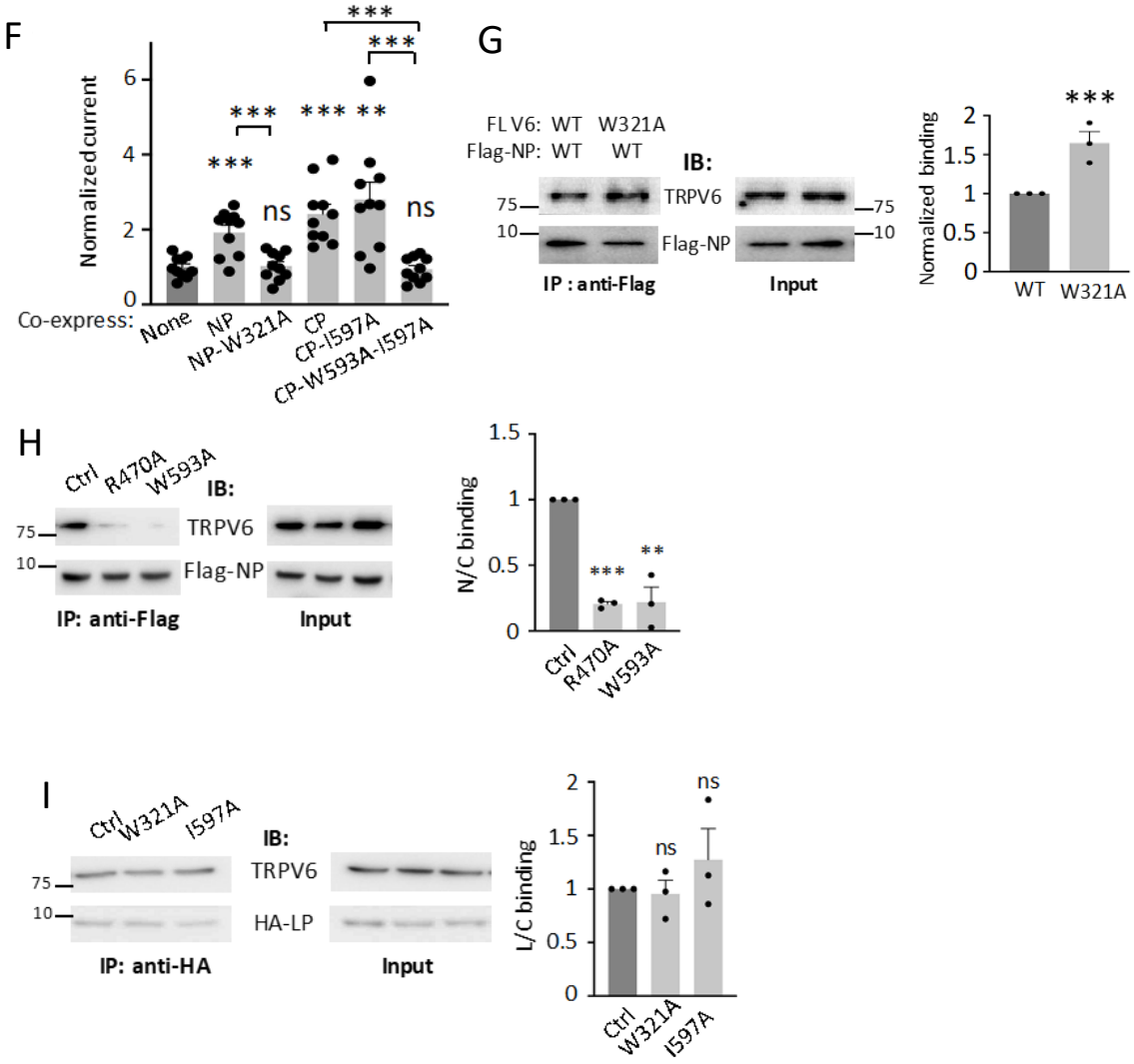
F
Normalized current
Co-express:
None
NP
NP-W321A
CP
CP-I597A
CP-W593A-I597A
ns
G
FLV6: WT W321A
Flag-NP: WT WT
IB:
TRPV6
Flag-NP
IP : anti-Flag
Input
Normalized binding
WT W321A
H
Ctrl
R470A
W593A
IP: anti-Flag
N/C binding
I
Ctrl
W321A
I597A
IP: anti-HA
HA-LP
L/C binding

Figure 2-4. Roles of the W321:I597 pair in the N/C interaction, colocalization and Channel function of TRPV6 and dependence between the N/C and L/C interaction. **A.** Upper panel: representative co-IP data from oocytes co-expressing full length (FL) TRPV6 and Flag-tagged TRPV6 NP with or without a mutation, as indicated. Lower panel: data from three independent co-IP experiments were quantified, normalized, and averaged. By Student's t-test, comparison with dark grey group. **B.** Upper panel: representative data from His pull-down showing binding between purified GST-tagged human TRPV6 N-terminal peptide (GST-NP1) and His-tagged human TRPV6 C-terminal peptide (His-CP1), with or without an indicated mutation. Lower panel: data from three independent *in vitro* binding experiments were quantified, normalized, and averaged. **C.** Representative co-IP data obtained using Flag-NP to precipitate TRPV6-ΔN, carrying an indicated mutation at 321 and 597, respectively. **D.** Inverse correlation between normalized binding strength (y) and normalized Ca-induced steady-state current (x). Data from three independent experiments as in the panel C were quantified, normalized and averaged. Curve represents the best fit using the inverse function $y = a/x$, with $a = 1.06$ and correlation coefficient $R = 0.97$. **E.** Representative co-IF images from oocytes expressing FL TRPV6 or a peptide, with or without mutation. Scale bar, 50 μm. **F.** Representative Ca-induced currents at -50 mV from oocytes expressing FL TRPV6 with or without indicated peptide. Data were normalized and averaged from 10-11 oocytes from three batches. $^{**}p < 0.01$ and $^{***}p < 0.001$, by Student's t-test. **G.** Left panel: Representative co-IP data showing the effect of mutation W321A within the TRPV6 pre-S1 domain on the NP/TRPV6 interaction. Right panel: statistical data after quantification and normalization from three independent experiments. $^{***}p < 0.001$, by Student's t-test. Data are presented as mean ± SEM. **H.** Left panel: representative co-IP data accessing the N/C interaction obtained using oocytes expressing Flag-tagged NP and FL TRPV6-W321A (Ctrl) carrying mutation R510A or W593A, as indicated. Right panel: data from three independent experiments as in the upper panel were quantified, normalized and averaged. **I.** Left panel: representative co-IP data assessing the L/C interaction obtained from oocytes expressing HA-LP and FL TRPV6-R470A (Ctrl) carrying mutation W321A or I597A, as indicated. Right panel: data from three independent experiments as in the left panel were quantified, normalized and averaged.

Rescue of Trpv5/6 knockdown-derived defects in zebrafish by TRPV6 activated mutant

We next examined potential rescue effect of human TRPV6 activated mutant W593A *in vivo* in zebrafish. A zebrafish homologue Trpv5/6 loss-of-function mutant R304X was previously found to result in loss of notochord tip ossification, a defective bone formation (Vanoevelen et al., 2011). We mimicked this condition through knocking down Trpv5/6 using CRISPR-Cas9 technique and confirmed by sequencing (Fig. 2-5A). A significant 77% reduction in Trpv5/6 mRNA expression was found in CRISPR-Cas9 injected embryos (Fig. 2-5B). Using Alizarin red S staining we found that larval fish at 7 days post-fertilization (dpf) with Trpv5/6 knockdown exhibits much increased likelihood of developing loss of ossification at the notochord tip (Fig. 2-5B). We then examined the effect of human TRPV6 activated mutant W593A on fish bone formation through mRNA co-injection into embryos. While 10 pg W593A mutant mRNA significantly rescued the bone abnormality 10 and 30 pg WT TRPV6 mRNA had no rescuing effect, respectively (Fig. 2-5C), indicating that mutant W593A acts as an activated (or gain-of-function) mutant *in vivo* in zebrafish.

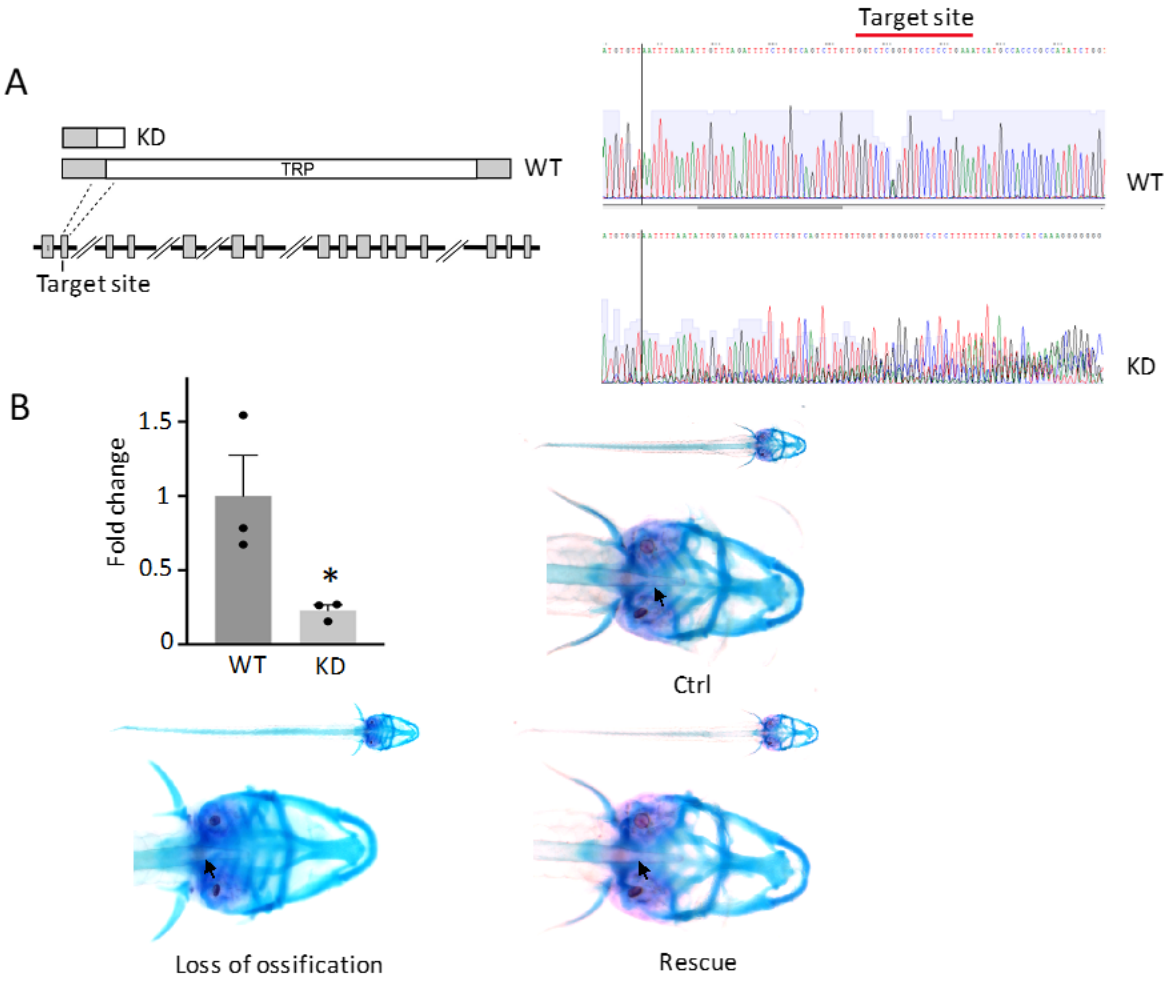
A
KD
TRP
WT
Target site
Target site
WT
KD
B
Fold change
1.5
1
0.5
0
*
WT
KD
Ctrl
Loss of ossification
Rescue

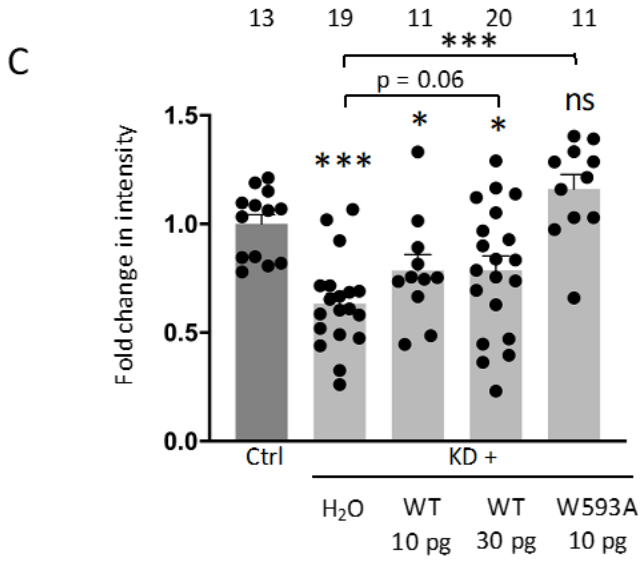
C
13
19
11
20
11
***
p = 0.06
ns
*
*
***
Fold change in intensity
1.5
1.0
0.5
0.0
Ctrl
KD +
H2O
WT
10 pg
WT
30 pg
W593A
10 pg

Figure 2-5. Rescue effect of TRPV6 activated mutant W593A on Trpv5/6 knockdown-induced bone abnormality in zebrafish. A. Left panel: schematic representation of the Trpv5/6 gene/protein domain architecture and CRISPR target site. The gene loci are shown with coding exons (grey boxes) and introns (solid black lines), with large introns not drawn to scale. The position of the CRISPR target site sequences at the beginning of exon 2 in Trpv5/6 is indicated and the predicted truncated proteins in the mutant lines are drawn above. Right panel: sequencing of WT and Trpv5/6 mutant fish at 3 dpf. Red lines indicate CRISPR target sites. **B.** Upper left panel: Trpv5/6 mRNA was detected by Q-PCR. The total RNA isolated from 5 dpf WT or Trpv5/6 mutant embryos (>10 embryos/sample) from three batches. Representative images of 7 dpf zebrafish embryos with cartilage (red) and bone (blue) staining. The notochord tip is indicated by an arrow. "Loss of ossification" was from an embryo injected with Trpv5/6 sgRNA and water while "rescue" was from an embryo co-injected with sgRNA and 10 pg of human TRPV6 W593A mutant mRNA. Ctrl, from a WT embryo. **C.** Fold change in the intensity in zebrafish notochord tip from indicated groups. Data were averaged from 11-18 embryos from three independent experiments. Ctrl, control zebrafish; KD, CRISPR-Cas9 injected Trpv5/6 knockdown zebrafish.

Characterization of the PIP2/TRPV6 binding

PIP2 was previously reported to up-regulate, and is required for, TRPV6 channel function (Thyagarajan et al., 2008; Zakharian et al., 2011). However, the mechanism of regulation and the PIP2 binding sites in TRPV6 are not well understood (Hughes et al., 2018). We examined the PIP2/TRPV6 binding by lipid dot blot assays using lysates of TRPV6-expressing oocytes, *E. coli* purified GST-NP1 and His-CP1, and PIP2 antibody for detection. We found that water-soluble PIP2 analogue diC_8-PIP2 binds to TRPV6 and CP1 but not NP1 (Fig. 2-6A). Because PIP2 was known to bind with cationic residues in other TRP channels (Nilius et al., 2008), we neutralized all cationic residues in the S2-S3 linker, inner S5 helix and CP1 by glutamine substitution to test their involvement in PIP2 binding. We found that K484Q, R589Q and R632Q, but not the other mutations, decrease the channel activity compared to WT TRPV6 (Fig. 2-6B-D). We and other groups have previously employed PIP2 monoclonal antibodies to precipitate TRP and other channels (Zheng et al., 2018a; Hamilton et al., 2014; Huang et al., 2013; Huang et al., 1998). By a similar approach we found that each of the K484Q, R589Q and R632Q mutations but not the R628Q mutation (Ctrl) abolishes the PIP2/TRPV6 interaction (Fig. 2-6E), consistent with the functional data (Fig. 2-6B). We also found that the W321A or W593A mutation has no effect on the PIP2/TRPV6 binding (Fig. 2-F), which further indicates that the two residues are not part of the PIP2 binding pocket. Further, we found that diC_8-PIP2, injected into oocytes by a third electrode, increases Ca-induced steady-state currents by nearly 13 folds in oocytes expressing WT TRPV6 but only by 2.3-4.2 folds in those expressing one of the three mutants (Fig. 2-6G). Consistently, we found that these three mutants are more sensitive to PIP2 depletion by wortmannin than WT channel and that neutralization of all the three residues abolishes the channel function (Fig. 2-6H and I). While according to the structural data, R632 locates in distal

C-terminus being away from inner cell membrane and may not directly bind to PIP2. These data together showed that K484, R589 and R632 may be involved in PIP2 binding.

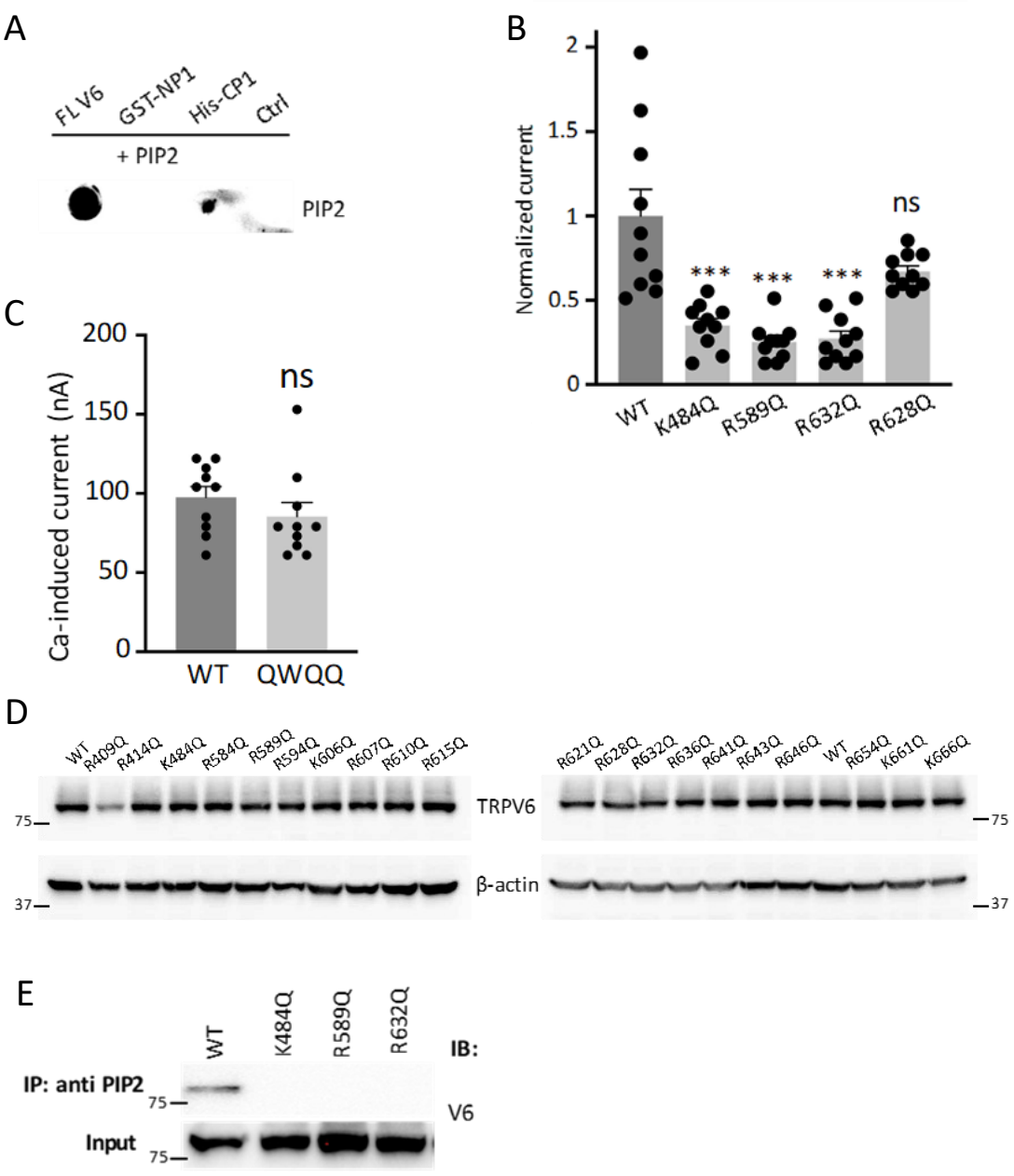
A
FL V6
GST-NP1
His-CP1
Ctrl
+ PIP2
PIP2
B
Normalized current
2
1.5
1
0.5
0
***
***
***
ns
WT
K484Q
R589Q
R632Q
R628Q
C
Ca-induced current (nA)
200
150
100
50
0
ns
WT
QWQQ
D
WT
R409Q
R414Q
K484Q
R584Q
R589Q
R594Q
K606Q
R607Q
R610Q
R615Q
R621Q
R628Q
R632Q
R636Q
R641Q
R643Q
R646Q
WT
R654Q
K661Q
K666Q
75
TRPV6
75
37
β-actin
37
E
WT
K484Q
R589Q
R632Q
IB:
IP: anti PIP2
75
V6
Input
75

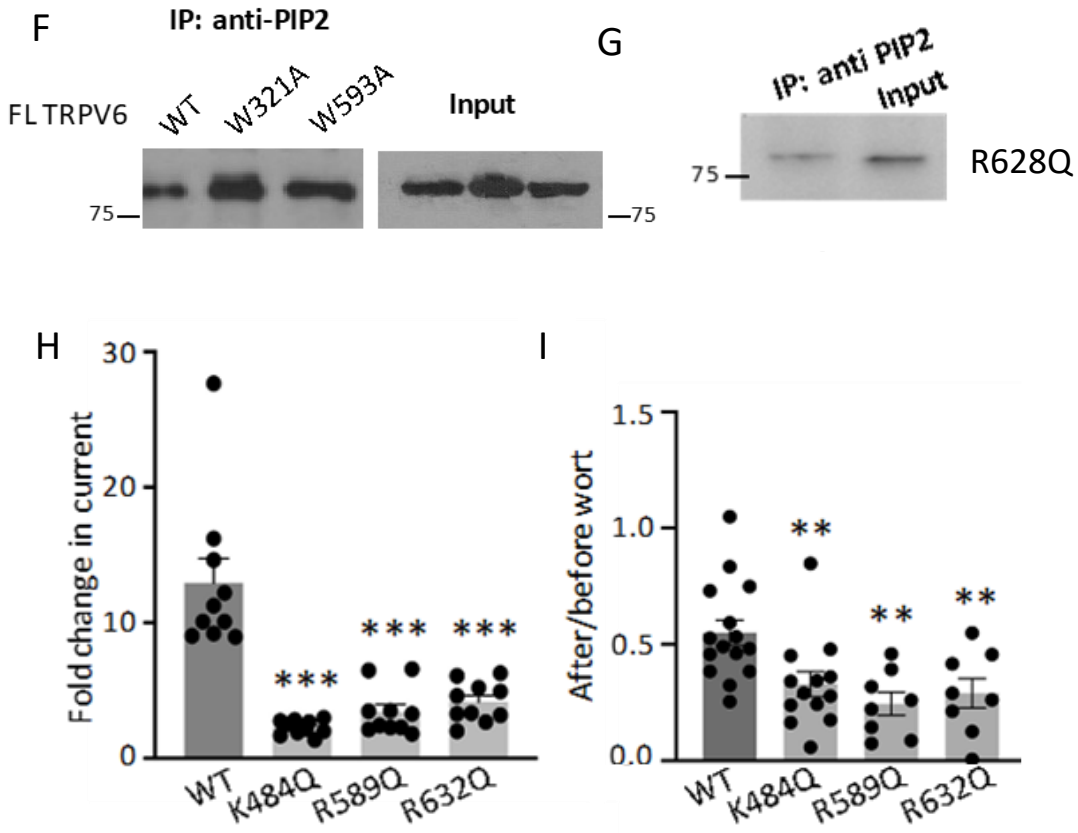

Figure 2-6. Characterization of the physical and functional PIP2/TRPV6 interaction. A. Representative dot-blot data obtained using diC$_8$-PIP2 with lysates of oocytes expressing FL TRPV6, GST-NP1, His-CP1 or None (Ctrl). **B.** Normalized Ca-induced currents obtained at -50 mV from oocytes expressing WT or a mutant TRPV6. Residues R409 and R414 are in the S2-S3 linker, K484 in the inner S5 helix and the others within CP1. Data were normalized and averaged from 10 oocytes from three batches. **C.** Ca-induced currents obtained from oocytes expressing WT or triple mutant QWQQ TRPV6. Currents were averaged from 10 oocytes (three batches). Data are presented as mean ± SEM. **D.** Representative WB data showing the oocyte expression of WT and neutralized (glutamine substituted) mutants used for function measurements (as in B). **E.** Representative co-IP data obtained from expressing oocytes showing the effect of mutations on the PIP2/TRPV6 interaction. **F.** Representative co-IP data obtained using expressing oocytes, showing the effect of mutation W321A or W593A on the PIP2/TRPV6 binding. **G.** Representative co-IP data obtained using oocytes showing the interaction between PIP2 and TRPV6 mutant R628Q. **H.** Effects of mutations on the activation of TRPV6 by diC$_8$-PIP2,

assessed by Ca-activated currents obtained from expressing oocytes. Fold change was calculated before and 10 min after injection of 25 nl of diC_8-PIP2 (5 mM) by a third electrode (see Methods), for an estimated final intracellular diC_8-PIP2 concentration of 0.25 mM. Injection of 25 nl of water was carried out as control and had no significant effect on the channel activity. Shown data were averaged from N = 10 oocytes from three batches. **I.** Ratios of monovalent currents from oocytes expressing WT or an indicated mutant after and before wortmannin treatment.

Modulation of TRPV6 intramolecular interactions by PIP2

Although the L/C and N/C interaction sites are not part of the PIP2 binding site, we wondered whether the PIP2 regulates TRPV6 channel function through altering the L/C or N/C interaction indirectly. We found by co-IP assays that addition of diC_8-PIP2, but not lipid phosphatidic acid (as control), into lysates of oocytes co-expressing TRPV6 and LP (or NP) reduces (or abolishes) the LP/TRPV6 (or NP/TRPV6) interaction (Fig.2-7A and B). In contrast, diC_8-PIP2 did not alter either interaction in the presence of triple mutation K484Q/R589Q/R632Q (referred to as TRPV6-3Q) or even single mutation K484Q and R589Q (Fig. 2-7C-F). These data indicated that PIP2 disrupts the two autoinhibitory L/C and N/C interactions through binding to TRPV6 protein thereby activating the channel. We also examined whether any of the four activated mutants R470A, W593A, W321A and I597A that correspond to the four residues mediating the L/C or N/C interaction has altered sensitivity to PIP2 regulation. We utilized membrane permeable wortmannin, a PI4K inhibitor, to block PIP2 synthesis thereby depleting the endogenous PIP2 (Downing et al., 1996). Distinct from WT TRPV6, none of the four mutants was inhibited by wortmannin (Fig. 2-7G), consistent with the conclusion that PIP2 activates TRPV6 through disrupting the L/C or N/C interaction. As expected, when both interactions were disrupted by alanine substitution, the resulting activated double mutant W321A-W593A was no longer inhibited by PIP2 depletion (Fig. 2-7G). However, we should keep in mind that the functional change in the double mutation might also be due to other structural changes that affect interaction with PIP2.

Taken together, our study suggested that PIP2 binds to cationic residues in the inner S5 helix and C-terminus of TRPV6, which disrupts the R470:W593-mediated L/C and W321:I597-mediated N/C interactions thereby activating the channel.

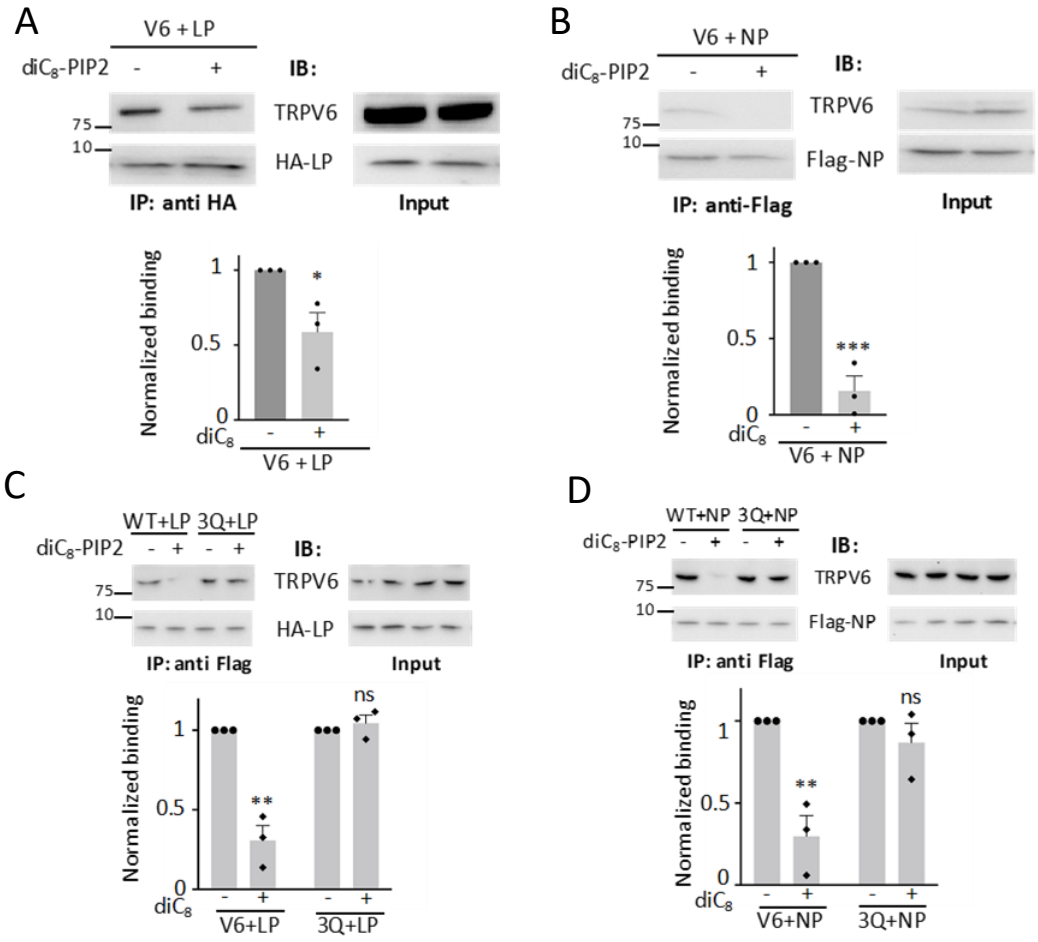
A
V6 + LP
diC8-PIP2 - +
IB:
75
10
TRPV6
HA-LP
IP: anti HA
Input
Normalized binding
1
0.5
0
*
diC8 - +
V6 + LP
B
V6 + NP
diC8-PIP2 - +
IB:
75
10
TRPV6
Flag-NP
IP: anti-Flag
Input
Normalized binding
1
0.5
0
***
diC8 - +
V6 + NP
C
WT+LP 3Q+LP
diC8-PIP2 - + - +
IB:
75
10
TRPV6
HA-LP
IP: anti Flag
Input
Normalized binding
1
0.5
0
**
ns
diC8 - + - +
V6+LP
3Q+LP
D
WT+NP 3Q+NP
diC8-PIP2 - + - +
IB:
75
10
TRPV6
Flag-NP
IP: anti Flag
Input
Normalized binding
1
0.5
0
**
ns
diC8 - + - +
V6+NP
3Q+NP

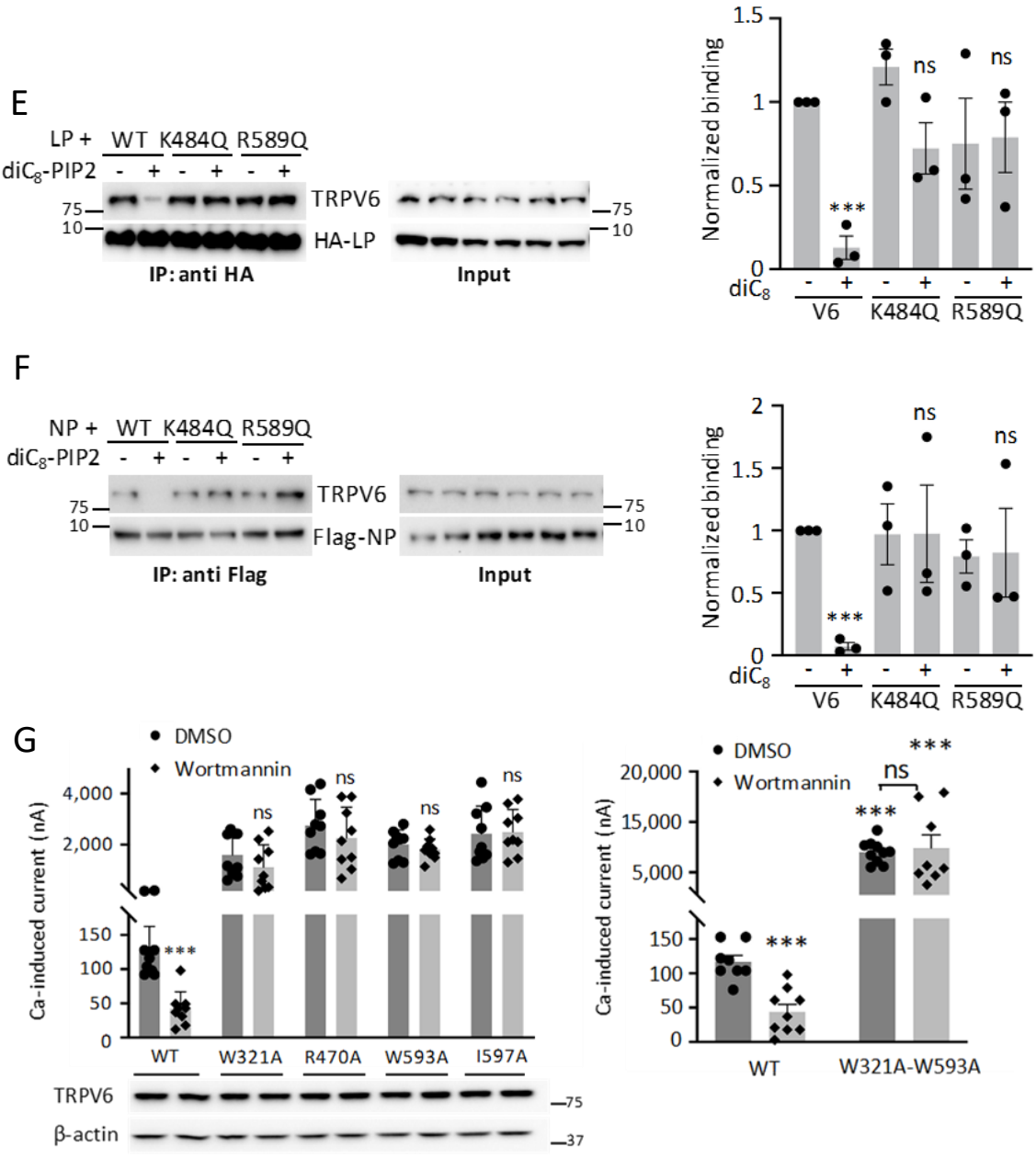

Figure 2-7. Regulation of the TRPV6 L/C and N/C interactions by PIP2. **A.** Upper panel: representative co-IP data showing the effect of PIP2 on HA-LP/FL TRPV6 interaction. Lower panel: statistical data from three independent experiments as in upper panel after quantification and normalization. **B.** Upper panel: representative co-IP data showing the effect of PIP2 on the Flag-NP/TRPV6 interaction. Lower panel: data from three independent experiments as in upper panel were quantified, normalized, and averaged. **C.** Upper panel: representative co-IP data

showing the effect of PIP2 on the interaction of HA-LP with WT TRPV6 or triple mutant K484Q/R589Q/R632Q (3Q). Lower panel: statistical data from three independent experiments as in upper panel after quantification and normalization. **D.** Upper panel: representative co-IP data showing the effect of PIP2 on the NP/TRPV6 interaction with or without 3Q mutation. Lower panel: data averaged from three independent experiments as in upper panel after quantification and normalization. **E.** Left panel: representative co-IP data showing the effect of PIP2 on the interaction of HA-LP with WT TRPV6 or single mutant K484Q or R589Q. Right panel: statistical data from three independent experiments as in the left panel after quantification and normalization. ***$p < 0.001$, by Student's t-test. **F.** Left panel: representative co-IP data showing the effect of PIP2 on the NP/TRPV6 interaction in the presence of a Q mutation. Right panel: data averaged from three independent experiments as in the upper panel after quantification and normalization. ***$p < 0.001$, by Student's t-test. Data are presented as mean ± SEM. **G.** Left upper panel: averaged Ca-induced currents obtained at -50 mV from expressing oocytes pre-incubated with wortmannin (10 μM) or DMSO (control) for 1 hr prior to measurements. Currents were averaged from 9-10 oocytes from three batches. Left lower panel: representative WB data obtained from oocytes after the wortmannin or DMSO treatment, as in the upper panel. Right panel: averaged Ca-induced steady-state currents obtained from expressing oocytes. Shown representative data were averaged from 5-6 oocytes from one of the three independent experiments.

2.5 DISCUSSION

The structure of TRPV6 has recently been resolved at high resolution by X-ray crystallography and cryo-EM, which revealed physical proximity between different domains such as S4-S5 linker/TRP helix, pre-S1/TRP helices and S4/S5 transmembrane helices (McGoldrick et al., 2018; Saotome et al., 2016). However, functional validation of potential physical interactions in this region has not been previously done. PIP2 activates TRPV6, but it is unclear where it binds in TRPV6 and how it affects the protein conformation (Thyagarajan et al., 2008; Zakharian et al., 2011). In the present study, we have characterized the physical interaction between the S4-S5 linker and TRP helix (L/C interaction), and between the pre-S1 and TRP helices (N/C interaction) and showed that disruption of the L/C or N/C interaction, by mutations at binding sites or blocking peptides, results in substantial activation of channel function, indicating that these intramolecular interactions present under basal conditions are autoinhibitory (Fig. 2-8). We found that the L/C and N/C interactions are not independent of each other, with the L/C binding as a requirement for the N/C binding, but the reverse. We also identified three cationic residues in TRPV6 involved in PIP2 binding and showed that the PIP2/TRPV6 binding represses the L/C and N/C association thereby suppressing the autoinhibition and activating the channel. Taken together, our study revealed a relay 'PIP2-L/C-N/C' in TRPV6 that mediates the regulation of the channel.

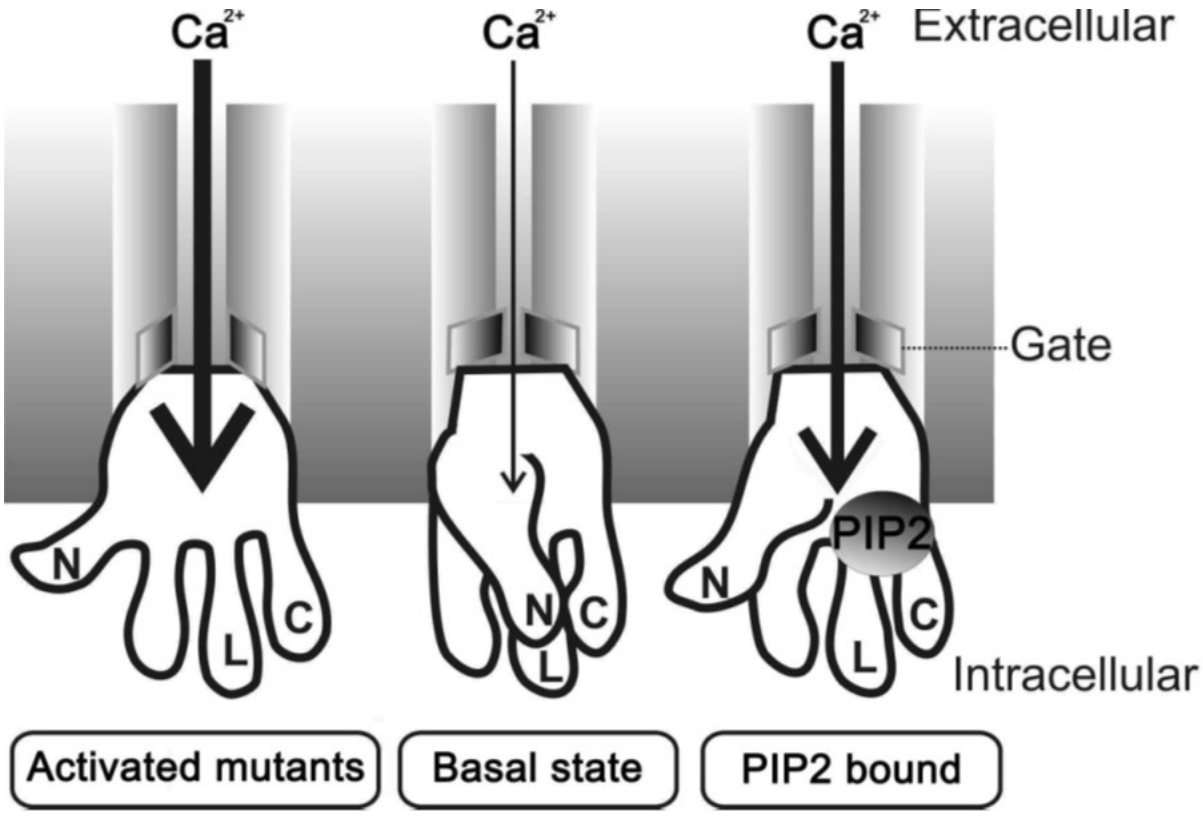

Figure 2-8. Schematic model illustrating the mechanism of TRPV6 activation-autoinhibition. For simplicity, only the intracellular pre-S1 helix (N), S4-S5 linker (L) and TRP helix (C) of one TRPV6 monomer are shown. The gate (or lower gate) is indicated. At the basal state, the autoinhibitory interactions among N, L and C maintain the channel at basal activity and prevent channel activation while an activating mutation or PIP2 binding disrupts the interactions thereby activating the channel.

We previously reported the functional importance of a conserved glycine residue in the S4-S5 linker of TRPV6, -C4 and -C5 (Hofmann et al., 2017; Beck et al., 2013). Functional importance of linker residues L596 of TRPV4, E571 of TRPV1 and K856 of TRPM8 have also been reported (Teng et al., 2015; Yang et al., 2015; Voets et al., 2007). Recently resolved Cryo-EM structures of TRPV2-cannabidiol complex revealed that the S4-S5 linker plays important roles in TRPV2 channel gating and activation induced by cannabidiol binding (Pumroy et al., 2019). The high-resolution cryo-EM structure of rat TRPV1, the first one in the TRP superfamily, displays close proximity of the S4-S5 linker and pre-S1 with TRP (or TRP-like) helix (Liao et al., 2013), an architectural arrangement now known to be shared by several other TRPs (Paulsen et al., 2015; Grieben et al., 2017; Saotome et al., 2016). However, it remains to be determined whether there is physical interaction between them and what are the functional consequences of breaking down the assembly. In rat TRPV1, the S4-S5 linker was suggested to interact with the TRP helix through the F559:W697 pair forming a hydrogen bonding between the indole ring of W697 and the main-chain carbonyl oxygen of F559 (Liao et al., 2013). While this has yet to be verified it is noted that the TRPV1 W697 corresponds to the functionally important W593 in human TRPV6 (Fig. 2-1A). Homology modeling proposed that hydrogen bonding mediated by the corresponding pair, the main-chain carbonyl oxygen of L596 and the indole ring of W733 in TRPV4, maintains a closed conformation (Teng et al., 2015). Indeed, both mutants L596P and W733R were found to be activated mutants, with increased open probability. However, this L596:W733 pairing was not seen in subsequently resolved TRPV4 crystal and cryo-EM structures (Deng et al., 2018). For TRPV6, the S4-S5 linker was not resolved in the crystal structure initially (Saotome et al., 2016). Subsequent structural studies by cryo-EM resolved the linker configuration and showed that the oxygen backbone of R470 is only

2.6 Å away from the indole ring of W593 (McGoldrick et al., 2018), consistent with our current finding of the R470:W593-mediated L/C interaction. Interestingly, we found that the channel activity of mutant R470F is comparable to WT channel (Fig. 2-1F), while R470A is an activated mutant (Fig. 2-1B and C). These data are inconsistent with the formation of hydrogen bonding at R470:W593, as suggested based on TRPV6 structure (McGoldrick et al., 2018), because of the invariable oxygen backbone in residues R, F and A, but support the presence of a F470:W593 (presumably π-π) bonding in mutant R470F and a R470:W593 (presumably cation-π) bonding in WT channel and the absence of an A470:W593 bonding. Of note, structural data suggested an alternative hypothesis that R470 interacts with lipids to stabilize the closed conformation of TRPV6 through unclear mechanisms (McGoldrick et al., 2018). We propose that lipid binding to R470 may competitively weaken the R470-W593 interaction, which opens the channel. Accordingly, the R470A mutation would mimic an extreme condition of lipid-TRPV6 binding, which couldn't be achieved physiologically, with total loss of the R470-W593 interaction, and acts as a gain-of-function mutation (Fig. 2-1C). Thus, it seems that a flexible S4-S5 linker may reflect a dynamic R470-W593 interaction (i.e., functional regulation) in response to upstream signaling such as binding of PIP2 and other ligands to TRPV6.

A salt bridge between K425 (pre-S1) and E709 (TRP helix) of rat TRPV1 was proposed based on cryo-EM structure (Liao et al., 2013). Molecular dynamics simulations on TRPV4 suggested the presence of pre-S1 to TRP helix interaction through a salt bridge formed by the corresponding K462:E745 pair (Garcia-Elias et al., 2015). However, mutation E745A that disrupts the putative bonding only had a moderate effect on protein folding, with undetermined roles of the two residues in the channel function. Thus, whether the K:E pair in TRPV1 and -V4 actually mediates the N/C binding and what is its functional role have yet to be determined. We

recently characterized the functionally critical N/C interaction in TRPP3, -P2, -M8, -V1 and -C4 that is mediated by a conserved residue W in pre-S1 and the last (cationic) residue K(R) in the W(Y)xxxK(R) (x indicates any amino acid) motif of their TRP (or TRP-like) helix, presumably by forming π-cation W:K(R) bonding (Zheng et al., 2018a), rather than a salt bridge based on a distance of 3.7 Å and 3.2 Å between the pre-S1 and TRP helices in TRPV1 and -V4, respectively, revealed from structures (Liao et al., 2013). In fact, the W residue in pre-S1 is conserved in all mammalian TRP members except TRPML (with residue F), while the K(R) residue in the W(Y)xxxK(R) motif is shared by the majority of the TRP members except TRPV4-V6, with the residue I(V) in the corresponding WxxxI(V) motif of TRPV6 and -V5. Thus, the mechanism of the W:I-mediated N/C interaction in TRPV6 discovered in the present study can be broadly interpreted as being shared by the W:K(R)-mediated N/C interaction in those other TRP channels (Zheng et al., 2018a). Reversely, it would be interesting to determine in future studies whether the TRPV6 L/C interaction is also shared by other TRP channels.

However, the TRPV6 N/C as well as L/C interaction is autoinhibitory, which is opposite to the N/C interaction of TRPP3/P2/V1/M8/C4 channels in that disruption of the N/C interaction in these channels results in loss of channel function (Zheng et al., 2018a). Also, the W321:I597 pair distance of 3.7 Å (McGoldrick et al., 2018) indicates the presence of weak van der Waals bonding, which would account for the detectable basal channel activity of WT TRPV6 (with W:I bonding), substantially activated activity with broken bonding (eg A:I), and inhibited activity in the presence of stronger π-π bonding (W:W) or salt bridge (E:R) (Fig. 2-3). This is further supported by the fact that the channel activity was inversely correlated with the 321:597 bonding strength (Fig. 2-4C and D).

While both the L/C and N/C interactions are functionally autoinhibitory, they are not independent of each other. In fact, our co-IP experiments showed that the L/C binding is required for the N/C binding but not reversely (Fig. 2-4H and I), which infers that the likelihood of the L/C binding would be higher than that of the N/C binding but not reversely. Indeed, LP/CP1 binding band was more intense than the NP1/CP1 band (i.e., L/C binding is more likely than the N/C binding) (Fig. 2-9). Disruption of either L/C or N/C binding in TRPV6 leads to channel activation, which is consistent with the activation of TRPV4 by mutation W733R (Teng et al., 2015), but is opposite in TRPP3/-P2/-V1/-M8/-C4 in which disrupting the N/C binding resulted in loss of function (Zheng et al., 2018a). In summary, the L/C and N/C interaction in TRPV6 play an autoinhibitory role in the prevention from channel activation; loss of either interaction by mutations (at endogenous levels of PIP2) or increased PIP2 suppresses the autoinhibition thereby activating the channel.

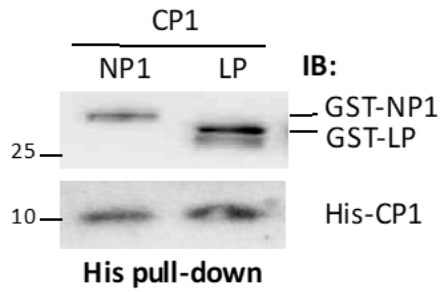

Figure 2-9. L/C and N/C binding assessed by pull-down assays. Representative data obtained from a His pull-down assay, showing the LP/CP1 and NP1/CP1 binding. GST-tagged pre-S1-containing human TRPV6 N-terminal peptide NP1 (GST-NP1), S4-S5 linker-containing peptide (GST-LP), and His-tagged TRPV6 C-terminal peptide CP (His-CP1) were expressed in and purified from *E. coli.*

PIP2 has been found to positively or negatively regulate most TRP channels. By electrophysiology with cultured cells PIP2 was shown to directly activate TRPV6 (Thyagarajan et al., 2009; Zakharian et al., 2011; Cao et al., 2013), which is consistent with our results (Fig. 2-6). Being negatively charged, PIP2 is known to bind with cationic residues in the C-terminus of several TRP channels including TRPC4, -C6, -V1, -V5, -M4, -M5 and -M8 (Nilius et al., 2008). Cationic residues involved in PIP2 binding have also been identified in the S4-S5 linker of TRPV1 (Poblete et al., 2015). In contrast, although surface plasmon resonance analysis suggested the presence of PIP2-binding cationic residues in the C-terminus of TRPM1 and -M4 so far this has not directly been shown by other methods (Bousova et al., 2015; Jirku et al., 2015). We recently found that a C-terminal cationic residue-rich domain ($_{594}$RLRLRK$_{599}$) and a conserved K residue in the TRP-like helix of TRPP3 form part of the PIP2 binding cassette (Zheng et al., 2018a). The specific PIP2 binding sites in TRPV6, however, have so far not been well characterized and PIP2 even failed to fit into the human TRPV6 cryo-EM structure and surrounding lipid (McGoldrick et al., 2018). A rabbit TRPV5 structure by cryo-EM revealed the involvement of the N-terminal R302, K484 in the S5 helix and C-terminal R584 (corresponding to R302, K484 and R584 of human TRPV6) in the PIP2/TRPV5 binding (Hughes et al., 2018). None of the R302Q and K484Q mutations in TRPV5 affected the function, although they increased sensitivity to wortmannin (Hughes et al., 2018); in contrast, the K484Q mutation in TRPV6 significantly reduced currents carried by monovalent cations (Hughes et al., 2018), supporting its involvement in PIP2 binding. The involvement of K484, but not R584, in the PIP2 binding is in fact consistent with our functional data on TRPV6 (Fig. 2-6). The inconsistency on the two other residues might be due to differences in the sequences (~70% amino acid identity with TRPV5) and experimental conditions. Our current study showed that K484 in the inner S5

and R589 and R632 in the C-terminus are involved in the PIP2 binding. Of note, according to TRPV6 structural data (McGoldrick et al., 2018) residue R632 in the distal C-terminus is far away from the inner cell surface. Thus, the role of R632 in PIP2 binding may be indirect and requires further studies. Proximity of R589 to W593 and I597, and of K484 to R470 may have facilitated regulation of TRPV6 by PIP2 through disrupting the R470:W593-mediated L/C interaction, and thereby for the N/C interaction as well (Fig. 2-4H). This is supported by our observation that PIP2 had no effect on the L/C or N/C interaction in mutant TRPV6-3Q lacking the PIP2 binding. Thus, TRPV6 shares with other TRPs (Zheng et al., 2018a) in terms of regulation by PIP2 in that PIP2 blocks the N/C interaction through which it modulates the channel function.

TRPV6 cryo-EM structures suggested that a salt bridge between Q473 and R589 in the S4-S5 linker and TRP helix, respectively, is present in an open conformation and that disruption of the interaction leads to channel closure (McGoldrick et al., 2018). In contrast, we found that R589 is involved in PIP2 binding and is thus critical for PIP2-induced channel activation (Fig. 2-6), whereas mutant Q473A has similar channel function as WT TRPV6 (Fig. 2-10), which does not support the presence of a Q473:R589 salt bridge under our conditions. This discrepancy may be due to differences in the experimental condition (cryo-EM vs oocyte) and thus in the protein conformation (Shoemaker and Ando, 2018). In basal conditions where PIP2 is low, TRP helix would be in firm association with the S4-S5 linker and pre-S1 helix, making the adjacent S6 stay in an α-helix configuration. When cellular PIP2 is elevated, the PIP2/TRPV6 binding results in disrupted or weakened L/C and N/C interaction, presumably leading to S6 helix to undergo α- to π-helix transition to activate the channel, similar to that of TRPV3 (Yin et al., 2018). In contrast, the S6 helix of TRPP2 undergoes an opposite, π- to α-helix, transition to activate the channels

(Zheng et al., 2018c). However, all these TRP channels together seem to broadly share a common mechanism of channel activation, i.e., when the intramolecular N/C (and L/C) binding is suppressed in TRPV6 (or increased in other TRPs), which forces the TRP helix to be in a conformation that renders the adjacent S6 helix to be in a π-helix (or α-helix in other TRPs) configuration to allow activation.

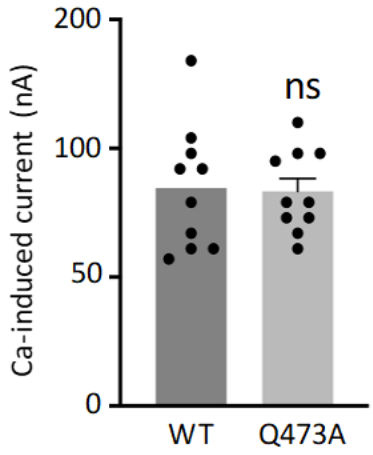

Figure 2-10. Effect of Q473A mutation on TRPV6 function. Ca-induced currents obtained from oocytes expressing WT or Q473A mutant TRPV6. Currents were averaged from 10 oocytes (three batches). Data are presented as mean ± SEM.

In summary, our present study characterized the autoinhibitory TRPV6 intramolecular L/C and N/C interactions presumably mediated by cation-π and van der Waals bonding, respectively. PIP2 directly binds to cationic residues in TRPV6 and suppresses the L/C and N/C interactions thereby activating TRPV6. Therefore, the 'PIP2-L/C-N/C' relay in TRPV6 represents a novel molecular switch that mediates the regulation of TRPV6 channel under physiological conditions.

CHAPTER 3

RESULTS #2

Modulation of TRPP3 by calmodulin through Ca2+/calmodulin -dependent protein kinase II phosphorylation

3.1 ABSTRACT

Transient receptor potential (TRP) polycystin-3 (TRPP3) is a non-selective cation channel activated by Ca^{2+} and protons and is involved in regulating ciliary Ca^{2+} concentration, hedgehog signaling and sour tasting. The molecular mechanisms underlying the Ca^{2+}-induced TRPP3 activation and ensuing inactivation remains poorly understood. Here we investigated regulation of TRPP3 by calmodulin (CaM) by means of electrophysiology and *Xenopus* oocytes as an expression model. We found that TRPP3 channel function is enhanced by calmidazolium, a CaM antagonist, and inhibited by CaM through binding of the CaM N-lobe to a TRPP3 C-terminal domain not overlapped with the EF-hand. We further identified that CaM interaction promoting phosphorylation at T591 by Ca^{2+}/CaM-dependent protein kinase II is a main mechanism of inhibition of TRPP3.

3.2 INTRODUCTION

TRP channels are a large family comprising six mammalian subfamilies: TRPC (canonical), TRPM (melastatin), TRPML (mucolipin), TRPP (polycystin), TRPV (vanilloid) and TRPA (ankyrin). They respond to a variety of stimuli, ranging from temperature, natural chemicals, pH, to mechanical force (Vangeel and Voets, 2019). TRPP3, also called polycystic kidney disease (PKD) protein 2 like 1 (PKD2L1), was first identified in 1998 (Nomura et al., 1998). Although mutations in TRPP2 (or PKD2) and PKD protein 1 (PKD1) account for around 15% and 80%, respectively, of human autosomal dominant PKD (ADPKD) (Pei, 2003), TRPP3 is unlikely involved in the disease. Despite the wide tissue distribution of TRPP3, including heart, skeletal muscle, brain, spleen, testis, retina, and liver (Nomura et al., 1998; Wu et al., 1998), the detailed physiological roles in these organs have not been well documented. TRPP3 has been reported to form a heterotetrametric channel with PKD protein 1 like 1 (PKD1L1) and 3 (PKD1L3) (Huque et al., 2009). The TRPP3-PKD1L1 complexing was reported to control Ca^{2+} concentration in primary cilia through a Ca^{2+}-dependent hedgehog signaling pathway, which seems to be developmentally important (Delling et al., 2013; DeCaen et al., 2013). For TRPP3 itself, studies have implied that it's involved in the regulation of fluid homeostasis (Shimizu et al., 2009). TRPP3 regulates body fluid homeostasis and heart function during pathological cardiac hypertrophy (Lu et al., 2018). TRPP3 in cerebrospinal fluid-contacting neurons is important for the maintenance of natural curvature of the spine (Sternberg et al., 2018).

CaM is a ubiquitous Ca^{2+}-binding protein with four EF-hand motifs forming two globular lobes (N- and C-lobes). Ca^{2+} binds to each lobe and triggers a structural rearrangement that changes the affinity of CaM binding to other target proteins such as voltage-gated Na+, K+ channels (Gabelli et al., 2016; Wen and Levitan, 2002), cyclic nucleotide-gated channels

(Trudeau and Zagotta, 2002), and TRP channels (Mercado et al., 2010). A growing body of reports have demonstrated the involvement of CaM in the functional regulation of several TRP channels (Hasan and Zhang, 2018), possibly through a shared mechanism. CaM antagonist calmidazolium (CMZ) was reported to activate TRPP3 but with an unclear mechanism (DeCaen et al., 2013; Park et al., 2018).

In the present study, we examined how CaM regulates TRPP3 channel function by two-electrode voltage clamp (TEVC) electrophysiology in *Xenopus* oocytes. We characterized the interaction between CaM and TRPP3 by means of co-immunoprecipitation (co-IP) and in vitro pull-down and examined the interplay among CaM, membrane-anchored phosphatidylinositol 4,5-bisphosphate (PIP2) and CaMK2 with respect to the regulation of TRPP3.

3.3 METHODS

Plasmids, reagents and antibodies

Flag-tagged human TRPP3 cDNA was subcloned into *Xenopus* oocytes expression vector pCHGF (Yang et al., 2012). WT CaM and mutant plasmids were obtained from Dr. Veit Flocerzi's lab and subcloned into PGEMHE for oocytes expression. WT CaMK2 and mutant plasmids were kindly provided by Dr. Khaled Machaca (Weill Cornell Medicine, NY). Q5 High-Fidelity 2X Master Mix from New England Biolabs (Ottawa, ON, Canada) was used to generate all mutations, which were verified by sequencing. Antibodies against β-actin, GST, His, HA and Flag were purchased from Santa Cruz Biotechnology (Santa Cruz, CA). The antibody against CaM was purchased from Cell Signaling Technology (Whitby, ON, Canada). The antibody against CaMK2 was purchased from Abcam (Cambridge, MA). Secondary antibodies were purchased from GE healthcare (Waukesha, WI). NFA, CMZ, KN93 and AIP were purchased from Sigma-Aldrich (St. Louis, MO). and diC8-PIP2 was from Echelon Biosciences (Salt Lake City, UT). For the drug application,

List of mutants used in this chapter

TRPP3
ΔN
ΔC
R594Q/R596Q/R598Q/R599Q
S581A
S581E
T591A
T591E
S603A
S603E

L593A
CaM
D21A/D57A (CaM_{12})
D94A/D130A (CaM_{34})
D21A/D57A D94A/D130A (CaM_{1234})
CaMK2
K42M
T286D

***Xenopus* oocyte expression**

Capped RNAs encoding human TRPP3, CaM, CaMK2 or their mutants were synthesized by an in vitro transcription T7 mMESSAGE mMACHINE kit (Invitrogen, Waltham, MA) and injected into oocytes (25-50 ng each) prepared as described (Cai et al., 2020). Same amount of water was injected to the oocytes served as control. Oocytes were incubated at 18℃ for 2-3 days before electrophysiological measurements. The present study was under the approvement of the Ethical Committee for Animal Experiments of the University of Alberta and performed in accordance with the Guidelines for Research with Experimental Animals of the University of Alberta and the Guide for the Care and Use of Laboratory Animals (NIH Guide) revised in 1996.

Two-electrode voltage clamp

The two-electrode voltage clamp electrophysiology experiments were performed as we described previously (Zheng et al., 2018a). Briefly, the electrodes (Capillary pipettes, Warner Instruments, Hamden, CT) that impaled an oocyte were filled with 3 M KCl to form a tip resistance of 0.3-2 MΩ. Duration of application of extracellular Ca^{2+}, CMZ (in DMSO) was

indicated in time course recordings. For other chemical applications, oocytes were incubated with 10 μM AIP or 10 μM KN93 for 30 mins to evaluate the effect of corresponding chemicals. before the recording. Unless described otherwise, measurements were performed when an oocyte was voltage clamped and held at -50 mV. Whole-cell currents and membrane potentials were recorded and analyzed using a Geneclamp 500B amplifier and Digidata 1322A AD/DA converter (Molecular Devices, Union City, CA) together with the pClamp 9 software (Axon Instruments, Union City, CA). Current and voltage signals were digitized at 200 μs/sample and filtered at 2 kHz through a Bessel filter. SigmaPlot 13 (Systat Software, San Jose, CA) and GraphPad Prism 8 (GraphPad Software, San Diego, CA) were used for data plotting.

Surface protein biotinylation

Xenopus oocytes after 3-times washing with ice-cold PBS solution were incubated with 0.5 mg/ml sulfo-NHS-SS-Biotin (Pierce, Rockford, IL) for 30 min at room temperature. Non-reacted biotin was quenched by 1 M NH_4Cl. Oocytes were then washed with ice-cold PBS solution and harvested in ice-cold CelLytic M lysis buffer (Sigma-Aldrich) supplemented with proteinase inhibitor cocktail (Thermo Scientific, Waltham, MA). Upon addition of 100 μl streptavidin (Pierce), lysates were incubated at 4℃ overnight with gentle shaking. The surface protein bound to streptavidin was resuspended in SDS loading buffer and subjected to SDS-PAGE.

Co-IP and *in vitro* pull-down

Co-IP experiments were performed as we described previously (Zheng et al., 2018a). Briefly, a group of 20-30 oocytes washed with PBS for three times. They were solubilized in ice-cold CelLytic-M lysis buffer (Sigma) supplemented with proteinase inhibitor cocktail.

Supernatants were collected after centrifugation at 13,200 rpm for 15 min and precleaned for 1 h with 50% protein G-Sepharose (GE Healthcare). The cell lysates were incubated with indicated antibodies at 4℃ for 4 h. Upon the addition of 100 µl of 50% protein G-Sepharose, the mixure was incubated at 4℃ overnight with gentle shaking. The immune complexes conjugated to protein G-Sepharose were washed five times with cold PBS solution containing 1% Nonidet P-40 and eluted by SDS loading buffer. Precipitated proteins were subjected to Western blot analysis.

GST- or His-tagged human TRPP3 peptides or CaM were purified from *E. coli* and solubilized in the CelLytic-M lysis buffer and incubated at the same amount (2 µg each) at 4℃ for 4 h with gentle shaking, followed by overnight incubation after addition of 50 µl Glutathione Sepharose 4B agarose beads (GE healthcare). The beads were then washed three times with PBS buffer with 1% Nonidet P-40, and the remaining proteins were eluted using SDS loading buffer and resolved by by Western blot analysis.

Statistical analysis

All statistical data in this study are represented as mean ± SEM (standard error of the mean) from N measurements. Student t tests were used to compare two groups of data; One-way ANOVA was used to compare multiple groups. *, ** and *** indicate $p < 0.05$, 0.01 and 0.001, respectively; ns indicates statistically not significant.

3.4 RESULTS

CMZ activates TRPP3 in *Xenopus* oocytes

We first used TEVC electrophysiology and verified that the channel activity of TRPP3 expressed in *Xenopus* oocytes is enhanced by CMZ, an inhibitor of CaM (Fig. 3-1A and B). The TRPP3 channel activity at -50 mV was assessed by the current elicited by 5 mM Ca^{2+} in the Na-containing bath solution that included 10 nm. 2-[(4-methoxynaphthalen-2-yl) amino]-5-nitrobenzoic acid (MONNA) to inhibit currents mediated by endogenous Cl channels activated by Ca^{2+} entry, similarly as we did previously (Wang et al., 2019). The stimulation effect of CMZ was also observed in other membrane potentials using a voltage ramp protocol (Fig. 3-1C). We next attempted to evaluate whether CMZ alters TRPP3 activation and inactivation kinetics. We measured the half-rise and half-decay times as parameters characterizing the time courses of Ca^{2+} induced activation and inactivation, respectively. We found that CMZ only enhances the current amplitude but does not affect the time courses of activation and inactivation (Fig. 3-1D). Of note, the basal TRPP3 channel activity, assessed by the difference of current between Na-containing solution and one that contains non-permeant NMDG, both in the absence of Ca^{2+}, was also enhanced by CMZ (Fig. 3-1 E, F and G). This CMZ-induced stimulation of the basal TRPP3 function is comparable to what was reported for TRPP3 expressed in human embryonic kidney (HEK) cells (DeCaen et al., 2013) (Park et al., 2018). Our data suggested possible involvement of CaM as a TRPP3 inhibitor.

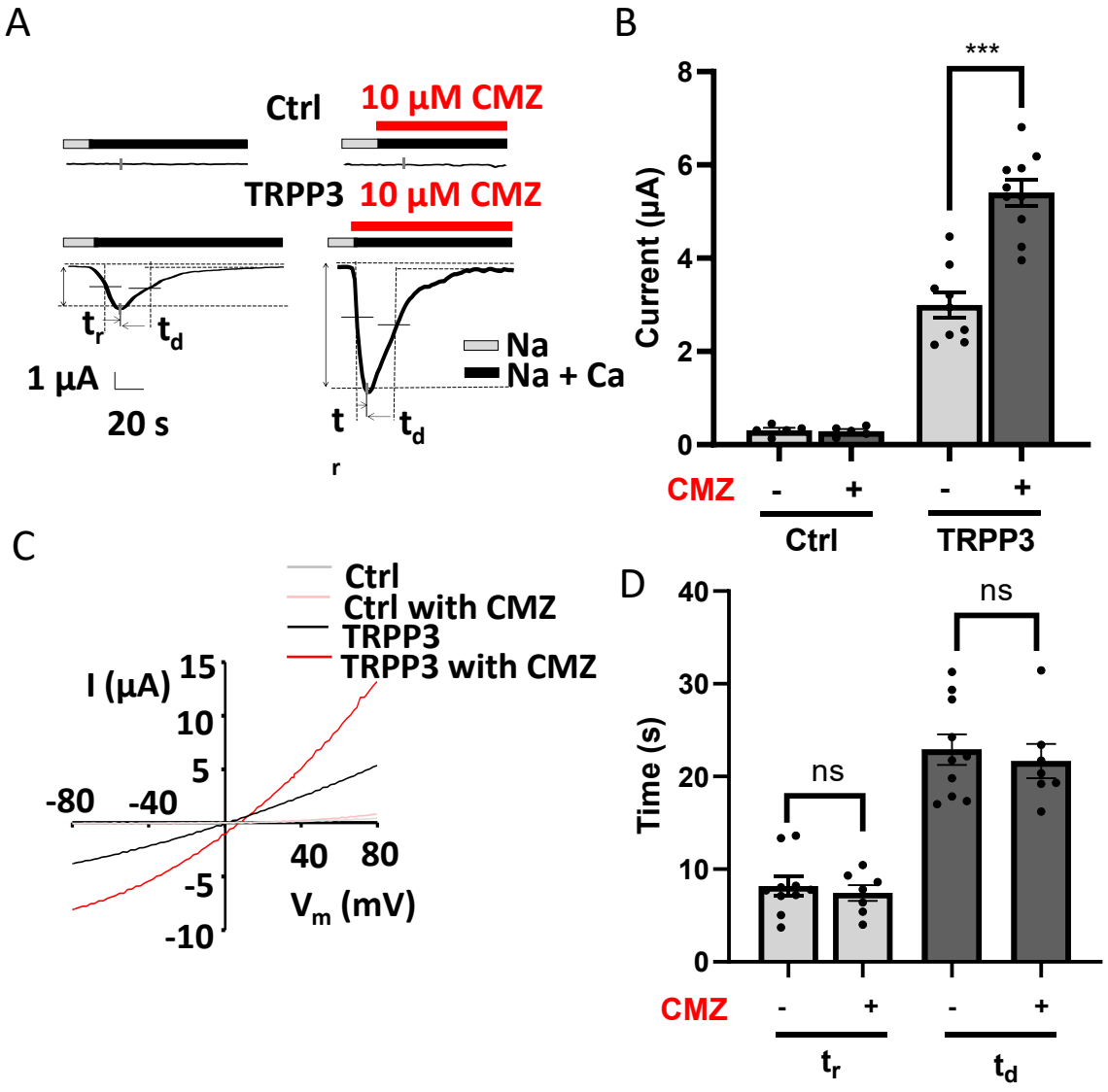
A
Ctrl
10 µM CMZ
TRPP3
10 µM CMZ
t_r
t_d
1 µA
20 s
Na
Na + Ca
B
Current (µA)
***
CMZ
Ctrl
TRPP3
C
Ctrl
Ctrl with CMZ
TRPP3
TRPP3 with CMZ
I (µA)
V_m (mV)
D
Time (s)
ns
ns
CMZ
t_r
t_d

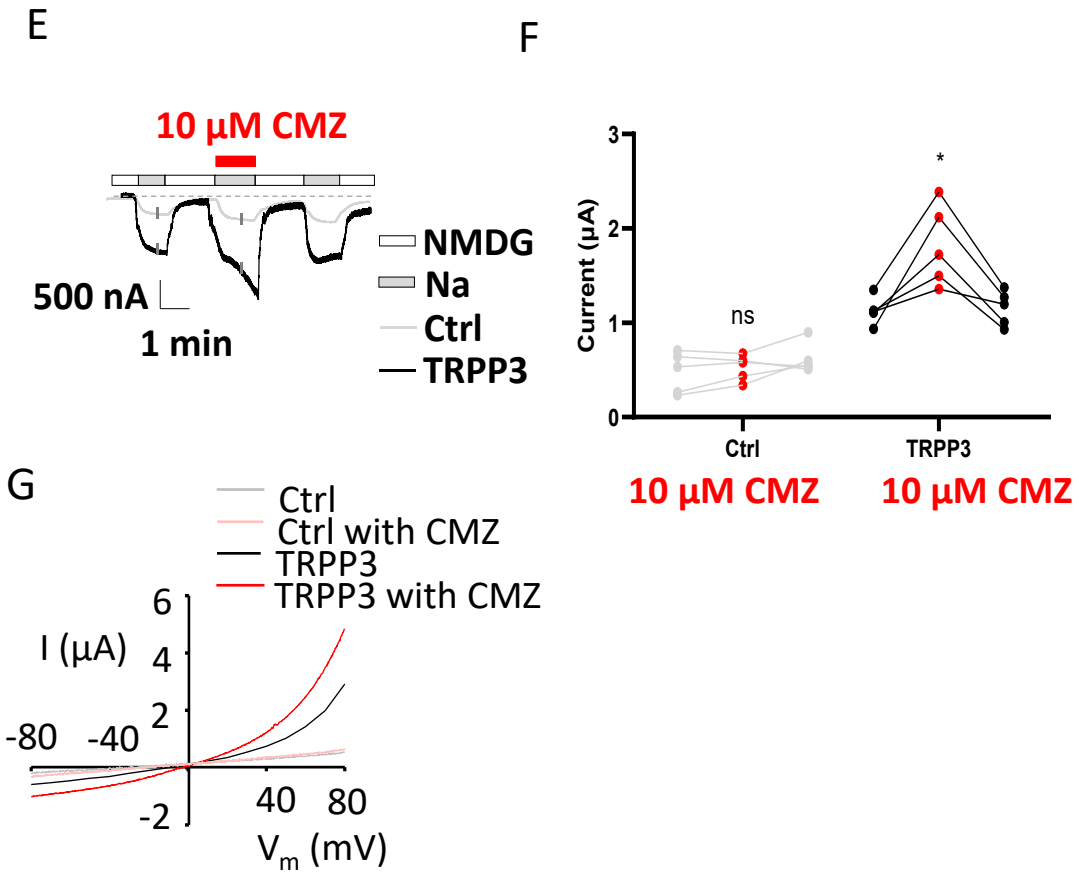

Figure 3-1. Roles of CMZ on TRPP3 channel function. A. Representative whole-cell current traces obtained from the water-injected (Ctrl) oocyte and the oocyte expressing human TRPP3. Oocytes were clamped at -50 mV and perfused with Na containing solution (Na) (in mM) (100 NaCl, 2 KCl, 1 $MgCl_2$, and 10 HEPES, pH 7.5) or added with 5 mM $CaCl_2$ (Na+Ca), in the presence of 10 µM MONNA throughout. TRPP3 channel activity was measured as Ca^{2+} induced peak current (Na + Ca) (e.g., current at ''Na+Ca'' - current at ''Na''), indicated by the double-arrowed line (Chen et al., 1999). The half-rising time (t_r) and half-decay time (t_d) obtained from each inward current time course following Ca^{2+} induced activation was defined. 10 µM CMZ was applied as the red bar showed. **B.** Averaged Ca^{2+} induced currents from Ctrl and TRPP3 expressing oocytes. ***$p < 0.001$. **C.** Representative I–V curves from Ctrl and TRPP3 expressing oocytes obtained at current points indicated by the vertical bars in the traces in A. **D.** Averaged t_r and t_d from TRPP3 expressing oocytes with or without CMZ. **E.** Representative

whole-cell current traces recorded by TEVC at −50 mV from a Ctrl oocyte and an oocyte expressing human TRPP3. Oocytes were perfused by extracellular solution containing *N*-methyl-D-glucamine (NMDG)-Cl (replacing NaCl to NMDG) (NMDG) or Na containing solution (Na). 10 μM CMZ was applied as the red bar showed. Current values were determined from dashed lines (baselines) to the plateau currents. **F.** Averaged Na currents from Ctrl and TRPP3 expressing oocytes. *$p < 0.05$. **G.** Representative I–V curves from Ctrl oocyte and TRPP3 expressing oocyte obtained at current points indicated by the vertical bars in the traces in E.

CaM inhibits TRPP3 through physical association

We next tested whether CaM indeed regulates the TRPP3 channel function. By co-expressing TRPP3 and CaM in oocytes, we found that CaM substantially decreases both the basal and Ca^{2+}-activated currents (Fig. 3-2A). To figure out whether CaM inhibited the TRPP3 channel function or decreased the TRPP3 surface membrane expression, we performed biotinylation assays and found that CaM does not have significant effect on the surface expression (Fig. 3-2B), indicating that CaM inhibits TRPP3. These data also indicated that CMZ increases the TRPP3 channel activity through inhibiting CaM. Given that CaM interacts with different channels to regulate the channel function, we next wanted to investigate whether CaM inhibits TRPP3 through physical association, as it regulates other ion channels by this manner (Saimi and Kung, 2002). For this, we performed co-IP assays using Flag-TRPP3 and HA-CaM for expression in oocytes and found that they are indeed in the same complex (Fig. 3-2C). We also carried out *in vitro* pull-down assays using CaM-coated agarose beads to incubate with lysates of TRPP3-expressing oocytes at different concentrations of Ca^{2+}. We found that the TRPP3/CaM interaction is Ca^{2+}-dependent (Fig. 3-2D). Besides, the TRPP3/CaM interaction was inhibited by CMZ (Fig. 3-2E), further supporting that CMZ activates TRPP3 through antagonizing CaM.

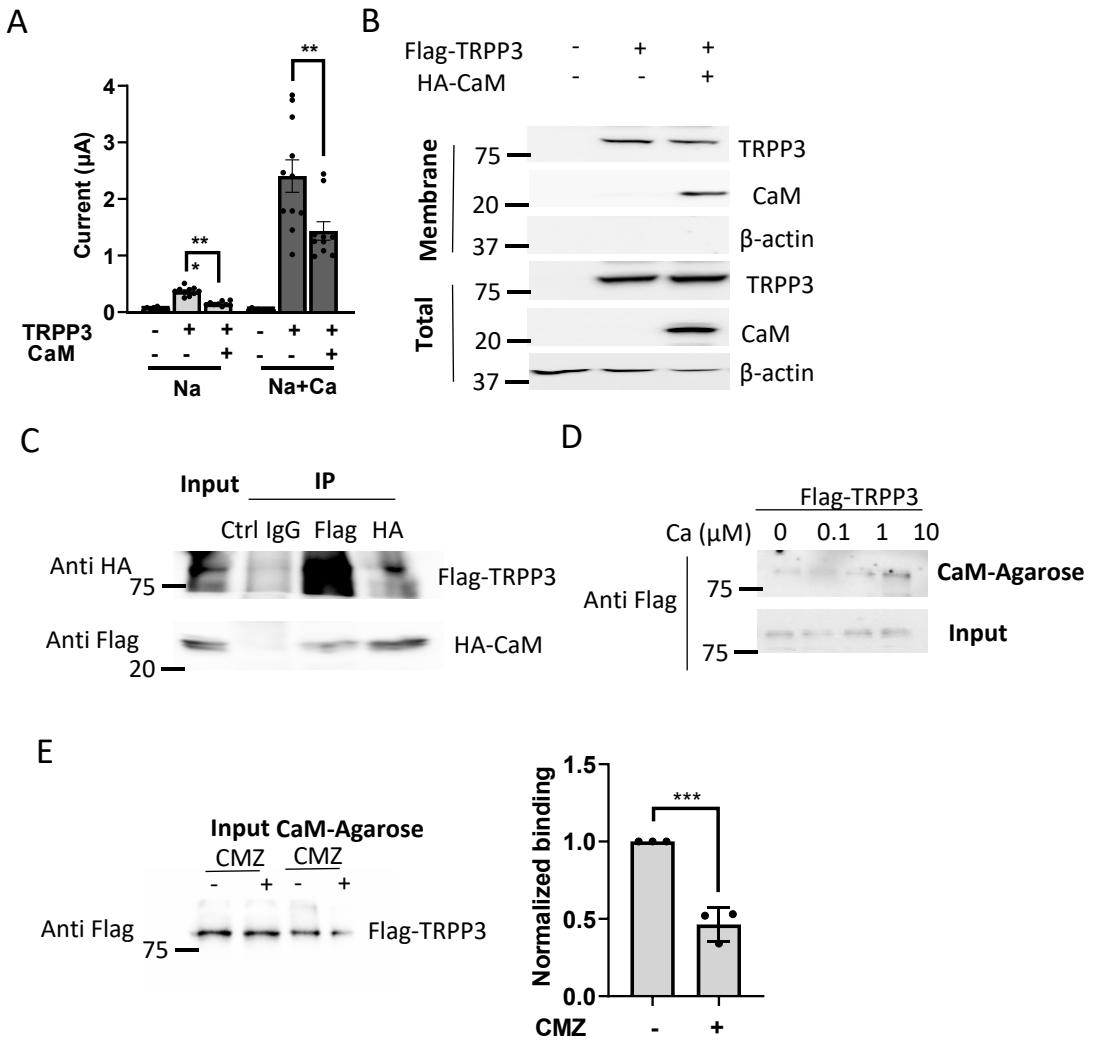

Figure 3-2. Roles of CaM on TRPP3 channel function and physical interaction between TRPP3 and CaM. A. Averaged currents of TRPP3 expressing oocytes and TRPP3-CaM co-expressing oocytes. Oocytes were from three batches. **p <0.01; ***p < 0.001; by One-way ANOVA with Holm-Sidak's correction. **B.** Representative surface and total expression of TRPP3 and CaM by biotinylation, with β-actin as the loading control. **C.** Representative co-IP data showing TRPP3 and CaM are in the same complex from one of the three independent experiments. **D.** Binding experiment performed in the presence of different buffered calcium concentration. **E.** Left panel: binding experiment between TRPP3 expressing oocytes lysates and CaM-agarose with or without CMZ. Right panel: data from three independent experiments in left panel were quantified, averaged, and normalized. ***p < 0.001.

The TRPP3/CaM binding is mediated by the CaM N-lobe and the E566-F621 fragment of the TRPP3 C-terminus

As a versatile Ca^{2+} sensor, CaM is capable of regulating various processes through Ca^{2+} binding at its two different lobes (Chin and Means, 2000).To further elucidate the functional significance of the Ca^{2+}-dependent TRPP3/CaM interaction we altered Ca^{2+} binding in CaM by mutations, with CaM_{12}, CaM_{34} and CaM_{1234} indicating CaM mutants in which D-to-A mutation was introduced to the Ca^{2+}-binding sites in the N-lobe, C-lobe and both lobes, respectively. We found that each of CaM and CaM_{34}, but not CaM_{12} or CaM_{1234}, are able to inhibit the TRPP3 channel function (Fig. 3-3A), while none of these mutants altered the plasma membrane expression of TRPP3 (Fig. 3-3B). These data indicated that Ca^{2+} binding to the CaM N-lobe, but not the C-lobe, is critical for its regulation of TRPP3 and supported the concept that the two lobes can work independently (Stefan et al., 2008). We further found that the N-lobe, but not the C-lobe, is important for the TRPP3/CaM binding. (Fig. 3-3C). Taken together, the data indicated that the N-lobe of CaM mediates its binding with and functional regulation of TRPP3.

We next wanted to identify the CaM-binding domain (CaMBD) in TRPP3. CaMBDs in several TRP channels were located in the N- or C-terminus and were mostly hydrophobic alpha helices (Gordon-Shaag et al., 2008). It was predicted that the CaM-binding site is located in the TRPP3 C-terminus (Park et al., 2019). But there have so far been no experimental data to support this. We therefore generated TRPP3 truncation mutants with deletion of the N-terminus (named P3*Δ*N) or C-terminus (named P3*Δ*C) and tested their interaction with CaM by pull-down assays using CaM-coated agarose beads. We found that mutant P3*Δ*N but not P3*Δ*C shows similar strength of binding with CaM as WT TRPP3 (Fig. 3-3D), indicating the CaM-binding site is located in the C-terminus. We also performed *in vitro* pull-down experiments to further

document the TRPP3/CaM interaction. For this, we constructed glutathione S-transferase (GST)-tagged CaM and His-tagged C-terminal peptide I560-K660 (His-P3CP) and purified from *E. coli* expression. By using GST and GST-tagged TRPP3 N-terminal peptide M1-L95 (GST-P3NP) as the negative and positive control, respectively (Zheng et al., 2018a), we confirmed that His-P3CP directly binds with GST-CaM (Fig. 3-3E). We next wanted to examine whether the EF-hand motif (H633-E668) within P3CP plays a role in the interaction with CaM. The EF-hand motif in the C-terminus of other channels were reported to mediate binding with CaM (Ben Johny et al., 2013). We found that, compared with WT TRPP3, truncation mutant T622X that lacks most of the C-terminus including the EF-hand motif has similar CaM-binding strength as revealed by co-IP and pull-down experiments (Fig. 3-3F and G). Further, CaM had similar inhibitory effect on the WT and mutant TRPP3 T622X (Fig. 3-3H), indicating EF-hand is not likely involved in CaM regulation. Taken together, these data indicate that the TRPP3 C-terminal fragment E566-F621 is a CaM-binding domain.

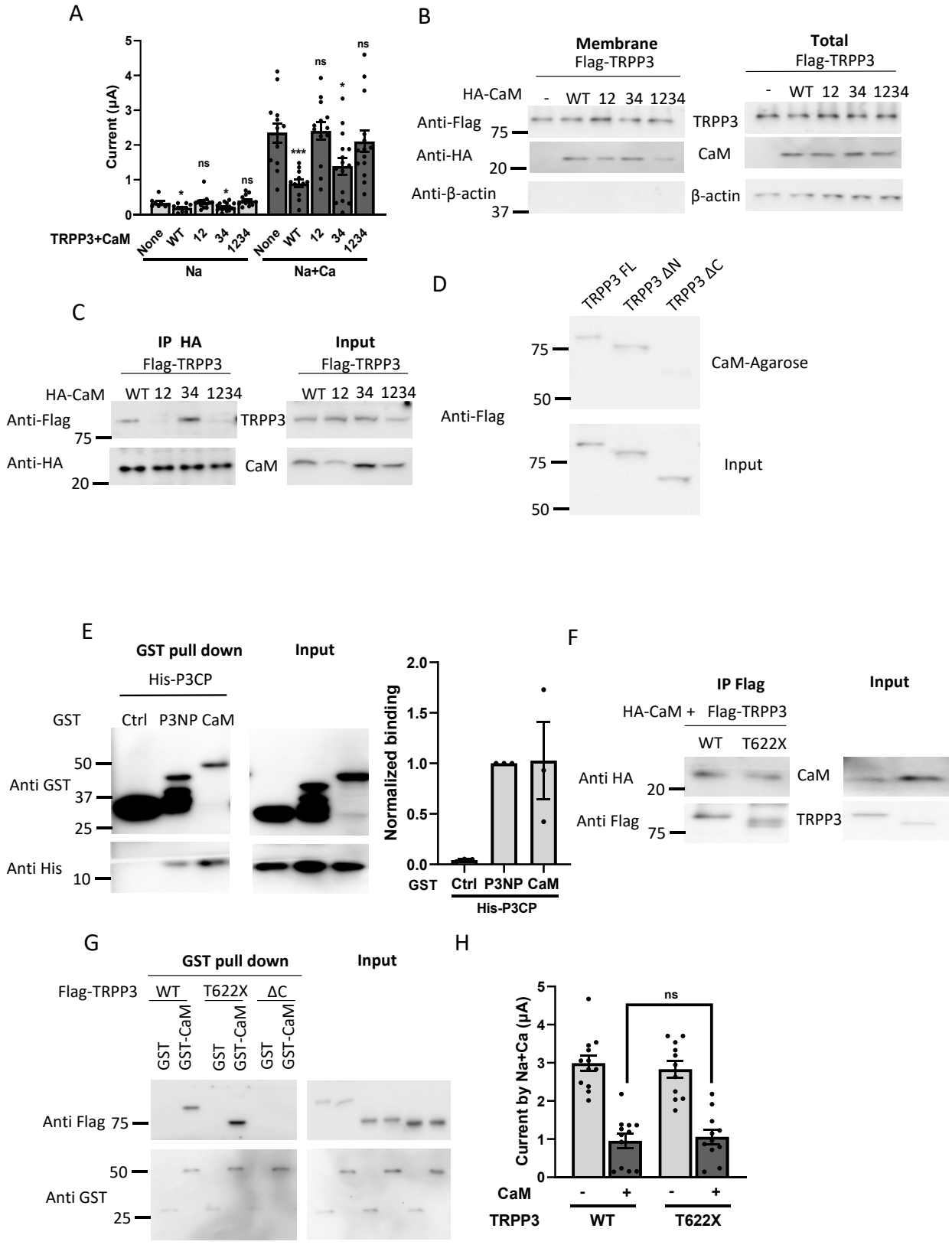
A
Current (μA)
TRPP3+CaM
None WT 12 34 1234 None WT 12 34 1234
Na
Na+Ca
B
Membrane
Flag-TRPP3
Total
Flag-TRPP3
HA-CaM - WT 12 34 1234
Anti-Flag
Anti-HA
Anti-β-actin
TRPP3
CaM
β-actin
C
IP HA
Flag-TRPP3
Input
Flag-TRPP3
HA-CaM WT 12 34 1234
Anti-Flag
Anti-HA
TRPP3
CaM
D
TRPP3 FL
TRPP3 ΔN
TRPP3 ΔC
CaM-Agarose
Anti-Flag
Input
E
GST pull down
His-P3CP
Input
GST Ctrl P3NP CaM
Anti GST
Anti His
Normalized binding
GST Ctrl P3NP CaM
His-P3CP
F
IP Flag
Input
HA-CaM + Flag-TRPP3
WT T622X
Anti HA
Anti Flag
CaM
TRPP3
G
GST pull down
Input
Flag-TRPP3 WT T622X ΔC
GST GST-CaM GST GST-CaM GST GST-CaM
Anti Flag
Anti GST
H
Current by Na+Ca (μA)
ns
CaM - + - +
TRPP3 WT T622X

Figure 3-3. Interaction between CaM and TRPP3 C-terminus. A. Averaged currents of TRPP3 expressing oocytes and different TRPP3-CaM mutants co-expressing oocytes. Oocytes were from three batches. *p <0.05, ns: not significant. **B.** Representative surface and total expression of TRPP3 and different forms of CaM by biotinylation, with β-actin as the loading control from one of the three independent experiments. **C.** Representative co-IP data showing the interaction between TRPP3 and different mutant forms of CaM from one of the three independent experiments. **D.** Representative binding experiment showing the interaction between CaM and TRPP3 full length, N-terminal truncation, C-terminal truncation from one of the three independent experiments. **E.** Left panel: Representative binding experiment showing the direct interaction between GST-tagged CaM and His-tagged TRPP3 C-terminal peptide (His-CP; I560-K660). Purified GST and GST-tagged TRPP3 N terminus (GST-P3N; M1-L95) served as negative and positive control, respectively. Right panel: Data from three independent experiments in left panel were quantified, averaged, and normalized. **F.** Representative co-IP data showing the interaction between CaM and WT TRPP3 or mutant T622X. **G.** Representative GST pull-down data showing the interaction between CaM and WT TRPP3 or mutant T622X with TRPP3 *Δ*C acting as the negative control from one of the three independent experiments. **H.** Averaged currents of WT TRPP3 and mutant T622X with or without CaM co-expression. Oocytes were from three batches. ns: not significant.

CaM and PIP2 competitively bind with TRPP3 but with distinct mechanisms of inhibition

We have recently reported that PIP2 interacts with TRPP3 C-terminal domain 594-RLRLRK-599 to disrupt the functionally critical intramolecular interaction between the N- and C-terminus of TRPP3 (called the N/C binding), thereby inhibiting the channel function (Zheng et al., 2018a). Because 594-RLRLRK-599 is within the CaM-binding domain E566-F621, it is possible that PIP2 and CaM interfere with each other with respect to their binding to TRPP3 or inhibition of the channel function. We found that CaM indeed significantly reduces the TRPP3/PIP2 binding (Fig. 3-4A), in support of the possibility that CaM and PIP2 compete for physical binding. We next wondered whether CaM and PIP2 have similar inhibitory effect on the TRPP3 N/C interaction which is functionally critical. We previously showed that PIP2 inhibits TRPP3 function through disrupting its N/C binding (Zheng et al., 2018a). For this, we assessed the TRPP3 N/C binding using purified GST-P3NP and over-expressed full-length TRPP3 by GST pull-down assays. Interestingly, unlike PIP2, CaM had no significant effect on the N/C binding (Fig. 3-4B). Taken together, our data indicated that CaM and PIP2 inhibit TRPP3 channel function through distinct mechanisms even though they compete for binding with TRPP3.

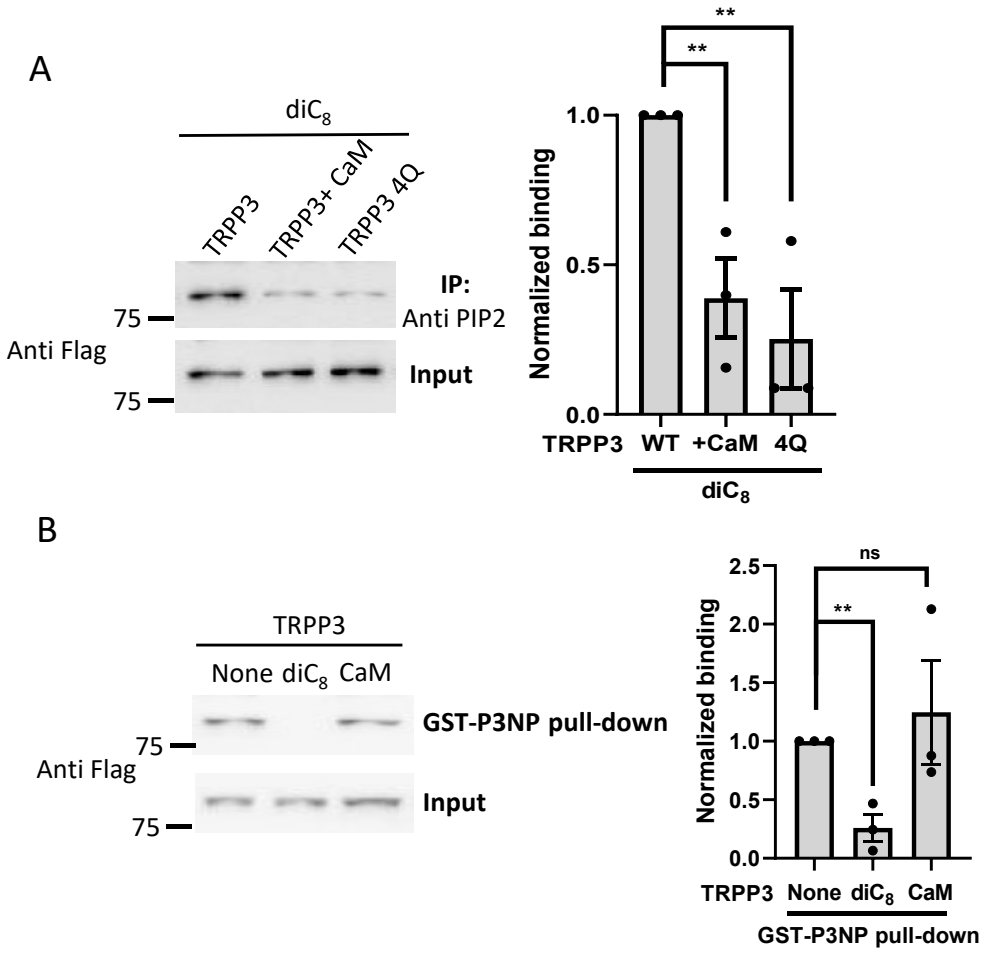

Figure 3-4. Relationship of CaM and PIP2 on TRPP3 regulation. A. Left panel: representative co-IP data showing the effect of CaM on the interaction of diC_8 PIP2 (a water-soluble dioctanoyl analog of PIP2) and TRPP3, TRPP3 4Q mutant (R594Q/R596Q/ R598Q/K599Q quadruple mutant) served as the negative control. Right panel: data from three independent experiments in left panel were quantified, averaged, and normalized. **$p < 0.01$. **B.** Left panel: representative GST pull down data showing the effect of CaM on the interaction of GST-P3NP and TRPP3 FL. diC_8 PIP2 served as a negative control. Right panel: data from three independent experiments in left panel were quantified, averaged, and normalized. **$p < 0.01$, ns: not significant.

CaMK2 mediates the regulation of TRPP3 by CaM

We next wanted to examine how CaM suppresses the TRPP3 channel function. Because phosphorylated TRPP3 has greatly reduced function, as we showed previously (Zheng et al., 2016b), we wondered whether CaM downstream kinase CaMK2 is involved in the phosphorylation of TRPP3. First, we found that treatment with KN93 or myristoylated autocamtide-2 related inhibitory peptide (AIP), potent inhibitors of CaMK2, significantly increases the TRPP3 channel activity (Fig. 3-5A). We next co-expressed TRPP3 with CaMK2, dominant negative mutant K42M, or constitutively active mutant T286D (Sun et al., 2008) and found that the high CaMK2 kinase activity is associated with the low TRPP3 channel activity, with the TRPP3 surface membrane expression is unaltered by CaMK2 co-expression (Fig. 3-5 B and C). Further co-IP experiments showed that CaMK2 and TRPP3 are in the same complex (Fig. 3-5D), further indicating TRPP3 is target of CaMK2. In an effort to examine the role of CaM in the TRPP3/CaMK2 interaction, we finally found that expression of CaM, but not of its mutant CaM_{1234}, significantly enhances the TRPP3/CaMK2 interaction, indicating that CaM binding with TRPP3 in the presence of Ca^{2+} is essential for the TRPP3/CaMK2 interaction. Taken together, our data indicated that CaM inhibits TRPP3 function through enhancing the TRPP3/CaMK2 interaction thereby increasing TRPP3 phosphorylation and functional inhibition.

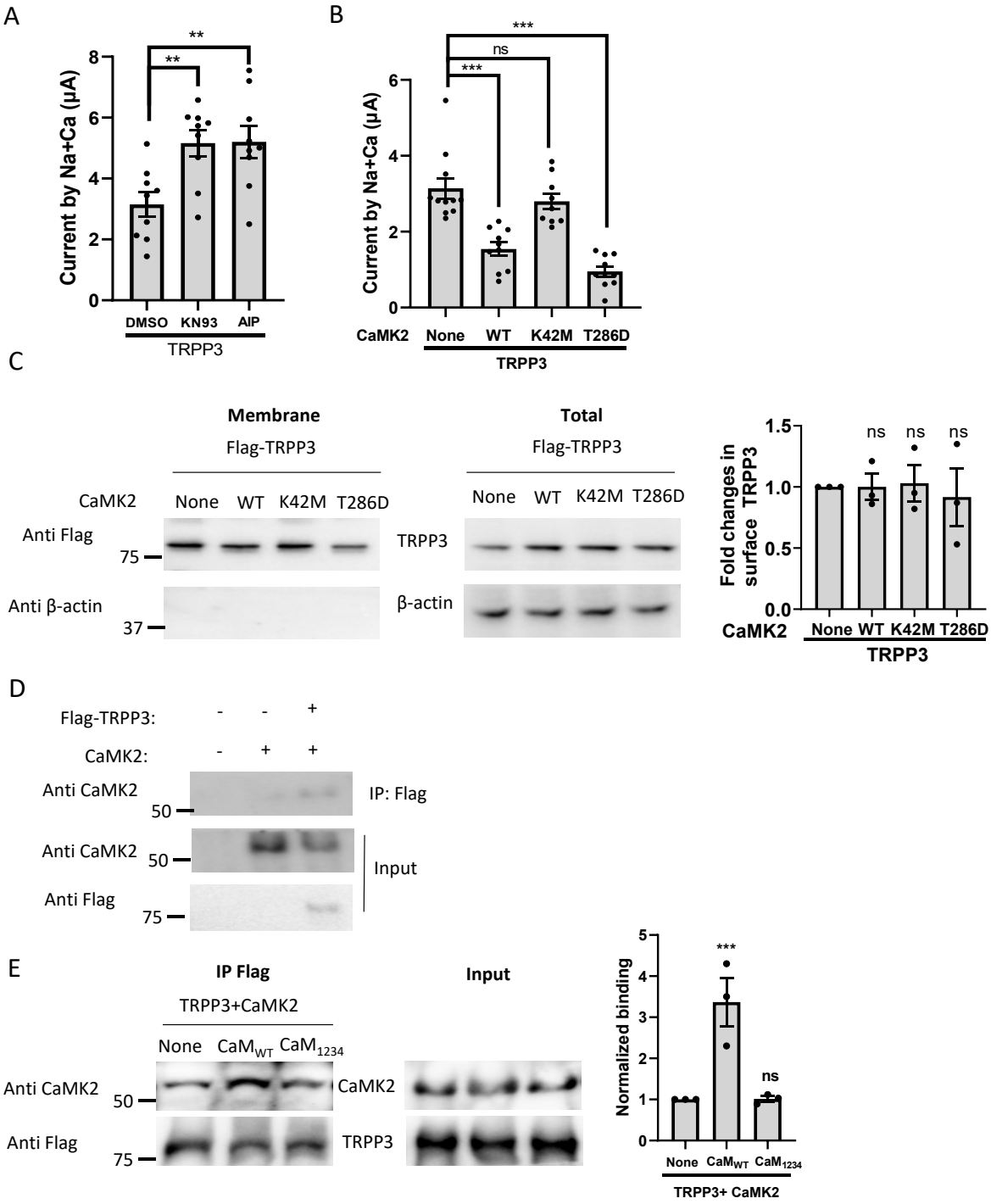
A
Current by Na+Ca (μA)
DMSO
KN93
AIP
TRPP3
B
Current by Na+Ca (μA)
CaMK2
None
WT
K42M
T286D
TRPP3
C
Membrane
Flag-TRPP3
Total
Flag-TRPP3
CaMK2
None WT K42M T286D
Anti Flag
TRPP3
Anti β-actin
β-actin
75
37
Fold changes in surface TRPP3
ns
D
Flag-TRPP3:
CaMK2:
Anti CaMK2
IP: Flag
Input
Anti Flag
50
75
E
IP Flag
Input
TRPP3+CaMK2
None
CaM$_{WT}$
CaM$_{1234}$
Anti CaMK2
Anti Flag
CaMK2
TRPP3
Normalized binding
TRPP3+ CaMK2

Figure 3-5. Roles of CaMK2 on TRPP3 channel function. A. Averaged currents of TRPP3 after the treatment of indicated chemicals. Oocytes were incubated with 10 μM KN93 or 10 μM AIP for 30 mins, with DMSO acting as the negative control. Oocytes were from three batches. **p < 0.01. **B.** Averaged currents of TRPP3 expressing oocytes and different TRPP3-CaMK2 mutants co-expressing oocytes. Oocytes were from three batches. ***p < 0.001, ns: not significant. **C.** Left panel: representative surface and total expression of TRPP3 by biotinylation, with β-actin as the loading control. Right panel: data from three independent experiments were quantified, normalized, and averaged. ns: not significant. **D.** Representative co-IP data showing the interaction between TRPP3 and CaMK2 from one of the three independent experiments. **E.** Left panel: representative co-IP data showing the role of CaM in TRPP3 and CaMK2 interaction. Right panel: data from three independent experiments were quantified, normalized, and averaged. *** p <0.001, ns: not significant.

We next wanted to determine how CaMK2 phosphorylates TRPP3. CaMK2 has a general phosphorylation motif RXX[pS/pT] in its target proteins (Songyang et al., 1996) but several exceptions have been reported (White et al., 1998; Dosemeci and Jaffe, 2010). Note that no such a motif is found near CaMBD in TRPP3. Due to the enhanced interaction between TRPP3 and CaMK2 by CaM, we decided to test the 3 candidate phosphorylation sites S581, T591 and S603 around CaMBD through alanine and glutamate substitutions to mimic dephosphorylation and phosphorylation, respectively (Fig. 3-6A). We found that mutations T591A and T591E substantially increases and decreases the channel function, respectively, while the same mutations at the other two sites had no effect (Fig. 3-6B). Of note, none of these mutations affected the plasma membrane expression of TRPP3 (Fig. 3-6C). We found that CaMK2-T286D has no inhibitory effect on the function of mutant T591A (Fig. 3-6D), suggesting that T591 could be the phosphorylation site of CaMK2 in TRPP3.

Because CaM binds with TRPP3 independently of CaMK2, we wondered whether CaM inhibits TRPP3 function also (in part) through the TRPP3/CaM binding. By CaM agarose beads pull-down experiments we found that while mutations at T591 do not affect the TRPP3/CaM binding (Fig. 3-6E), CaM has no effect on the function of mutant T591A (Fig. 3-6F). These data together demonstrated that CaM inhibits TRPP3 function through its downstream kinase CaMK2 phosphorylating T591 but not through the direct TRPP3/CaM binding.

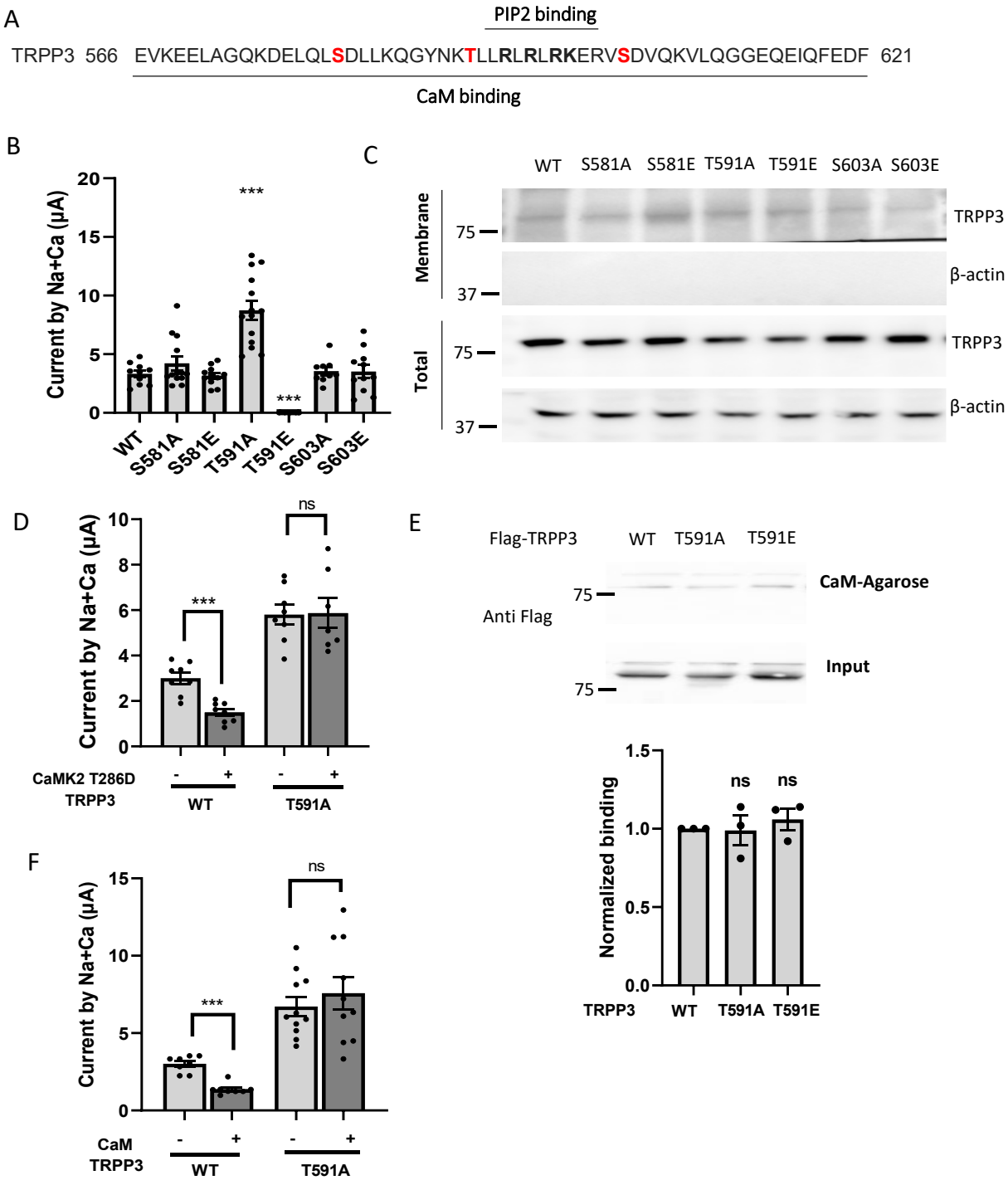
A
PIP2 binding
TRPP3 566 EVKEELAGQKDELQLSDLLKQGYNKTLLRLRLRKERVSDVQKVLQGGEQEIQFEDF 621
CaM binding
B
Current by Na+Ca (μA)
***
***
WT
S581A
S581E
T591A
T591E
S603A
S603E
C
WT S581A S581E T591A T591E S603A S603E
Membrane
Total
75
37
TRPP3
β-actin
D
Current by Na+Ca (μA)
***
ns
CaMK2 T286D
TRPP3
WT
T591A
E
Flag-TRPP3 WT T591A T591E
Anti Flag
CaM-Agarose
Input
Normalized binding
ns
ns
TRPP3 WT T591A T591E
F
Current by Na+Ca (μA)
***
ns
CaM
TRPP3
WT
T591A

Figure 3-6. The role of T591 on TRPP3 channel function. A. CaM binding sequence identified on TRPP3 C-terminus. PIP2 binding sites are indicated. **B.** Averaged currents of WT TRPP3 and indicated mutants. Oocytes were from three batches. ***$p < 0.001$. **C.** Representative surface and total expression of WT TRPP3 and mutants by biotinylation, with β-actin as the loading control. **D.** Effect of CaMK2 T286D on the function of WT TRPP3 and T591A mutant. Oocytes were from three batches. ***$p < 0.001$. ns: not significant. **E.** Upper panel: representative data showing the interaction between WT TRPP3, T591A, T591E and CaM-agarose. Lower panel: data from three independent experiments were quantified, normalized, and averaged. ns: not significant. **F.** Effect of CaM on the function of WT TRPP3 and T591A. Oocytes were from three batches. ***$p < 0.001$. ns: not significant.

3.5 DISCUSSION

We previously reported that human TRPP3 expressed alone in *Xenopus* oocytes is regulated by a number of factors including Ca^{2+}, voltage, pH, amiloride analogs, large monovalent organic cations, troponin I, α-actinin and receptor for activated protein kinase 1 (RACK1) (Yang et al., 2012; Liu et al., 2002; Li et al., 2003; Li et al., 2007; Dai et al., 2006; Dai et al., 2007). Extracellular Ca^{2+} has been shown to activate TRPP3, which is followed by channel inactivation. One hypothetical mechanism is that outward-moving Ca^{2+} block the TRPP3 conducting pore through interacting with residue D523 in the selectivity filter (DeCaen et al., 2016). However, Ca^{2+} electrochemical gradients (e.g., at a membrane potential of -50 mV) across the membrane would be highly unfavorable for the outward movement. Besides, we previously showed that mutant D523N exhibits no Ca^{2+}-induced activation in oocytes and thus no ensuing inactivation either (Hussein et al., 2015), indicating that D523 is essential for channel activation. Besides this direct Ca^{2+} blockage hypothesis, here we showed that Ca^{2+}-induced TRPP3 activation is inhibited by Ca^{2+}/CaM through CaMK2 phosphorylation. However, disturbing the Ca^{2+}-dependent CaM-CaMK2 regulatory pathway by pharmacological or mutational approaches, including inhibiting CaM, only reduced the current amplitude but did not affect the TRPP3 inactivation kinetics, indicating that CaM and its associated pathway are mainly involved in the activation process.

CaM is known to regulate membrane receptors (Zhang et al., 1998), transporters (Iwamoto et al., 2010)and a variety of ion channels including voltage-gated Ca^{2+} (DeMaria et al., 2001), Na^{+} (Ben-Johny et al., 2015) and K^{+} channels (Schumacher et al., 2001) and TRP channels (Hasan and Zhang, 2018). Compared to other membrane proteins, how CaM regulates TRP channels is less well understood, possibly because they are impacted by other stimuli such as

temperature, natural chemicals, and mechanical force (Falcón et al., 2019). Several residues in TRPs have been reported to be involved in CaM binding through functional studies and in vitro or in vivo binding assays (Gordon-Shaag et al., 2008) but overall whether the regulation by CaM is through direct TRP/CaM binding or through an intermediate cellular factor requires further studies. Indirect CaM modulation through altering channel/lipid interaction (Wang et al., 2001), channel biosynthesis (Deutsch, 2003) or membrane trafficking (Joiner et al., 2001) has been reported.

The highly Ca^{2+}-selective TRPV5 and TRPV6 possess CaMBDs in the N- and C-termini as well as in transmembrane domains but some of these bindings remain debatable (Derler et al., 2006). Binding of CaM to one of these CaMBDs is known to act as a rapid feedback mechanism to prevent Ca^{2+} overload and maintain Ca^{2+} homeostasis (Kovalevskaya et al., 2012). In a proposed "two-tail" CaM modulation model, the CaM C-lobe constitutively binds to TRPV6 with the N-lobe sensing calcium increment to adjust the conformation to promote TRPV6 inactivation (Bate et al., 2018). However, this model was strongly challenged by recently resolved structures for the TRPV6/CaM and TRPV5/CaM complex, which revealed that the CaM C-lobe plugs the channel through a unique cation-π interaction by inserting the side chain of K115 (TRPV6) to the pore's intracellular entrance to directly block the conducting pore (Singh et al., 2018a; Hughes et al., 2018). Interestingly, an indirect CaM blockade strategy was adopted based on the structures of the TRPC4 apo and TRPC4/CaM complex so that their conducting pores have similar conformations (Vinayagam et al., 2020).CaM binding resulted in a more stabilized closed state in which the channel periphery displays pronounced differences compared to that in the absence of CaM. However, due to the lack of a fully resolved CaM

structure in the TRPC4/CaM complex, it remains to be determined how CaM affects the overall conformation of TRPC4.

Instead of inducing the channel conformational change directly, we here identified a regulation mechanism by CaM through CaMK2 on TRPP3. Ca^{2+} dependent CaM binding to TRPP3 might be similar as other CaM targets, as CaM/Ca^{2+} complex binding to TRPP3 initiates the channel inactivation. Notably, weak CaM binding was still detectable even without extracellular Ca^{2+} (Fig. 3-2D) or when abolishing Ca^{2+}-binding sites via mutations (Fig. 3-3C), which was similarly observed for L-type Ca^{2+} channel and TRPV1 (Peterson et al., 1999; Numazaki et al., 2003). Binding of CaM to a channel protein may ensure a relatively rapid response of the channel to changes in the local Ca^{2+} concentration. We found that CaM binding to TRPP3 is a necessary process, but it does not seem to be sufficient for channel inhibition because TRPP3 mutant T591A became irresponsive to CaM while retaining its CaM binding ability (Fig. 3-6 E and F). This is because the mutation T591A abolishes the phosphorylation site for CaMK2. In fact, our study demonstrated that CaM facilitates TRPP3 phosphorylation at T591 by kinase CaMK2, a mechanism that was initially proposed for a Na^{+} channel (Deschênes et al., 2002).

We noticed that CaM regulation on TRPP3 has also been explored by another group. And they proposed CaM N-lobe is involved in TRPP3 EF-hand autoinhibition with L593 playing as the CaM anchor residue (Baik et al., 2020). Indeed, through the Ca^{2+} dependent conformational change, EF-hand motif has been believed to be mediated in channel gating (Braun and Sy, 2001). For example, in the predominant cardiac voltage-gated sodium channel, Nav1.5, intramolecular interaction between EF-hand and III-IV intracellular linker loop is involved in channel inactivation (Gardill et al., 2018). And in TRPP2, which shares 70% overall sequence similarity

with TRPP3, calcium binding in the EF-hand is required by TRPP2 channel activity and normal cellular function (Petri et al., 2010). However, it's recently strongly challenged by another group with both TRPP2 heterologous expression and native expression (Vien et al., 2020). They found that Ca^{2+}/EF-hand association is not required for TRPP2 channel function or related to ADPKD. Similarly, on TRPP3, no difference on channel function has been observed when EF-hand was removed from TRPP3 (Li et al., 2002; DeCaen et al., 2016). And we also found that removing EF-hand has nearly no impact on CaM inhibition or interaction (Fig. 3-3 F and G), suggesting EF-hand may be not involved in CaM regulation on TRPP3. Also, our data is not in agreement with L593 working as the CaM anchor residue since no functional difference had been detected in our setup (Fig. 3-7A). Then we compared the CaM-binding strength of L593A mutant and TRPP3 WT through CaM agarose pull-down experiment. Consistent with functional data, no difference was detected (Fig. 3-7B). Thus, this result strongly challenged the idea that L593 works as the binding site. Although we cannot completely rule out the involvement of L593 in CaM interaction, this residue may not be the critical one. CaM is known to bind to the IQ motif or a hydrophobic alpha helix (Rhoads and Friedberg, 1997), but also varies depending on different channels (Mercado et al., 2010). Considering there is no classical IQ motif in TRPP3, double or even triple mutations may be generated to identify the key residues involved in CaM interaction.

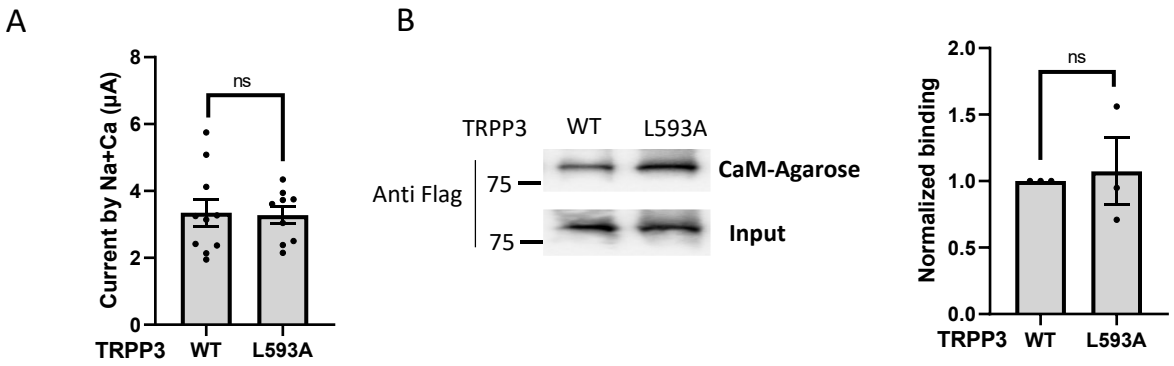

Figure 3-7. L593 is not involved in the CaM regulation on TRPP3. A. Averaged currents of WT TRPP3 and L593A. Oocytes were from three batches. ns: not significant. **B.** Left panel: Representative CaM-agarose pull-down data showing that the interaction between CaM and WT TRPP3 or L593A mutant. Right panel: data from three independent experiments in left panel were quantified, averaged, and normalized. ns: not significant.

Although we found the competition between CaM and PIP2 for binding with TRPP3, unlike PIP2, CaM did not affect the TRPP3 N/C interaction (Fig. 3-4). In fact, several reports have found even more complex interplays between CaM and PIP2 (Cao et al., 2013; Tobelaim et al., 2017; Alberdi et al., 2015). Due to the opposite functional effect of CaM and PIP2 on TRPP3, it raises the possibility that they compete for the same polycationic/hydrophobic domains. Although CaM and PIP2 bind to overlapping regions in TRPV1 and TRPC6, they were found to bind with distinct amino acid residues (Nilius et al., 2008; Kwon et al., 2007). In contrast, CaM and PIP2 demonstrate similar effects on other channels such as Kv7.1 in which they similarly modulate the gating by stabilizing the open state (Trudeau and Zagotta, 2003). This may serve as a supplementary strategy that can be of physiological significance because PIP2 in cardiomyocytes is substantially depleted due to the activation of phospholipase C via Gq protein-coupled receptors like M1-muscarinic receptors (Kobrinsky et al., 2000). CaM in this case can still activate the channel to prevent compromised channel gating and may relieve cardiac arrhythmias such as long-QT syndrome (LQT) (Trudeau and Zagotta, 2003). In the case of TRPP3, although CaM and PIP2 may have distinct ways of inhibition, CaM may still play a supplementary role, to prevent Ca^{2+} overload through the channel when the cellular PIP2 level becomes low, given that TRPP3 has a large conductance (120-150 pS) and is around 5 times more permeable to Ca^{2+} than Na^{+} or K^{+} (DeCaen et al., 2016; Chen et al., 1999).

Although there are 70% overall sequence similarity between TRPP3 and TRPP2, we found that TRPP2 gain-of-function mutant F604P (Arif Pavel et al., 2016) is not sensitive to CaM (Fig. 3-8A). However, our CaM-agarose pull-down experiments showed the interaction between CaM and TRPP2 F604P mutant (Fig. 3-8B). Sequence alignment found that TRPP3 T591 corresponds to TRPP2 A711 (Fig. 3-8C), suggesting that TRPP2 may be kept constitutively in its

‘dephosphorylated’ state at 711. Indeed, changing A711 to E or D in TRPP2-F604P to mimic phosphorylation completely abolished the channel function (Fig. 3-8D).

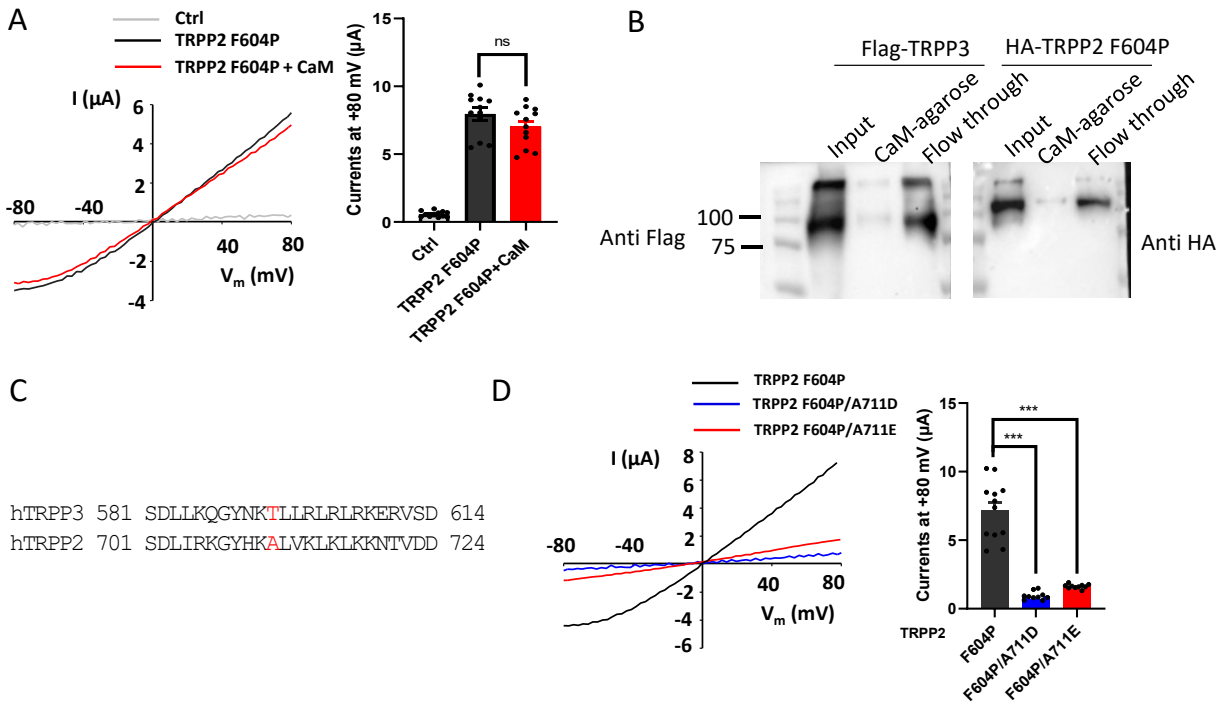

Figure 3-8. TRPP2 is not under the regulation of CaM. A. Left panel: representative I-V curves obtained from oocytes expressing TRPP2 F604P or TRPP2 F604P+CaM as indicated, in the presence of Na^+-containing, divalent-free solution (in mM): 100 NaCl; 2 KCl; and 10 HEPES (pH 7.5). Right panel: averaged currents at +80 mV are shown. Ctrl, water-injected oocytes. Oocytes were from three batches. ns: not significant. **B.** Representative CaM-agarose pull-down data showing that the interaction between CaM and TRPP2 F604P. TRPP3 acts as the positive control. **C.** Sequence alignment of TRPP3 and TRPP2 CaM binding domain. **D.** Left panel: representative I-V curves obtained from oocytes expressing TRPP2 F604P TRPP2 F604P/A711D or TRPP2 F604P/A711E as indicated in the same solution described in A. Right panel: averaged currents at +80 mV are shown. Oocytes were from three batches. ***p <0.001.

In summary, we reported that an important channel regulator, CaM, which binds to TRPP3 competitively with PIP2, regulates TRPP3 through a totally different mechanism. As our schematic diagram (Fig. 3-9) illustrated, Ca^{2+} entry through TRPP3 increases the formation of the CaM/Ca^{2+} complex that binds to the TRPP3 C-terminus to enhance the TRPP3/CaMK2 interaction thereby promoting the T591 phosphorylation, which inhibits the channel function.

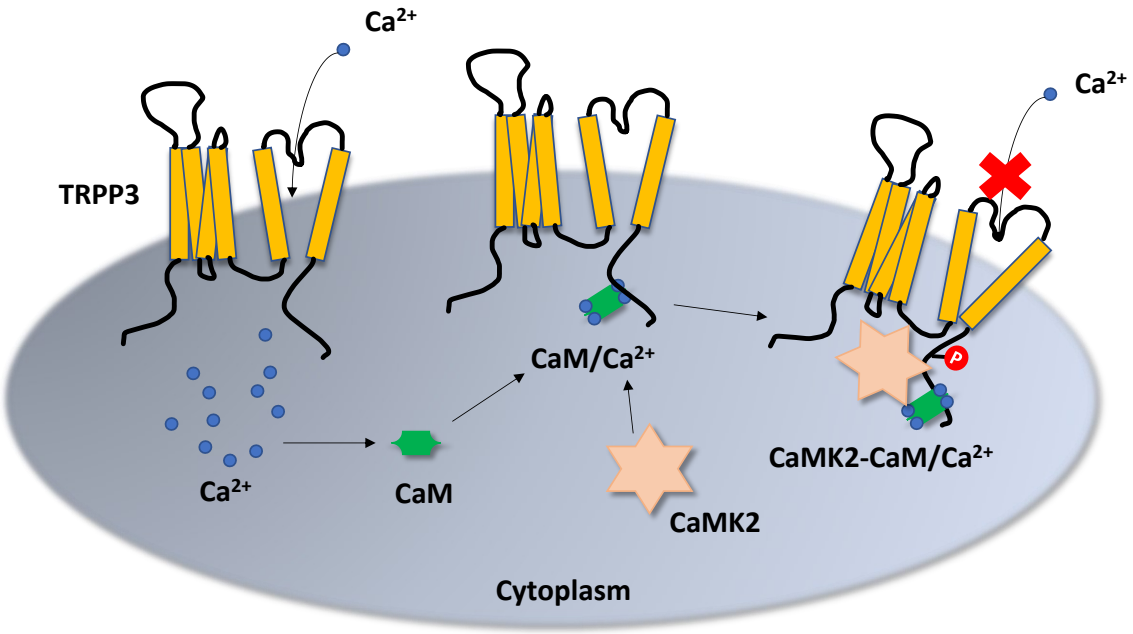

Figure 3-9. Model of the mechanism of how CaM regulates TRPP3 through CaMK2. CaM senses the Ca^{2+} entering through TRPP3. CaM/Ca^{2+} complex will interact with TRPP3 and recruit CaMK2 to TRPP3. With the following enhanced phosphorylation of T591, TRPP3 is inhibited.

CHAPTER 4

RESULTS #3

TACAN is a novel regulator of TRPP2

4.1 ABSTRACT

Autosomal dominant polycystic kidney disease (ADPKD) is caused by mutations in membrane receptor PKD1 or cation channel TRPP2. TACAN (also named TMEM120A), recently reported as an ion channel in neuron cells for mechano- and pain-sensing, is also distributed in diverse non-neuronal tissues such as heart, intestine and kidney, suggesting its involvement in other roles. In this study, we found that TACAN is in complex with TRPP2 in renal primary cilia and *Xenopus* oocytes. We found that while the first and last transmembrane domains of TACAN interact with transmembrane domains of TRPP2, only the last transmembrane domain of TACAN is functionally relevant. TACAN inhibited the channel activity of TRPP2 gain-of-function mutant F604P in oocytes. In mammalian cells TACAN inhibited both the single channel conductance and open probability of wild-type TRPP2 and mutant F604P. Further, we found that co-expressed TACAN and TRPP2, but not TRPP2 alone, exhibit sensitivity to mechanical force in mammalian cells. In summary, this study revealed that TACAN acts as a TRPP2 regulator mediating mechanosensitivity of the TRPP2/TACAN channel complex.

4.2 INTRODUCTION

Autosomal dominant polycystic kidney disease (ADPKD), characterized by accumulation of numerous cysts in both kidneys, is one of the most common human genetic diseases (Harris and Torres, 2009). Although it is widely accepted that mutations in polycystin-1 (also called PKD1) or polycystin-2 (also called PKD2 or TRPP2) act as the genetic basis of ADPKD, the biophysical and physiological function of the two proteins remains poorly understood (Douguet et al., 2019). PKD1 is a receptor-like membrane protein with 11 transmembrane (TM) segments (S1-S11) and a large extracellular N-terminus. TRPP2 belongs to the transient receptor potential (TRP) ion channel superfamily and to a group of six-TM (S1-S6) cation channels with the pore domain formed by the last two segments (S5 and S6) (Bergmann et al., 2018).

TRP proteins, including TRPP2, retain the ability of forming heterotetrametric ion channels to fulfill different functions (Cheng et al., 2010). Recently reported cryo-EM structure of the PKD1/TRPP2 complex revealed that they form a heteromer in a 1:3 stoichiometry and suggested that PKD1 acts as a dominant-negative subunit to block the channel complex (Su et al., 2018). Through functional studies, we identified that PKD1 enhances the calcium permeability (Wang et al., 2019). It was reported that the extracellular N-terminus of PKD1 functions as an activation ligand of the PKD1/TRPP2 complex (Ha et al., 2020). Additional reports demonstrated that TRPP2 interacts with other ion channels including TRPV4 (Köttgen et al., 2008), TRPC1 (Kobori et al., 2009), and Piezo1 (Peyronnet et al., 2013) to form channel complexes with distinct biophysical properties. How TRPP2 is regulated by these or other interacting partners remains largely unknown.

TMEM120A (transmembrane protein 120A, also called TACAN) was initially reported to be a nuclear envelope transmembrane protein and be critical for adipocyte differentiation

(Batrakou et al., 2015). Recently, it was shown to target to the plasma membrane to form a mechano-sensitive ion channel involved in pain sensation (Beaulieu-Laroche et al., 2020), but this was challenged by subsequent studies (Del Rosario et al., 2021; Ke et al., 2021; Niu et al., 2021; Parpaite et al., 2021; Rong et al., 2021; Xue et al., 2021). Global knockout of TACAN led to embryo death, indicating its important role in embryonic development. Furthermore, wide distribution of TACAN in non-neuronal tissues, such as kidney, indicated other potential roles besides pain sensation (Beaulieu-Laroche et al., 2020). A previous proteomic screen suggested a potential interaction between TACAN and TRPP2 (Sharif-Naeini et al., 2009), but whether and how TACAN is associated with TRPP2 has never been explored.

In the present study, we examined how TACAN modulates the TRPP2 channel function using the two-electrode voltage clamp (TEVC) in *Xenopus* oocytes and patch-clamp in Chinese hamster ovary (CHO) cells. We characterized the interaction between TACAN and TRPP2 by means of co-immunoprecipitation (co-IP) and explored the relationship between physical interaction and functional association. We further used zebrafish models to examine the effect of TACAN on TRPP2-dependent disorders.

4.3 METHODS

Plasmids, reagents, and antibodies

HA-tagged human TRPP2 (HA-TRPP2) in vector pGEMHE for *Xenopus* oocyte expression and TRPP2 mutant F604P in vector pcDNA3.1 for mammalian cell expression were obtained from Dr. Yong Yu (St. John's University, NY). Human HA-TACAN in a modified vector pCMV for mammalian cell expression was a kind gift from Dr. Reza Sharif-Naeini (McGill University, QC, Canada). It was then subcloned into vector PGEMHE for oocyte expression, with a Flag tag inserted at the 5' side. Human TRPP2, TRPP2-N, TRPP2-TM and TRPP2-C in vector pEGFP for oocyte expression were constructed previously (Wang et al., 2012). All mutations were carried out using Q5 High-Fidelity 2X Master Mix from New England Biolabs (Ottawa, ON, Canada) and verified by sequencing. Antibodies against β-actin and Arl13b were from Santa Cruz Biotechnology (Santa Cruz, CA) and those against Flag, HA, TMEM120A and TRPP2 were from Proteintech Group (Rosemont, IL). Secondary antibodies were purchased from GE Healthcare (Waukesha, WI). DTT was purchased from Thermo Fisher Scientific (Ottawa, ON, Canada) and disuccinimidyl tartrate (DST) were from CovaChem (Loves Park, IL).

List of mutants and peptides used in this chapter

TRPP2
F604P
F604P/A711D
F604P/A711E
L677G
M1-K215 (N)
D682-V968 (C)
S209-K688 (TM)

A594X
N580-L700
TACAN
K135X
T60X
K190X
G243X
L276X
L296X
R327X
K135-D343
T160-D343
N184-D343
G213-D343
G243-D343
R270-D343
L296-D343

Xenopus oocyte expression

Capped RNAs encoding human TRPP2, human TACAN or their mutants were synthesized by in vitro transcription using the T7 mMESSAGE mMACHINE kit (Invitrogen, Waltham, MA) and injected into oocytes (25 ng each) prepared as described (Cai et al., 2020). Control oocytes were injected with the same amount of water. Oocytes were incubated at 18℃ for 2-3 days before measurements. The present study was approved by the Ethical Committee for Animal Experiments of the University of Alberta and performed in accordance with the Guidelines for

Research with Experimental Animals of the University of Alberta and the Guide for the Care and Use of Laboratory Animals (NIH Guide) revised in 1996.

Cell culture and protein expression

CHO cells were cultured in Dulbecco's Modified Eagle Medium/Nutrient Mixture F-12 (DMEM/F12) supplemented with L-glutamine, penicillin-streptomycin and 10% fetal bovine serum (FBS). MDCK, IMCD and LLC-PK1 cells were cultured in DMEM supplemented with L-glutamine, penicillin-streptomycin and 10% FBS. All cultured cells were kept at 37°C and supplied with 5% CO2. Transfection of cDNAs was performed using Lipofectamine 3000 (Invitrogen) according to the manufacturer's protocol.

Two-electrode voltage clamp

The two-electrode voltage clamp electrophysiology experiments in *Xenopus* oocytes were performed as we described previously (Zheng et al., 2018a) Briefly, an electrode made of a capillary glass pipette (Warner Instruments, Hamden, CT) was filled with 3 M KCl. The tip resistance was measured to be 0.3-2 MΩ and the electrode was impaled into the oocyte. The Geneclamp 500B amplifier and Digidata 1322A AD/DA converter (Molecular Devices, Union City, CA) were used to record the whole-cell currents and membrane potentials. The pClamp 9 software (Axon Instruments, Union City, CA) was used to analyze the data. Both signals were digitized at 200 μs/sample and filtered at 2 kHz through a Bessel filter. Data were plotted using SigmaPlot 13 (Systat Software, San Jose, CA) or GraphPad Prism 8 (GraphPad Software, San Diego, CA).

Patch-clamp

Patch-clamp recordings were carried as we described previously (Fatehi et al., 2017), under voltage clamp at room temperature (~22°C). The recording pipette and chamber were coupled by Ag/AgCl electrodes to an Axopatch 200B patch-clamp amplifier and Digidata 1200A BNC data-acquisition system, controlled by pCLAMP 10 software (Axon Instruments). Both bath and pipette solutions were the same, composed of (in mM) 140 NaCl, 5 KCl, 2 CaCl2, 2 MgCl2, 10 HEPES, 10 glucose and pH 7.4. The seal resistance was no less than 5 GΩ for all cell-attached recordings. The recordings were low pass filtered at 1 kHz following acquisition. Linear stepwise negative pressures (by suctions) of various magnitudes were applied to the interior of the glass pipettes using a high-speed pressure clamp system (HSPC-1, ALA Scientific, Farmingdale, NY).

Western-blot and surface protein biotinylation

Xenopus oocytes after 3-times washing with ice-cold PBS solution were incubated with 0.5 mg/ml sulfo-NHS-SS-Biotin (Pierce, Rockford, IL) for 30 min at room temperature. Non-reacted biotin was quenched by 1 M NH4Cl. Oocytes were then washed with ice-cold PBS solution and harvested in ice-cold CelLytic M lysis buffer from Sigma-Aldrich (St. Louis, MO) supplemented with proteinase inhibitor cocktail (Thermo Fisher Scientific) Upon addition of 100 µl streptavidin (Pierce) lysates were incubated at 4℃ overnight with gentle shaking. The surface protein bound to streptavidin was resuspended in SDS loading buffer and subjected to SDS-PAGE.

Chemical cross-linking

Chemical cross-linking assays were performed as previously described (Yu et al., 2009). Oocytes expressing the desired proteins were harvested in ice-cold CelLytic M lysis buffer (Sigma-Aldrich) supplemented with proteinase inhibitor cocktail (Thermo Fisher Scientific). Fresh crosslinker stock solutions were prepared by dissolving DST (CovaChem) into dimethylsulfoxide (DMSO) (Sigma-Aldrich). Cross-linking reactions were carried out by diluting the stock solution into the cell lysate samples, followed by incubation on ice for 4 h. SDS loading buffer was used to stop the reaction. The samples were incubated at 37 °C for 30 min and subjected to SDS-PAGE.

Immunofluorescence

Whole-mount immunofluorescence assays using *Xenopus* oocytes were performed as described (Zheng et al., 2018a). Briefly, oocytes were washed in PBS, fixed in 4% paraformaldehyde for 15 min, washed three times in PBS plus 50 mM NH4Cl, and then permeabilized with 0.1% Triton X-100 for 4 min. Oocytes were then blocked in PBS plus 3% skim milk for 30 min and then incubated overnight with indicated primary antibodies, followed by incubation with secondary Alexa-488-conjugated donkey anti-rabbit or Cy3-conjugated goat anti-mouse antibody (Jackson ImmunoResearch Laboratories, West Grove, PA) for 30 min. Oocytes were then mounted in Vectashield (Vector Labs, Burlington, ON, Canada) and examined on an AIVI spinning disc confocal microscopy (Cell Imaging Facility, Faculty of Medicine and Dentistry, University of Alberta).

Co-IP

Co-IP experiments were performed as we previously described (Zheng et al., 2018a). Briefly, a group of 20-30 oocytes washed with PBS were solubilized in ice-cold CelLytic-M lysis buffer (Sigma-Aldrich) supplemented with proteinase inhibitor cocktail. Supernatants were collected after centrifugation at 13,200 rpm for 15 min and precleaned for 1 h with 50% protein G-Sepharose (GE Healthcare), followed by incubation with an indicated antibody at 4℃ for 4 h. Upon addition of 100 μl of 50% protein G-Sepharose, the mixture was incubated at 4℃ overnight with gentle shaking. The immune complexes conjugated to protein G-Sepharose were washed three times with cold PBS solution containing 1% Nonidet P-40 and eluted by SDS loading buffer. Precipitated proteins were subjected to Western blot analysis.

Zebrafish experiments

Zebrafish experiments were performed as previously described (Zheng et al., 2018c). Briefly, embryos of WT zebrafish AB strain were kept in E3 solution. A translation-blocking antisense MO (Gene Tools LLC, Philomath, OR) was injected at the fertilized eggs within 1 h postfertilization for zebrafish TRPP2 knock-down. The TRPP2 MO sequence was 5′-AGGACGAACGCGACTGGAGCTCATC-3′. Human TACAN mRNA was the same as what we used for *Xenopus* oocytes expression.

Statistical analysis

All statistical data in this study were represented as mean ± SEM (standard error of the mean) from N measurements. Two sets of data were analyzed by student t tests, while multiple sets were analyzed by one-way ANOVA. *, ** and *** indicate $p < 0.05$, 0.01 and 0.001, respectively; ns indicates statistically not significant.

4.4 RESULTS

Functional interaction between TRPP2 and TACAN

TACAN was indicated as a potential interactor of TRPP2 through a proteomic screen using smooth muscle cells as a model and TRPP2 C-terminal truncation mutant R742X as a negative control (Sharif-Naeini et al., 2009). To study whether TACAN modulates the TRPP2 channel function, both proteins were expressed in *Xenopus* oocytes for electrophysiological analysis. Because of relatively low expression of wild-type (WT) TRPP2 to the oocyte plasma membrane and unknown agonist, no appreciable whole-cell current was evoked. In contrast, as expression of gain-of-function (GOF) mutant F604P induced large currents in oocytes (Arif Pavel et al., 2016), we used currents mediated by mutant F604P as a functional readout, similarly as we used previously (Zheng et al., 2018a; Zheng et al., 2018c). First, we found that oocytes expressing TACAN alone do not exhibit any significant increase in the current compared with water-injected oocytes (Fig. 4-1A and B). Co-expression of TRPP2 F604P and TACAN significantly decreased the current amplitude compared with TRPP2 F604P expressed alone (Fig. 4-1A and B). To address the question of whether the TACAN's effect was simply through decreasing the surface expression of TRPP2 F604P, we performed whole-cell immunofluorescence (IF) and biotinylation assays. IF assays nicely displayed the plasma membrane co-localization of the two proteins (Fig. 4-1C). Biotinylation assays demonstrated that neither the total nor the surface membrane expression of F604P is not affected by TACAN (Fig. 4-1D), indicating that TACAN reduced the F604P channel activity. Interestingly, expression of F604P reduced both the total and surface expression of TACAN while the surface/total expression ratio remained unaffected (Fig. 4-1E), indicating that it is the expression of TACAN, but not the membrane trafficking, that was affected by F604P, possibly because expression of F604P significantly increased the steady-

intracellular Ca^{2+} concentration, since the Ca^{2+} is related to the gene expression (Negulescu et al., 1994).

Next, we examined whether TACAN affected the F604P ion selectivity using extracellular solutions containing 100 mM Na+, Li+, K+ or non-permeable N-methyl-d-glucamine (NMDG, negative control). We found that the reversal potential shifts due to changes in the solution remain the same between F604P alone and F604P + TACAN (Fig. 4-1F), indicating that TACAN does not significantly affect the cation permeability ratios (PNa : PLi : PK = 1 : 1.65 : 2.15 for F604P, consistent with previous reports(Shen et al., 2016); PNa : PLi : PK = 1 : 1.66 : 2.15 for F604P + TACAN). Extracellular Ca^{2+} is known to block the TRPP2 conductance of monovalent cations (Arif Pavel et al., 2016; Shen et al., 2016). We found that TACAN does not affect the effect of Ca^{2+} on TRPP2 mutant F604P (Fig. 4-1G and H). Taken together, our data indicated that TACAN inhibits TRPP2 F604P channel activity but does not affect the cation selectivity or the inhibitory effect of extracellular Ca^{2+} on the permeation of monovalent cations.

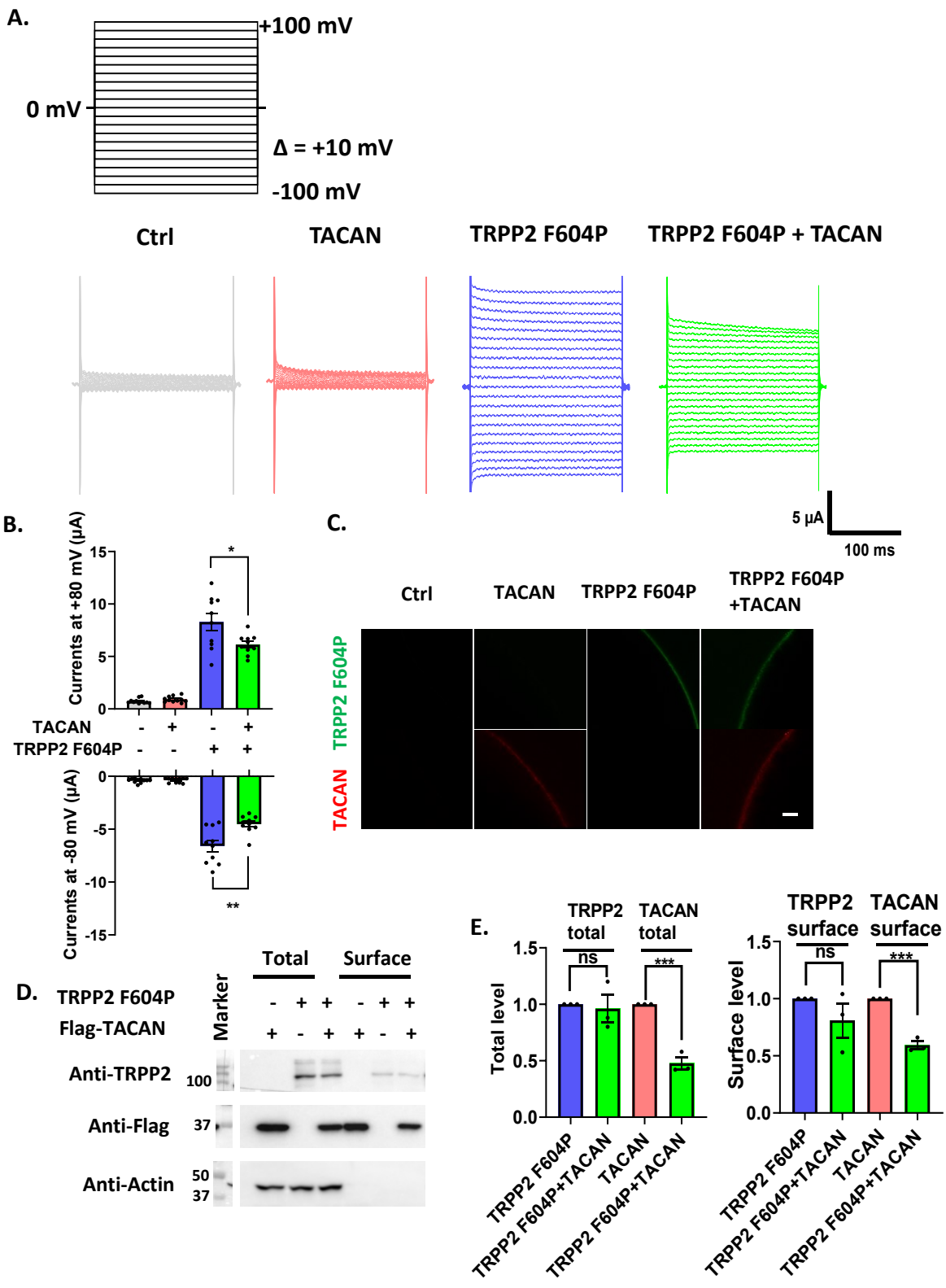
A.
+100 mV
0 mV
Δ = +10 mV
-100 mV
Ctrl
TACAN
TRPP2 F604P
TRPP2 F604P + TACAN
5 μA
100 ms
B.
Currents at +80 mV (μA)
Currents at -80 mV (μA)
TACAN
TRPP2 F604P
C.
Ctrl
TACAN
TRPP2 F604P
TRPP2 F604P +TACAN
TRPP2 F604P
TACAN
D.
Total
Surface
TRPP2 F604P
Flag-TACAN
Marker
Anti-TRPP2
Anti-Flag
Anti-Actin
100
37
50
37
E.
TRPP2 total
TACAN total
TRPP2 surface
TACAN surface
Total level
Surface level
ns
***
TRPP2 F604P
TRPP2 F604P+TACAN
TACAN
TRPP2 F604P+TACAN

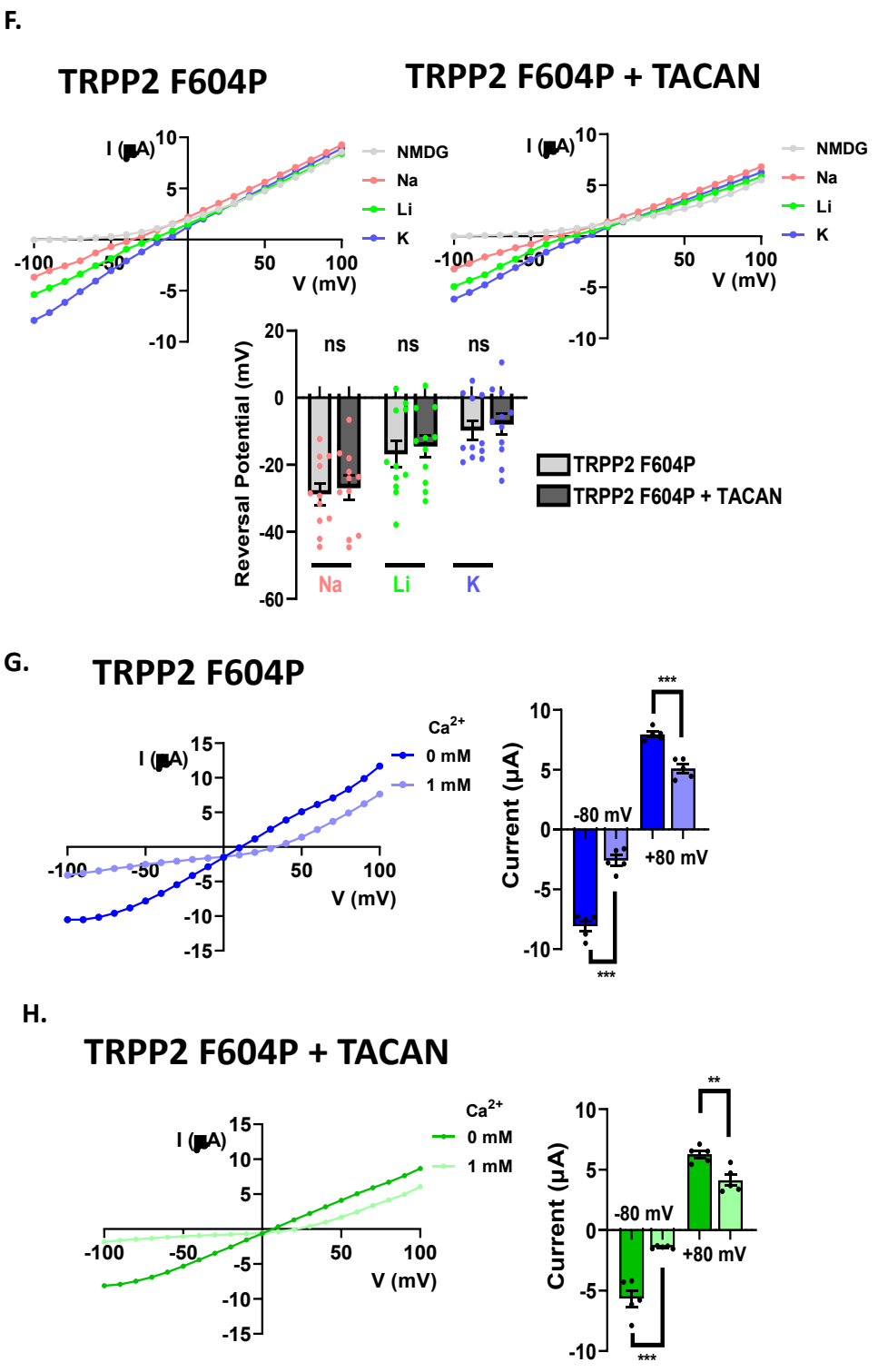

Figure 4-1. Functional regulation of TRPP2 by TACAN in *Xenopus* oocytes. A. Representative current traces obtained using a voltage jump protocol in oocytes expressing TACAN, TRPP2 F604P or TRPP2 F604P + TACAN, in the presence of the divalent-free Na-

containing solution (in mM): 100 NaCl, 2 KCl, 10 HEPES and pH 7.5. Data from water-injected oocytes served as negative control (Ctrl). **B.** Statistical bar graphs of currents recorded at +80 mV obtained under the same experimental conditions as in **A**. Data are presented as mean ± SEM. * $p < 0.05$; ** $p < 0.01$; by One-way ANOVA with Holm-Sidak's correction. **C.** Representative IF images showing oocyte surface expression of TACAN or TRPP2 F604P. Scale bar, 50 μm. **D.** Representative Western blot analysis of the biotinylated (surface) and total protein of TACAN, TRPP2 F604P or TRPP2 F604P + TACAN. **E.** Averaged data obtained as those from **D** (n = 3). Data are presented as mean ± SEM. ns, not significant; *** $p < 0.001$. **F.** Upper panel: representative I-V curves for TRPP2 F604P or TRPP2 F604P + TACAN when 100 mM of an indicated ion was used in the divalent ion-free bath solution. Lower panel: averaged reversal potentials. Data are presented as mean ± SEM. ns, not significant. **G** and **H.** Left panel: representative I-V curves for TRPP2 F604P (**G**) and TRPP2 F604P + TACAN (**H**) in bath solution with or without 1 mM Ca^{2+}. Right panel: Ca^{2+} inhibition of inward (-80 mV) and outward (+80 mV) currents for TRPP2 F604P (**G**) and TRPP2 F604P + TACAN (**H**). Data are presented as mean ± SEM. * $p < 0.05$; ** $p < 0.01$; *** $p < 0.001$.

To further characterize how TACAN inhibits the TRPP2 F604P channel function, we also examined its effects on single-channel parameters of the mutant using Chinese hamster ovary (CHO) cells with patch clamp electrophysiology. Similar as what was observed in *Xenopus* oocytes, we did not detect any single-channel events in CHO cells expressing TACAN alone in the presence of negative pressure in the 0 to -30 mm Hg range (Fig. 4-2A). Of note, increasing the pressure beyond -30 mm Hg generated non-specific leak currents, presumably due to broken cell membrane in our setup. We found that both the unitary current and open probability of mutant F604P at +80 mV are substantially reduced in the presence of TACAN (Fig. 4-2B), which is consistent with our whole-cell data obtained from using oocyte expression. We next also explored the effect of TACAN on WT TRPP2. Compared with mutant F604P, WT TRPP2 exhibited relative smaller unitary current and much smaller open probability, which is also consistent with quasi undetectable whole-cell currents mediated by WT TRPP2(Zheng et al., 2018c). Similar to TRPP2 F604P, the unitary current and open probability of WT TRPP2 were also inhibited by TACAN (Fig. 4-2B and C). Taken together, our data demonstrated that TACAN is an inhibitor of TRPP2.

Although TRPP2 itself has no mechano-sensing activity, it was reported that some interacting partners such as PKD1 and TRPV4 may serve to sense the mechanical force (Köttgen et al., 2008; Nauli et al., 2003). We wanted to determine whether TACAN modulates mechano sensitivity of TRPP2. While WT TRPP2 exhibited no response to the mechanical force, co-expression of TACAN appeared to confer some pressure dependence, as open probability increased with negative pressure in the -10 to -30 mm Hg range (Fig. 4-2D and E). In contrast, the unitary current at +80 mV remained independent of the pressure in the same range. In summary, our data showed that co-expression of TACAN allowed complex TRPP2/TACAN

gaining mechano-sensitivity through increasing the single-channel open probability, but not the unitary current.

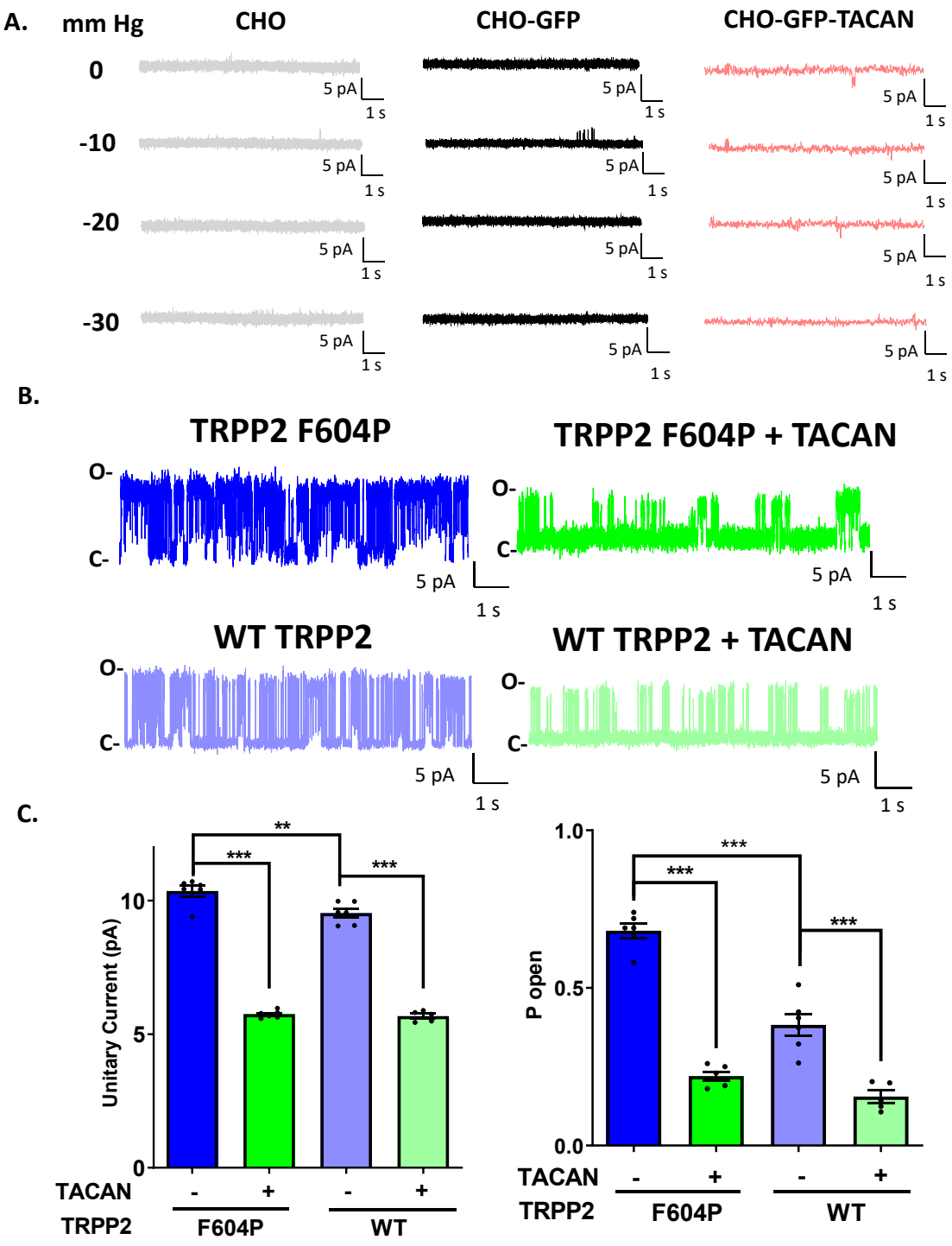
A.
mm Hg
CHO
CHO-GFP
CHO-GFP-TACAN
0
-10
-20
-30
5 pA
1 s
B.
TRPP2 F604P
TRPP2 F604P + TACAN
WT TRPP2
WT TRPP2 + TACAN
O-
C-
C.
Unitary Current (pA)
P open
TACAN
TRPP2
F604P
WT
**
***

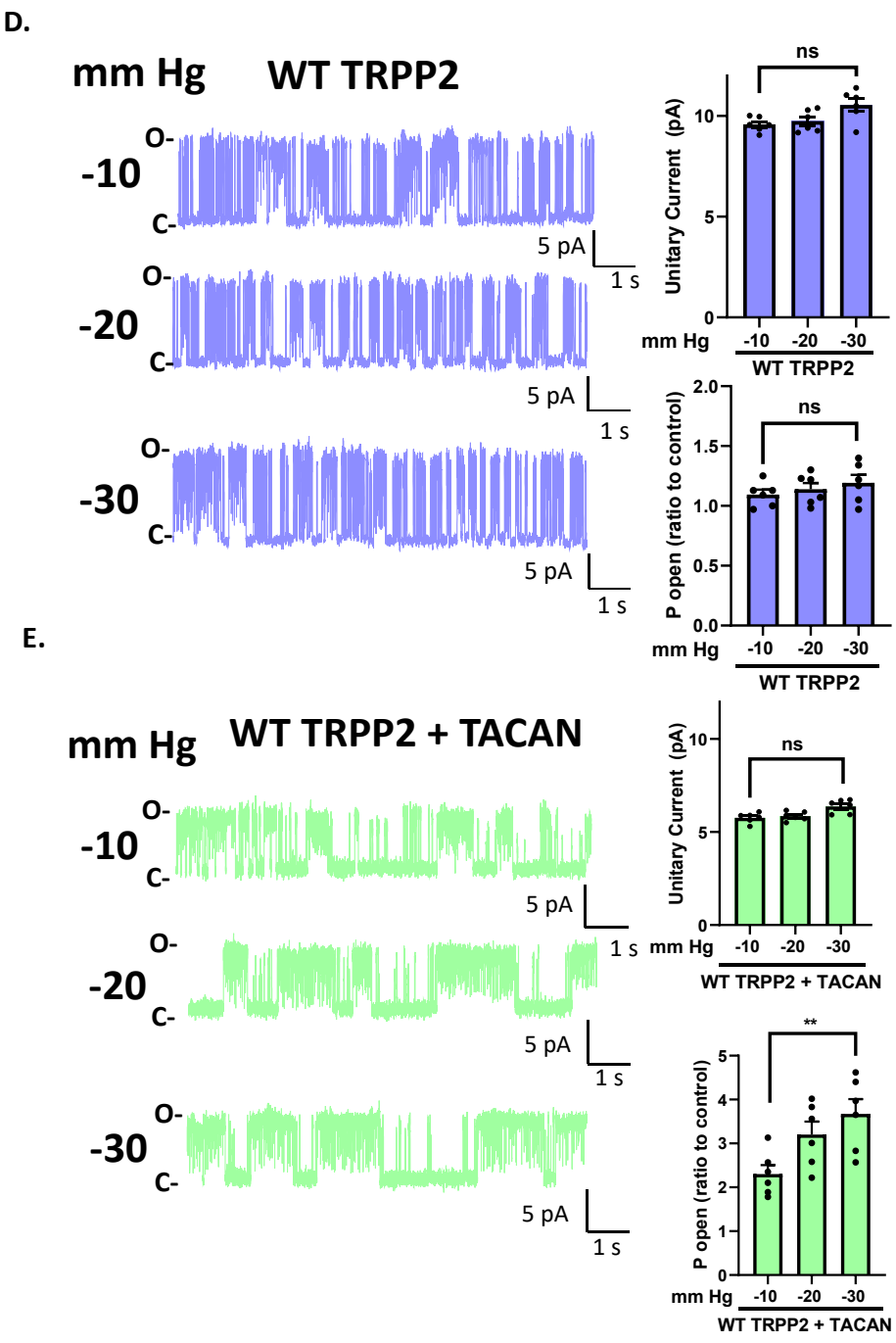

Figure 4-2. Functional regulation of TRPP2 by TACAN in CHO cells. A. Representative single channel recordings of non-transfected, GFP-transfected, and GFP-TACAN transfected CHO cells under the application of the indicated negative pressure. **B.** Representative single-channel recordings of CHO cells transfected with indicated proteins and voltage clamped at +80 mV. Symmetrical buffers (in mM: 140 NaCl, 5 KCl, 2 $CaCl_2$, 2 $MgCl_2$, 10 HEPES, 10 glucose,

and pH 7.4) were used in the pipette and bath. **C.** Effects of TACAN on the unitary current amplitudes and open probabilities of WT TRPP2 and mutant F604P. Data are presented as mean ± SEM. ** $p < 0.01$; *** $p < 0.001$. **D** and **E.** Left panel: representative single-channel recordings in CHO cells transfected with WT TRPP2 (**D**) or WT TRPP2 + TACAN (**E**) and voltage clamped at +80 mV showing the effect of negative pressure. Right panel: effect of pressure on the unitary current amplitudes and normalized open probabilities of WT TRPP2 (**D**) or WT TRPP2 + TACAN (**E**) under the application of the corresponding negative pressures. Data are presented as mean ± SEM. ns, not significant; ** $p < 0.01$.

Besides the inhibition of the F604P steady-state currents by TACAN, we noticed that TACAN induced modest inactivation of the F604P-mediated currents at depolarization (Fig. 4-3A). The decay in the current at +100 mV was associated with time constant (τ) of 33.8 ± 4.4 ms (N = 7) when fitted with an exponential (Fig. 4-3B). Interestingly, inactivation at depolarized voltages was present in TRPP2 GOF gate mutant L677G in the absence of TACAN (Fig. 4-3C). Unlike the F604P mutation, which locks TRPP2 in an activated configuration, the L677G mutation is proposed to directly enlarge the pore size, ie, the protein would still be in a basal configuration similar to WT TRPP2(Zheng et al., 2018c). Co-expression of TACAN did inhibit the steady-state currents of L677G while it did not further enhance the inactivation (Fig. 4-3D-F). These data together seemed to suggest that inactivation occurs when TRPP2 protein is in an inhibited (F604P+TACAN) or a basal state (L677G alone or L677G+TACAN) but not in an activated state (F604P alone).

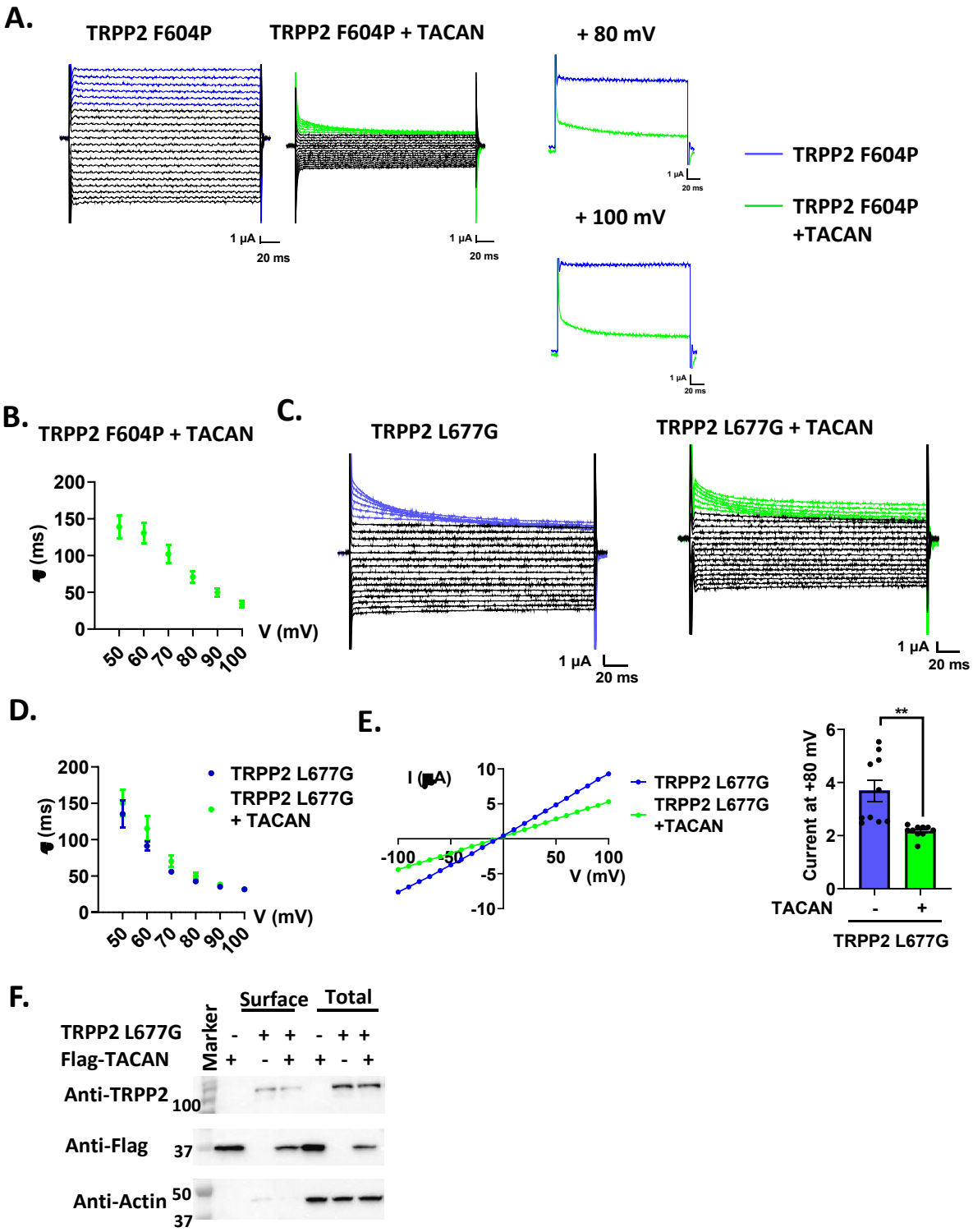

Figure 4-3. Effect of TACAN on inactivation of TRPP2-mediated currents in *Xenopus* oocytes. A. Representative recording traces for oocytes expressing TRPP2 F604P or TRPP2

F604P + TACAN. Traces obtained at +50 mV to +100 mV corresponding to TRPP2 F604P (blue) or TRPP2 F604P + TACAN (green) and superimposed traces of TRPP2 F604P and TRPP2 F604P + TACAN at +80 mV and +100 mV are indicated. **B.** Time constants (τ) of current decay for TRPP2 F604P + TACAN under the indicated voltages (+50 mV to +100 mV are shown). **C.** Representative recording traces of oocytes expressing TRPP2 L677G (left) or TRPP2 L677G + TACAN (right). Traces obtained at +50 mV to +100 mV corresponding to TRPP2 L677G (blue) or TRPP2 L677G + TACAN (green) are indicated. **D.** Time constants (τ) of current decay for TRPP2 L677G (blue) and TRPP2 L677G + TACAN (green) under the indicated voltages (+50 mV to +100 mV are shown). **E.** Left panel: Representative I-V curves from oocytes expressing TRPP2 L677G (blue) or L677G + TACAN (green). Right panel: Averaged currents at +80 mV obtained from oocytes expressing TRPP2 L677G (blue) or TRPP2 L677G + TACAN (green). Data are presented as mean ± SEM. ** $p < 0.01$. **F.** Representative Western blot analysis of the surface (biotinylated) and total proteins of TACAN, TRPP2 L677G or TRPP2 L677G + TACAN.

Physical interaction between TRPP2 and TACAN

To explore how TACAN inhibits TRPP2, we tested whether TACAN physically interacts with TRPP2. Indeed, TACAN co-immunoprecipitated WT TRPP2 and mutant F604P in oocytes and reversely, mutant F604P was able to precipitate TACAN (Fig. 4-4A-C), indicating that TRPP2 and TACAN are in the same complex in oocytes. We next used chemical cross-linking to examine the subunit stoichiometry of the TRPP2/TACAN complex. However, the complex could not be detected under our conditions although we successfully detected a dimeric TACAN dimers and different TRPP2 oligomers (Fig. 4-4D). The coiled-coil domain (amino-acid (aa) G9-L100) in the TACAN N-terminus was proposed to be important for oligomerization(Batrakou et al., 2015). Indeed, we found aggregation of the N-terminus in our chemical cross-linking experiments. Further, TACAN lacking the entire N-terminus still formed the dimer (Fig. 4-4E), indicating that the TACAN dimeric assembly is independent of its coiled-coil domain. Furthermore, we generated different fragments of TACAN, which is predicted to possess six TMs (S1-S6), to narrow down the domain(s) mediating physical and functional interaction with TRPP2 (Fig. 4-4F). By co-IP assays we found that TACAN fragments containing S1 (L135-T160) or S6 (L296-D343), but not the N-terminus (L135X), interacts with TRPP2 F604P (Fig.4-4G). Interestingly, the S6-containing fragment inhibited the F604P function while the S1-containing fragment exhibited no functional effect on mutant F604P (Fig. 4-4H).

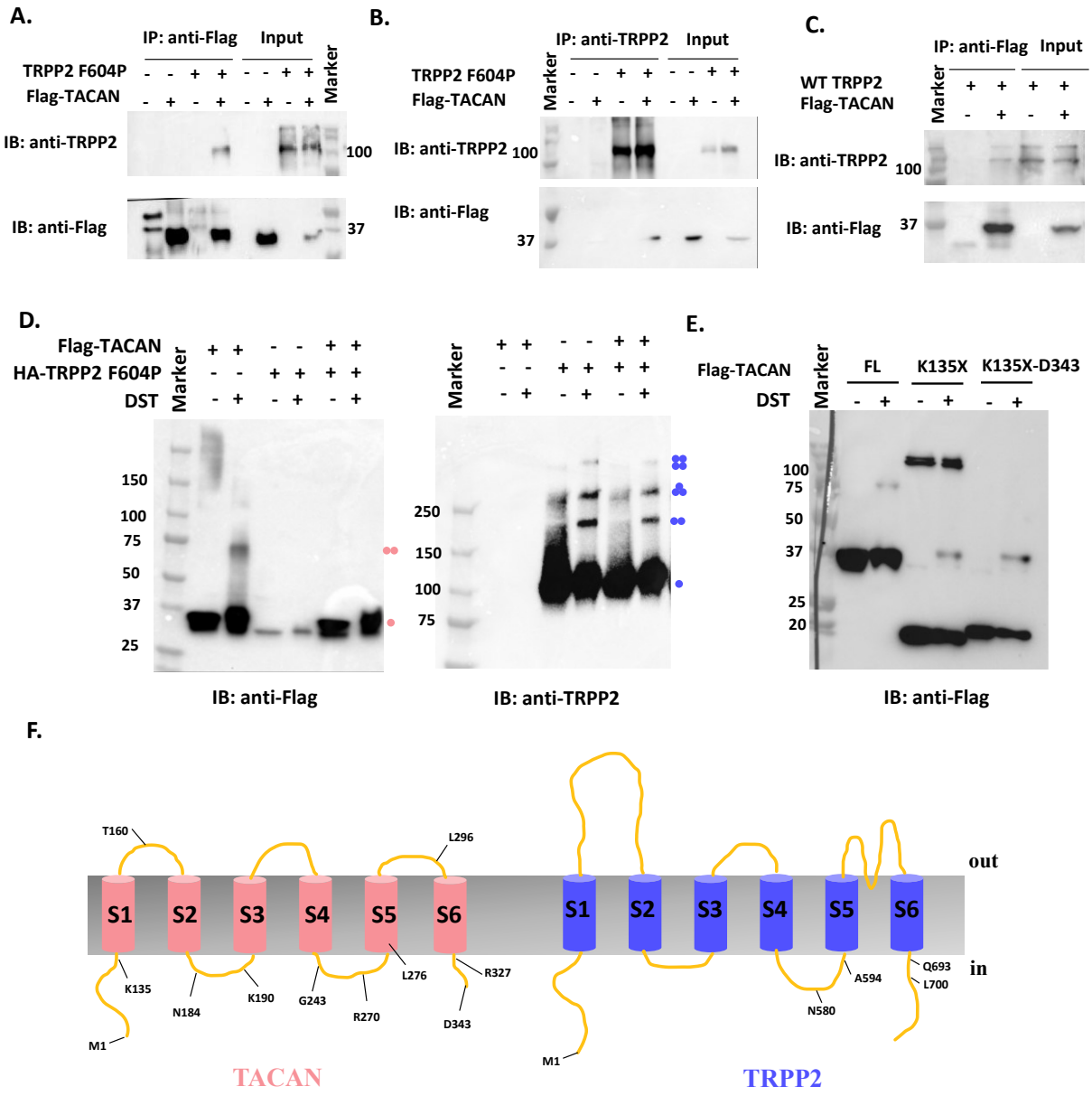
A.
IP: anti-Flag
Input
TRPP2 F604P
Flag-TACAN
Marker
IB: anti-TRPP2
100
IB: anti-Flag
37
B.
IP: anti-TRPP2
Input
TRPP2 F604P
Flag-TACAN
Marker
IB: anti-TRPP2
100
IB: anti-Flag
37
C.
IP: anti-Flag
Input
WT TRPP2
Flag-TACAN
Marker
IB: anti-TRPP2
100
IB: anti-Flag
37
D.
Flag-TACAN
HA-TRPP2 F604P
DST
Marker
150
100
75
50
37
25
IB: anti-Flag
250
150
100
75
IB: anti-TRPP2
E.
Flag-TACAN
DST
Marker
FL
K135X
K135X-D343
100
75
50
37
25
20
IB: anti-Flag
F.
T160
L296
S1
S2
S3
S4
S5
S6
out
in
K135
N184
K190
G243
L276
R270
R327
D343
M1
TACAN
S1
S2
S3
S4
S5
S6
A594
N580
Q693
L700
M1
TRPP2

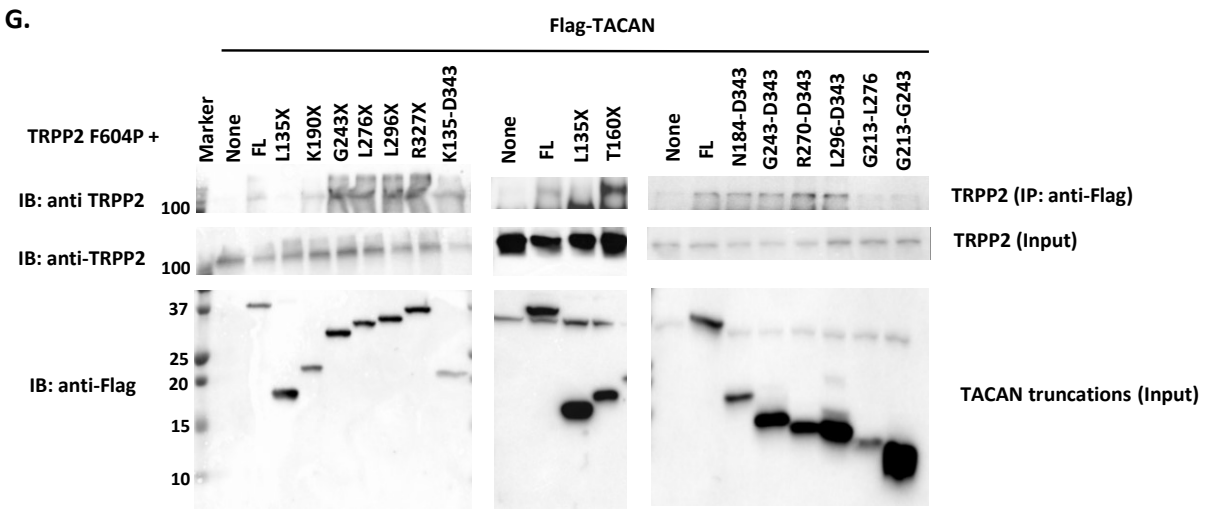
G.
Flag-TACAN
TRPP2 F604P +
Marker
None
FL
L135X
K190X
G243X
L276X
L296X
R327X
K135-D343
None
FL
L135X
T160X
None
FL
N184-D343
G243-D343
R270-D343
L296-D343
G213-L276
G213-G243
IB: anti TRPP2
100
IB: anti-TRPP2
100
IB: anti-Flag
37
25
20
15
10
TRPP2 (IP: anti-Flag)
TRPP2 (Input)
TACAN truncations (Input)

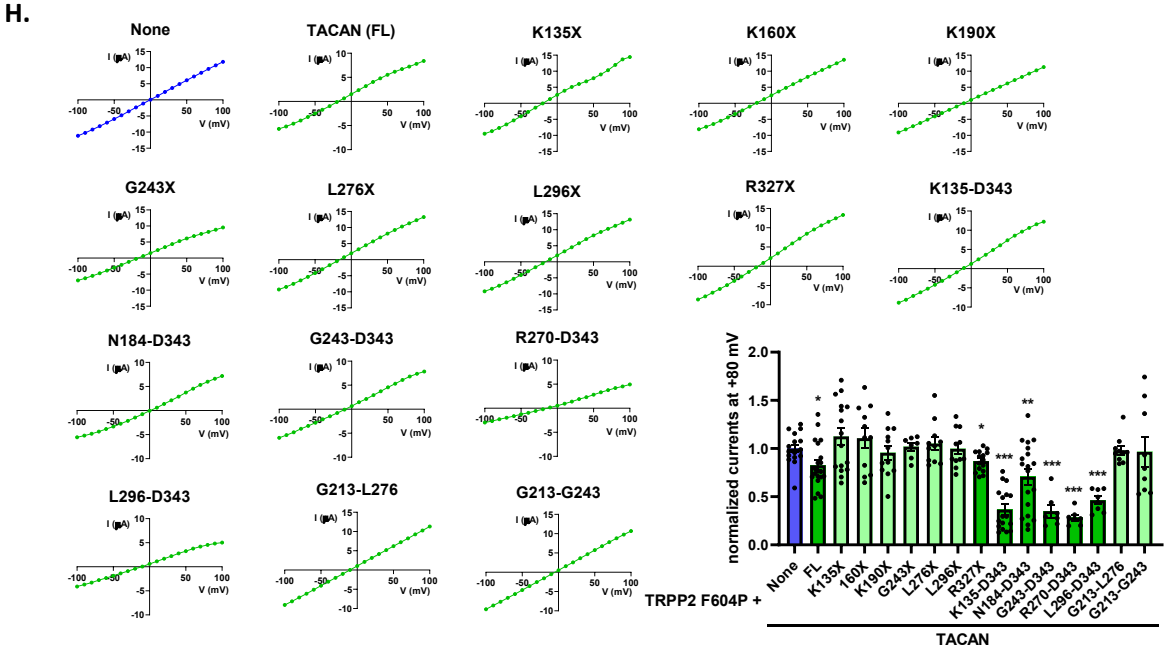
H.
None
TACAN (FL)
K135X
K160X
K190X
G243X
L276X
L296X
R327X
K135-D343
N184-D343
G243-D343
R270-D343
L296-D343
G213-L276
G213-G243
I (pA)
V (mV)
normalized currents at +80 mV
TRPP2 F604P +
None
FL
K135X
160X
K190X
G243X
L276X
L296X
R327X
K135-D343
N184-D343
G243-D343
R270-D343
L296-D343
G213-L276
G213-G243
TACAN

Figure 4-4. Domains in TACAN mediating association with TRPP2. A. Representative co-IP data showing the interaction between TRPP2 mutant HA-F604P and Flag-TACAN using Flag antibody for precipitation. **B.** Representative co-IP data showing the interaction between HA-F604P and Flag-TACAN using TRPP2 antibody for precipitation. **C.** Representative co-IP data showing interaction between WT HA-TRPP2 and Flag-TACAN using Flag antibody for precipitation. **D.** Western blot analysis after showing the cross-linking products of TACAN and TRPP2 F604P. Cross-linking was carried out with 1 mM disuccinimidyl tartrate (DST). The putative subunit composition of the bands is indicated. **E.** Western blot analysis after showing the cross-linking products of TACAN FL, K135X, K135X-D343. Cross-linking was carried out with 1 mM DST. **F.** The relative location of each specific key residue for the truncation mutant generation was indicated. **G.** Representative co-IP data showing the interaction between mutant HA-F604P and an indicated TACAN truncation mutant using Flag antibody for precipitation. **H.** Representative I-V curves and averaged currents at +80 mV in oocytes expressing TRPP2 mutant F604P with or without a TACAN truncation mutant. Data are presented as mean ± SEM. * $p < 0.05$; ** $p < 0.01$; *** $p < 0.001$.

Reversely, we next wanted to identify which part(s) in TRPP2 is involved in the interaction with TACAN. We performed co-IP experiments in CHO cells expressing TACAN together with the TRPP2 N-terminus (TRPP2N, M1-K215), C-terminus (TRPP2C, D682-V968), or TRPP2 lacking both the N- and C-termini (TRPP2TM, S209-K688). TRPP2TM but not TRPP2N or TRPP2C conferred interaction with full-length (FL) TACAN (Fig. 4-5A), which is not consistent with the previous proteomic screen study indicating that TACAN binds to the TRPP2 C-terminus (Sharif-Naeini et al., 2009).

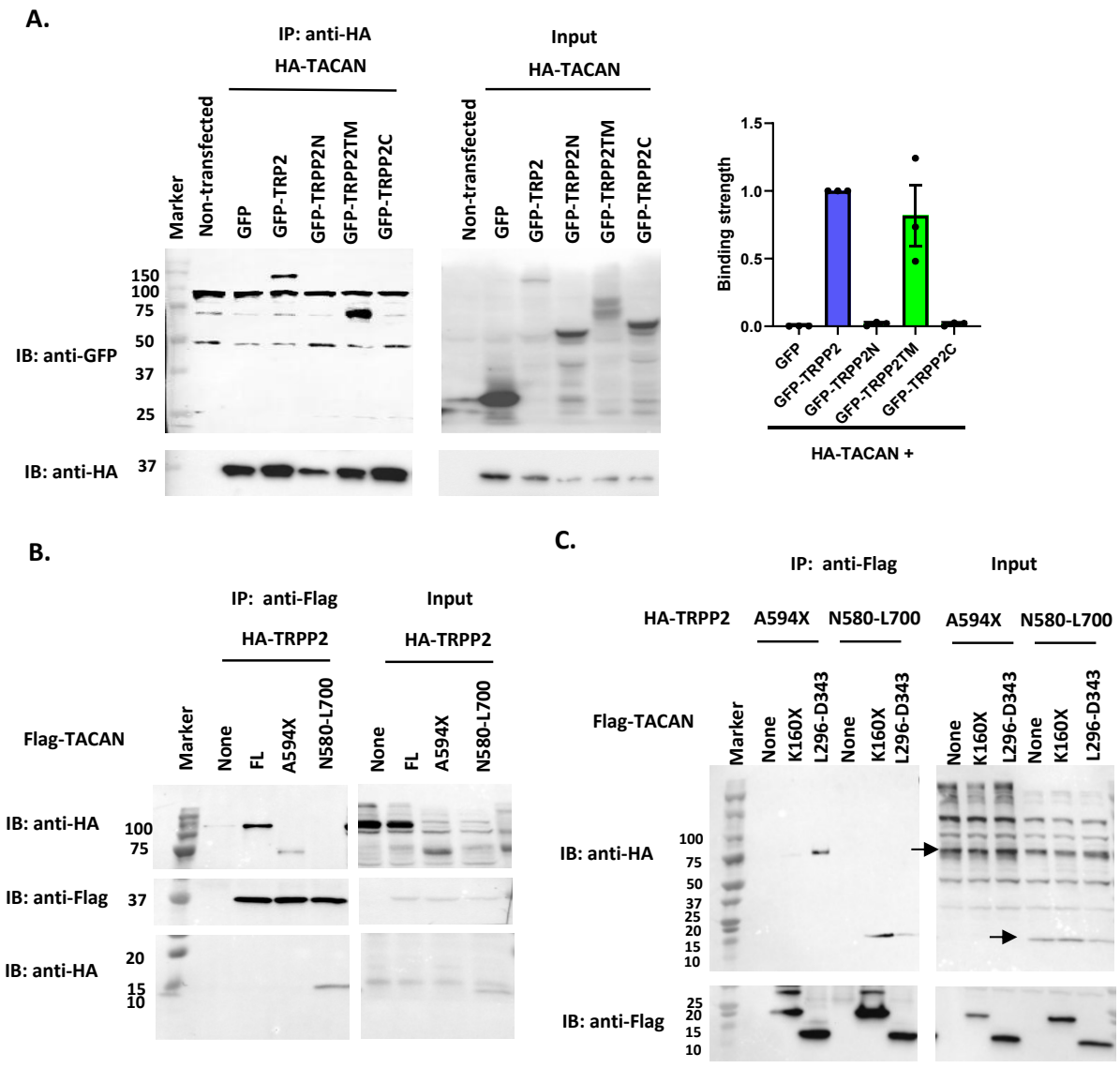

Figure 4-5. Domains in TRPP2 mediating association with TACAN. A. Left panel: representative co-IP data showing the interaction between GFP-TRPP2 and HA-TACAN using HA antibody for precipitation. Non-transfected and GFP-transfected CHO cell lysates served as negative control. Right panel: binding strength averaged from three independent experiments. **B.** Representative co-IP data showing the interaction between Flag-TACAN and a TRPP2 truncation mutant (A594X or N580-L700) using Flag antibody for precipitation. TRPP2

expressed in oocytes with or without co-expressed Flag-TACAN served as positive and negative controls, respectively. **C.** Representative co-IP data showing the interaction between TRPP2 mutant A594X and TACAN mutant L296-D343, and between TRPP2 mutant N580-L700 and TACAN mutant K160X using Flag antibody for precipitation. TRPP2 mutants A594X and N580-L700 alone served as negative controls, which were indicated by the arrow.

The TRPP2 pore domain is formed by S5, S5-S6 loop and S6 (A594-Q693) (Shen et al., 2016). We next examined whether TACAN participates in the pore formation in the TRPP2/TACAN channel complex. For this purpose, we tested whether TACAN interacts with truncation mutant A594X (no pore domain) or fragment N580-L700 containing the pore domain (Fig. 4-S3). Surprisingly, TACAN can interact with either of them (Fig. 4-5B), indicating that TRPP2 also contains at least two domains interacting with TACAN. Because the TACAN S1 and S6 interacted with TRPP2, we continued to narrow down the corresponding binding domains in TRPP2. We found by co-IP that TRPP2 A594X interacts with TACAN S6, while TRPP2 N580-L700 interacts with TACAN S1 (Fig. 4-5C). Since the interaction between S6 was functionally critical, it highly suggested that instead of acting as a pore-forming subunit, TACAN mainly binds at the peripheral domain (S1-S4) to regulate TRPP2 channel function.

TACAN was shown to be highly expressed in the kidney (Beaulieu-Laroche et al., 2020). We next wanted to check the subcellular localization of TACAN. For this, we performed double immunofluorescence assays to determine the subcellular localization of TACAN and TRPP2 in epithelia Madin-Darby Canine Kidney (MDCK), inner medullary collecting duct (IMCD), and Lilly Laboratories Cell-Porcine Kidney 1 (LLC-PK1) cell lines. We found that the endogenous TRPP2 and TACAN both display enhanced staining in the primary cilia in all three cell lines (Fig. 4-6A), indicating a similar distribution of the two proteins. To document their interaction in vivo, we performed co-IP experiments using native MDCK, IMCD, and LLC-PK1 cell lines. TRPP2 was detected in the immunoprecipitates of all cells with an anti-TMEM120A antibody, but not in the control (Fig. 4-6B), demonstrating that TRPP2 interacts with TACAN in vivo.

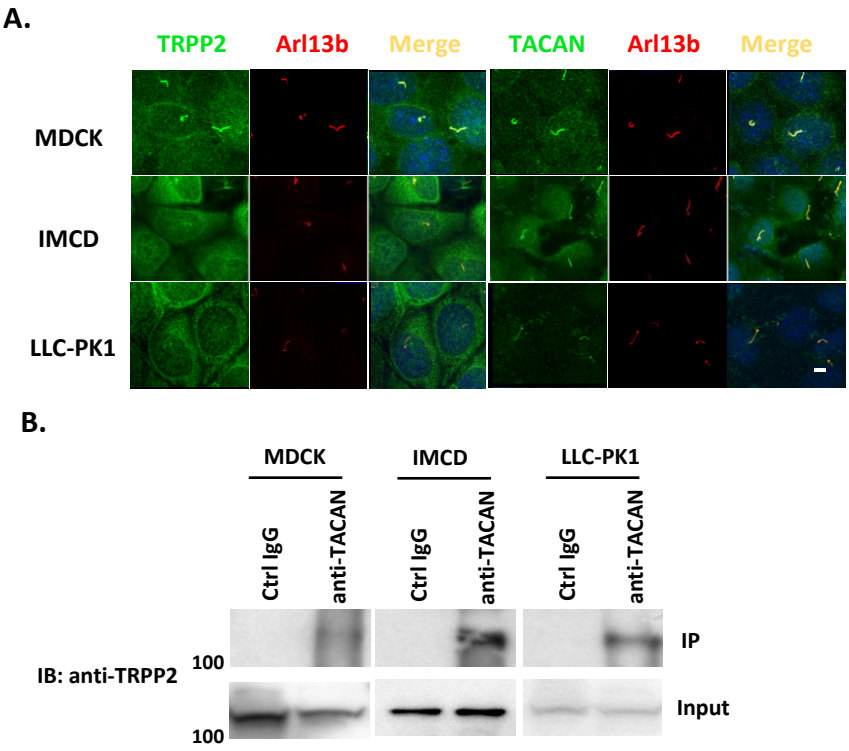

Figure 4-6. Interaction and colocalization of endogenous TRPP2 and TACAN in renal cell lines. A. Subcellular localization of endogenous TRPP2 and TACAN in MDCK, IMCD and LLC-PK1 cells by means of IF. Arl13b served as a primary cilia marker. Scale bar, 5 μm. **B.** Representative co-IP data showing association between endogenous TRPP2 and TACAN in MDCK, IMCD and LLC-PK1 cells.

Regulation of the TRPP2 function in zebrafish by TACAN

We next wanted to examine the role of TACAN in the regulation of TRPP2 in vivo. TRPP2 knockdown in zebrafish is associated with the presence of tail curvature and pronephric cysts resembling renal cysts in mammals (Zheng et al., 2018c). We previously showed that the injection of human TRPP2 morpholino oligonucleotide (MO) into zebrafish embryos induces tail curling in zebrafish at 3 days post fertilization (dpf)(Zheng et al., 2016a). We wondered whether TACAN overexpression in the zebrafish embryos might also lead to the tail curvature phenotype. Here, we found that the injection of TACAN mRNA induces the tail curvature of the zebrafish. Further, TRPP2 MO and TACAN mRNA co-injection significantly increased the occurrence of tail curling induced by TRPP2 MO knockdown (Fig. 4-7A and B), indicating that TACAN further inhibits TRPP2 channels, consistent with our results using cell models (Fig. 4-1A and B, and 4-2A and B). Taken together, our data demonstrated that TACAN regulates TRPP2-dependent disease phenotypes in larval zebrafish, presumably through repressing the TRPP2 channel function.

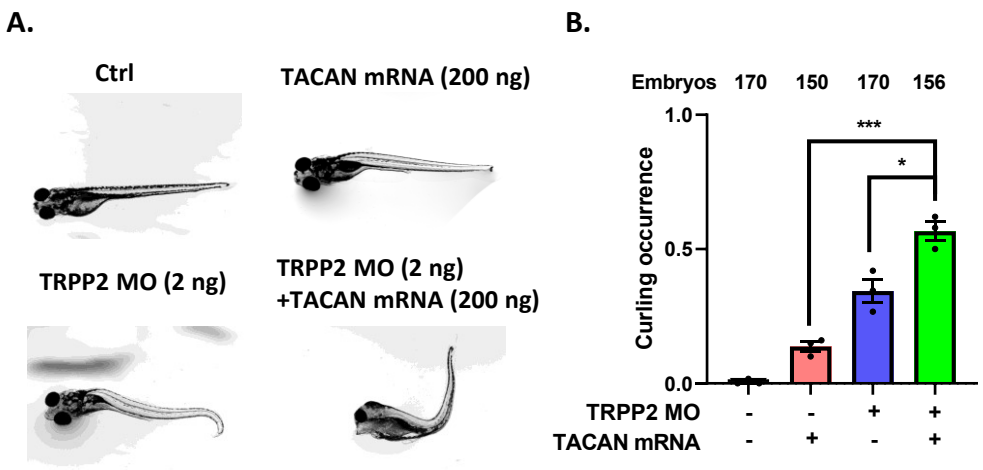

Figure 4-7. Effect of TACAN overexpression on the tail curling of larval zebrafish. A. Representative pictures showing tails of 3 dpf zebrafish with injection of water (ctrl), TACAN mRNA, TRPP2 MO, or both TRPP2 MO + TACAN mRNA within 1 h postfertilization. **B.** Average percentages of fish having a curled tail under different conditions. Data were from three independent experiments with the indicated total numbers of embryos. *P < 0.05; ***P < 0.001.

4.5 DISCUSSION

TACAN is a transmembrane protein that is evolutionally conserved and was recently reported to be an ion channel involved in sensing mechanical stimuli(Beaulieu-Laroche et al., 2020). TACAN is predicted to possess six TM domains, with intracellular N- and C-termini. Its N-terminal coil-coiled domain (aa G9-L100) was reported to be important for oligomerization (Batrakou et al., 2015), consistent with our cross-linking results showing that deletion of the N-terminal significantly reduced the amount of dimers (Fig. 4-4F). However, the fact that TACAN dimers were still present in the absence of the N-terminus indicates the presence of another domain important for dimerization. Interestingly, there is also a coil-coiled domain in the TRPP2 (and TRPP3 as well) C-terminus, which is important for the interaction with PKD1(Qian et al., 1997; Tsiokas et al., 1997; Yu et al., 2009) and was proposed to be critical for interaction with TACAN(Sharif-Naeini et al., 2009). However, recent cryo-EM structures of homotetrameric TRPP2(Shen et al., 2016), TRPP3(Su et al., 2018b) and heterotetrameric PKD1/TRPP2 complex(Su et al., 2018a) in the absence of the TRPP2 or TRPP3 coiled-coil domain demonstrate that the coiled-coil domain is not required for oligomerization of these TRPP channels. Consistently, TM domains (S1 and S6) but not the N- or C-terminus of TACAN were involved in interaction with TRPP2.

While homotetrameric organization of TRPP2 has been confirmed by its structures revealed by means of cryo-EM, it was also reported to heteromerize with PKD1 and other TRP channels including TRPC1, -C3, -C4, -C7 and -V4(Cheng et al., 2010; Grieben et al., 2017; Shen et al., 2016) TRPP2 homo-and heterotetrameric channels have distinct biophysical properties as well as distinct subcellular localizations(Cheng et al., 2010). One of the physiologically most important TRPP2 channel complexes is PKD1/TRPP2 in which defects are associated with

ADPKD(Su et al., 2018a). While it is well known PKD1 promotes the plasma membrane trafficking of TRPP2, studies on its role in the biophysical properties of the PKD1/TRPP2 channel complex only started recently(Wang et al., 2019; Ha et al., 2020). PKD1/TRPP2 channel complex in primary cilia of renal epithelial cells was previously shown to mediate mechano sensing through modulating Ca^{2+}-dependent currents(Nauli et al., 2003) but subsequent studies found that the currents are PKD1-independent(Liu et al., 2018). The TRPP2/TRPC4 complexing in the primary cilia of MDCK cells was found to be involved in flow sensing but even the role of primary cilia in mechano sensing is debatable(Köttgen et al., 2008; Delling et al., 2016). Even the involvement of mammalian TRP channels in mechano sensing has been questioned(Nikolaev et al., 2019). In our current study we found that TRPP2 alone does not confer mechano sensitivity and that the mechano sensitivity of the TRPP2/TACAN channel complex is mediated by TACAN (Fig. 4-3C). It will be interesting to investigate whether TACAN is relevant to ADPKD.

TMEM120B, as a homologue of TACAN (TMEM120A, 70.5% identity), is generated as a result of gene duplication in mammals. However, TMEM120B has different properties from those of TACAN; for example, expression of TACAN, but not TMEM120B, in CHO cells was found to induce mechano-sensitive currents (Beaulieu-Laroche et al., 2020). TACAN, but not TMEM120B, was reported to inhibit Piezo2 (Del Rosario et al., 2021). It will be of interest to determine whether TMEM120B regulates TRPP2 as TACAN does.

Since TACAN acted an inhibitor of TRPP2 and colocalized with TRPP2 in the primary cilia of different renal cells, we explored whether it exacerbates the TRPP2-dependent cystogenesis. Using the tail curling phenotype in zebrafish as a readout to examine the functional implications of the regulation of TRPP2 by TACAN, we found significant increased tail curling

occurrences of TACAN on TRPP2-dependent tail curling. Interestingly, it was reported that TMEM33, an activator of TRPP2, which forms a complex in the endoplasmic reticulum (ER) membrane, but not in the primary cilia, show no impact on the TRPP2-dependent renal cystogenesis(Arhatte et al., 2019). These findings further indicates that primary cilia TRPP2 is directly related to ADPKD, but not TRPP2 in the ER, and that TRPP2 and TACAN might also form a complex in the primary cilia.

The conclusion that TACAN acts as an ion channel has been challenged by recent structural and functional studies (Beaulieu-Laroche et al., 2020; Del Rosario et al., 2021; Ke et al., 2021; Niu et al., 2021; Parpaite et al., 2021; Rong et al., 2021; Xue et al., 2021). Based on its involvement in regulation of the expression of different proteins including Ca^{2+} ATPase, ATP2a1 and TMEM150C, a general regulator of mechano-sensitive channels such as Piezo1, Piezo2, and the potassium channel TREK-1(Anderson et al., 2018), it was indicated that TACAN is involved in regulating ion transport. Thus, it would be helpful to examine whether TACAN up-regulates the expression or activities of an ion channel, but this can not explain the reported channel activity of purified TACAN reconstituted in lipid bilayers(Beaulieu-Laroche et al., 2020), which was strongly challenged by recent reports(Ke et al., 2021; Niu et al., 2021; Rong et al., 2021; Xue et al., 2021). Structural studies found that TACAN resembles the structure of long-chain fatty acid elongase 7 (ELOVL 7)(Ke et al., 2021; Niu et al., 2021; Rong et al., 2021; Xue et al., 2021). TACAN was then found to be an inhibitor of Piezo2, but not Piezo1 or TREK-1, with an unclear mechanism of inhibition(Del Rosario et al., 2021). Our present study found that TACAN inhibits the TRPP2 function through physical association of the TACAN-S6 helix with TRPP2 S1-S4 domain. It is therefore unlikely that TACAN participates in the pore formation in the TRPP2/TACAN channel complex since TACAN-S6 still exhibited an inhibitory

effect (Fig. 4-4H). It will be interesting to determine whether TACAN inhibits the Piezo2 function through a similar mechanism.

In this study, we demonstrated that TACAN inhibits TRPP2 through decreasing both the single channel conductance and open probability and through physical association between them. We found that the TACAN S6 associates with S1-S4 of TRPP2 and that the TACAN S1 associates with S5-S6 of TRPP2. The TACAN-S6/TRPP2-S1-S4, but not the TACAN-S1/TRPP2-S5-S6, association was functionally important. We demonstrated that TACAN is localized in the primary cilia of MDCK, IMCD and LLC-PK1 renal cell lines. In line with these findings, we found that TACAN affects TRPP2-dependent disorders in larval zebrafish, indicating the presence of this regulation *in vivo*.

CHAPTER 5

GENERAL DISCUSSION

5.1 Intramolecular interactions in TRPV6 and PIP2 regulation mechanism

Most members in the TRP channel superfamily have been reported to be regulated by PIP2. However, the effect of PIP2 varies (Rohacs, 2014). TRPV1 was originally reported to be inhibited by PIP2 (Prescott and Julius, 2003). However, it was challenged by a following study in a different experimental condition (Stein et al., 2006). It was further supported by the finding that PIP2 enhances the regulation of TRPV1 by Pirt, a positive regulator of TRPV1. The important roles of PIP2 have also been implicated in other ion channels. For instance, PIP2 stimulates TRPM4, M5, M8 and V5 possibly through suppression of desensitization, while it inhibits TRPC channels (Numata et al., 2011). Since PIP2 is coupled with the PLC pathway, downstream molecules DAG (diacyl glycerol) and IP3 (inositol 1,4,5 triphosphate) also complicate interpretation of studies of these regulatory mechanisms (Hardie, 2004). For PIP2 direct regulation, we previously identified that PIP2 disrupts the intramolecular N/C interactions in TRPP2 and TRPP3 to inhibit channel activity, showing that the N/C interaction is essential for the channel function. However, we also found that PIP2 enhances N/C interactions of TRPV1 and TRPM8, which is consistent with the activation effect of PIP2 on these two channels (Zheng et al., 2018a). Experiments on these four channels demonstrated that disrupting the N/C interaction results in decreased channel function, which is consistent with the functional regulation by PIP2. Here in Chapter 2, we found that PIP2 disrupts the N/C and L/C interactions in TRPV6 thereby substantially increasing the channel function. These data indicated a shared PIP2 regulation mechanism on TRP channel gating. It remains unclear as to how PIP2 affects these intramolecular interactions. Future structural resolution of TRP channels in complex with PIP2 may help answering to the question.

5.2 Calcium and TRPP3

TRPP3 was cloned in 1999 and was found to be a Ca^{2+}-activated and Ca^{2+} permeable non-selective cation channel when expressed in *Xenopus* oocytes (Chen et al., 1999). Since then, how Ca^{2+} regulates TRPP3 has been further explored but the underlying mechanism of regulation has remained unclear. Intracellular Ca^{2+} increases due to TRPP3-mediated Ca^{2+} entry must be necessary for the Ca-induced channel activation because pre-loading of the Ca^{2+} chelator EGTA abolished the activation (Chen et al., 1999; DeCaen et al., 2016) Meanwhile, several inactivation processes would be triggered, including Ca^{2+} activated PLC pathway and CaM/CaMK2 pathway we identified. Direct Ca^{2+} inhibition on TRPP3 has also been proposed by another group (DeCaen et al., 2016). So far, it is still unclear how Ca^{2+} activates TRPP3. Reported Ca^{2+} activation on TRP channels include TRPM2 (Huang et al., 2018), M4 (Autzen et al., 2018) and TRPM8 (Diver et al., 2019). A Ca^{2+} binding site is formed by several negative charged residues in S2 and S3 of these ion channels. Interestingly, these residues are also conserved in TRPP3, indicating that the role of Ca^{2+} activation could be shared. Mutations at those negatively charged residues may render TRPP3 Ca^{2+} unresponsive. So far, the solved TRPP3 structure appears to be in an open configuration (Su et al., 2018b). Mutated TRPP3 with decreased Ca^{2+} binding affinity might result in a closed conformation, which will better illustrate the relationship between Ca^{2+} and TRPP3.

5.3 Functional role of TACAN

TACAN was initially found to be localized in the nuclear envelope and important in adipocyte differentiation (Batrakou et al., 2015). It was then found to be expressed on the plasma membrane of neurons and proposed to act as a mechano-sensitive ion channel involved in pain

sensing (Beaulieu-Laroche et al., 2020). However, the statement that TACAN acts as a pore-forming ion channel has been challenged recently by functional and structural studies (Niu et al., 2021; Rong et al., 2021; Xue et al., 2021). The functional studies failed to generate channel activity and the structural studies found that TACAN proteins form tightly packed dimers that may rather act as an enzyme for fatty acid metabolism due to its similarity to very long-chain fatty acid elongase 7 (ELOVL7). Also, TACAN can be co-purified with CoA based on mass spectrometry analyses, suggesting the possibility that CoA acts as a substrate. However, MacKinnon group found no enzymatic activity using TACAN in assays in the absence of CoA, arguing physiological relevance of the TACAN/CoA association (Niu et al., 2021). Thus, the physiological role of TACAN remains elusive although it appears unlikely that TACAN is a pore forming ion channel. Our present study found that TACAN acts as a binding partner of TRPP2 and thereby represses the TRPP2's channel activity and confers the mechano sensitivity of the TRPP2/TACAN channel complex.

5.4 Future directions

In Chapter 2, we identified that PIP2 regulates TRPV6 by disrupting the intramolecular L/C and N/C interactions thereby substantially enhancing the channel function. We previously also reported the functional importance of and the regulatory role of PIP2 in the N/C interaction in TRPP2, -P3, -V1 and -M8 (Zheng et al., 2018a). Since the Pre-S1, S4-S5 and TRP domains are highly conserved across the TRP channels (Vangeel and Voets, 2019), it would be interesting to explore whether this PIP2/intramolecular interaction regulatory axis is shared by other TRP channels. Because TRP channels are involved in different human diseases, elucidating the involvement of this regulatory axis would be clinically and therapeutically relevant. For

example, blocking peptides that disrupt PIP2/TRP association may represent a first step towards drug discovery as they would interfere with TRP channel function affected either by pathogenic mutations or by altered expression.

It was proposed that Ca^{2+} blocks the pore domain to initiate long-term inhibition (DeCaen et al., 2016) and our current study (Chapter 3) revealed the inhibitory effect of CaM on the Ca^{2+}-induced activation TRPP3, but how Ca induces TRPP3 activation has remained unknown. Structures resolved by recent cryo-EM studies show that the negatively charged residues in S2 and S3 form a Ca^{2+} binding site (Huang et al., 2018; Autzen et al., 2018; Diver et al., 2019). The corresponding residues in TRPP3 are also conserved and thus it will be interesting to determine whether Ca^{2+} binding to these residues plays a central role in the TRPP3 activation. So far, the physiological function of TRPP3 is not fully understood. Although TRPP3 knockout mice show decreased sour tasting response (Horio et al., 2011) and mild intestinal development abnormality (Delling et al., 2013), the disease relevance is still debatable. It would be interesting to investigate its physiological function using mice with knock-in of a GOF mutant of TRPP3. We here proposed that TRPP3 could be the target of CaMK2 through pharmacological and mutational studies, no direct evidence has been shown. Further *in vitro* phosphorylation assay or mass spectrometry assay are needed to verify this.

Although TACAN was reported to be localized at the nuclear envelope and to be an ion channel on the plasma membrane (Beaulieu-Laroche et al., 2020), subsequent studies render its ion channel function controversial (Niu et al., 2021; Rong et al., 2021; Xue et al., 2021). Thus, further functional characterizations and structural studies would be helpful to elucidate its biophysical and physiological functions. To follow up with our finding about a mechano-sensing role of TACAN (Chapter 4), together with the proposal that the TRPP2/TRPV4 channel complex

be involved in the flow-induced Ca^{2+} entry in MDCK cells (Köttgen et al., 2008), it will be interesting to investigate the physiological relevance of this increased mechano sensitivity. Another interesting question is to determine the potential stoichiometry of TRPP2/TACAN complex, for which our cross-linking experiments failed. Further, it will also be interesting to examine possible involvement of TACAN in ADPKD *in vivo* because TACAN and TRPP2 are colocalized in primary cilia that have been shown to play critical roles in various types of PKD. And the confirmation of this regulation mechanism in vivo.

5.5 Limitations of the studies

In this thesis, we mainly used *Xenopus* oocytes as an expression model to functionally characterize TRPV6, TRPP3 and TRPP2. Since there are a limited number of ion channels or receptors expressed in oocytes, exogenously expressed ion channels are studied with a relatively clean background. On the other hand, as oocytes are quite distant from human cells also used mammalian cells to study regulation of TRPP2 by TACAN and intramolecular interactions in TRPV6. However, mammalian cell lines are not suitable models for illustrating disease phenotypes. To explore the clinic relevance of the regulation of TRP channels we considered using animal models. TRPV6 knockout mice were reported to demonstrate significant destruction of bone microarchitecture, indicating that TRPV6 plays a critical role in bone homeostasis (Chen et al., 2014). Given the time-consuming genetic manipulations in mice, we choose *in vivo* zebrafish models which allowed us to easily and rapidly alter the TRPV6 expression and observe the resulting bone formation phenotypes. Further experiments are needed to control the amount of mRNA, although we inject the same amount of WT TRPV6 mRNA or mutant forms. By similar reasons zebrafish has also been used to model disease phenotypes

associated with defective TRPP2 and was used by us to study regulation of TRPP2 by TACAN. However, as zebrafish has a highly simplified kidney system, it would be important in the future to use a more *in vivo* model such as mouse to determine the role of TACAN in regulating TRPP2-associated cystic phenotypes. On the other hand, as the disease phenotype associated with altered TRPP3 has been unclear or controversial in mice we have yet to find a suitable *in vivo* model to study regulation of TRPP3 by CaM and CaMK2.

We examined protein-protein interactions (intramolecular interactions in TRPV6, CaM/TRPP3 and TACAN/TRPP2) by co-IP experiments which, however, can't tell whether the two proteins or peptides directly bind with each other. We thus also performed GST pull-down experiments to further document the interactions and to determine whether an interaction is through direct binding. However, we are aware that they are only of semi-quantitative methods for characterizing the strength of a protein-protein interaction. In Chapter 2 we also utilized blocking peptides to interfere with protein interactions. Because blocking peptides may induce unknown structural changes to the two interacting proteins or protein fragments, we also used negative controls (mutant blocking peptides with only one point mutation) to verify the specificity of the action of a blocking peptide.

We utilized whole-cell immunofluorescence to show the plasma membrane localization of TRP channels. As this is not a quantitative method, we also performed biotinylation assays to quantify the surface membrane localization. However, a biotinylation assay depends largely on the interaction between protein potions facing the extracellular environment and biotin but some reactive sites may be occluded due to the conformational changes induced by low temperature during the experiment. Thus, an additional labeling method would be helpful for characterizing the surface expression of proteins.

6. REFERENCES

Alberdi, A., Gomis-Perez, C., Bernardo-Seisdedos, G., Alaimo, A., Malo, C., Aldaregia, J., Lopez-Robles, C., Areso, P., Butz, E., Wahl-Schott, C.*, et al.* (2015). Uncoupling PIP2-calmodulin regulation of Kv7.2 channels by an assembly destabilizing epileptogenic mutation. J Cell Sci *128*, 4014-4023.

Anderson, E.O., Schneider, E.R., Matson, J.D., Gracheva, E.O., and Bagriantsev, S.N. (2018). TMEM150C/Tentonin3 Is a Regulator of Mechano-gated Ion Channels. Cell Rep *23*, 701-708.

Arhatte, M., Gunaratne, G.S., El Boustany, C., Kuo, I.Y., Moro, C., Duprat, F., Plaisant, M., Duval, H., Li, D., Picard, N.*, et al.* (2019). TMEM33 regulates intracellular calcium homeostasis in renal tubular epithelial cells. Nat Commun *10*, 2024.

Arif Pavel, M., Lv, C., Ng, C., Yang, L., Kashyap, P., Lam, C., Valentino, V., Fung, H.Y., Campbell, T., Møller, S.G.*, et al.* (2016). Function and regulation of TRPP2 ion channel revealed by a gain-of-function mutant. Proc Natl Acad Sci U S A *113*, E2363-2372.

Autzen, H.E., Myasnikov, A.G., Campbell, M.G., Asarnow, D., Julius, D., and Cheng, Y. (2018). Structure of the human TRPM4 ion channel in a lipid nanodisc. In Science, pp. 228-232.

Baik, J.Y., Park, E.Y.J., and So, I. (2020). Ca(2+)/calmodulin-dependent regulation of polycystic kidney disease 2-like-1 by binding at C-terminal domain. Korean J Physiol Pharmacol *24*, 277-286.

Bassi, M.T., Manzoni, M., Monti, E., Pizzo, M.T., Ballabio, A., and Borsani, G. (2000). Cloning of the gene encoding a novel integral membrane protein, mucolipidin-and identification of the two major founder mutations causing mucolipidosis type IV. Am J Hum Genet *67*, 1110-1120.

Bate, N., Caves, R.E., Skinner, S.P., Goult, B.T., Basran, J., Mitcheson, J.S., and Vuister, G.W. (2018). A Novel Mechanism for Calmodulin-Dependent Inactivation of Transient Receptor

Potential Vanilloid 6. Biochemistry *57*, 2611-2622.

Batrakou, D.G., de Las Heras, J.I., Czapiewski, R., Mouras, R., and Schirmer, E.C. (2015). TMEM120A and B: Nuclear Envelope Transmembrane Proteins Important for Adipocyte Differentiation. PLoS One *10*, e0127712.

Bautista, D.M., Jordt, S.E., Nikai, T., Tsuruda, P.R., Read, A.J., Poblete, J., Yamoah, E.N., Basbaum, A.I., and Julius, D. (2006). TRPA1 mediates the inflammatory actions of environmental irritants and proalgesic agents. Cell 124, 1269-1282.

Beaulieu-Laroche, L., Christin, M., Donoghue, A., Agosti, F., Yousefpour, N., Petitjean, H., Davidova, A., Stanton, C., Khan, U., Dietz, C.*, et al.* (2020). TACAN Is an Ion Channel Involved in Sensing Mechanical Pain. Cell *180*, 956-967.e917.

Beck, A., Speicher, T., Stoerger, C., Sell, T., Dettmer, V., Jusoh, S.A., Abdulmughni, A., Cavalie, A., Philipp, S.E., Zhu, M.X.*, et al.* (2013). Conserved gating elements in TRPC4 and TRPC5 channels. J Biol Chem *288*, 19471-19483.

Ben-Johny, M., Dick, I.E., Sang, L., Limpitikul, W.B., Kang, P.W., Niu, J., Banerjee, R., Yang, W., Babich, J.S., Issa, J.B.*, et al.* (2015). Towards a Unified Theory of Calmodulin Regulation (Calmodulation) of Voltage-Gated Calcium and Sodium Channels. Curr Mol Pharmacol *8*, 188-205.

Ben Johny, M., Yang, P.S., Bazzazi, H., and Yue, D.T. (2013). Dynamic switching of calmodulin interactions underlies Ca2+ regulation of CaV1.3 channels. Nat Commun *4*, 1717.

Bergmann, C., Guay-Woodford, L.M., Harris, P.C., Horie, S., Peters, D.J.M., and Torres, V.E. (2018). Polycystic kidney disease. Nat Rev Dis Primers *4*, 50.

Bernal, L., Sotelo-Hitschfeld, P., König, C., Sinica, V., Wyatt, A., Winter, Z., Hein, A., Touska, F., Reinhardt, S., Tragl, A.*, et al.* (2021). Odontoblast TRPC5 channels signal cold pain in teeth.

Sci Adv *7*.

Bhardwaj, R., Lindinger, S., Neuberger, A., Nadezhdin, K.D., Singh, A.K., Cunha, M.R., Derler, I., Gyimesi, G., Reymond, J.L., Hediger, M.A.*, et al.* (2020). Inactivation-mimicking block of the epithelial calcium channel TRPV6. Sci Adv *6*.

Bianco, S.D., Peng, J.B., Takanaga, H., Suzuki, Y., Crescenzi, A., Kos, C.H., Zhuang, L., Freeman, M.R., Gouveia, C.H., Wu, J.*, et al.* (2007). Marked disturbance of calcium homeostasis in mice with targeted disruption of the Trpv6 calcium channel gene. In J Bone Miner Res, pp. 274-285.

Bolanz, K.A., Hediger, M.A., and Landowski, C.P. (2008). The role of TRPV6 in breast carcinogenesis. Mol Cancer Ther *7*, 271-279.

Bourinet, E., Altier, C., Hildebrand, M.E., Trang, T., Salter, M.W., and Zamponi, G.W. (2014). Calcium-permeable ion channels in pain signaling. Physiol Rev 94, 81-140.

Bousova, K., Jirku, M., Bumba, L., Bednarova, L., Sulc, M., Franek, M., Vyklicky, L., Vondrasek, J., and Teisinger, J. (2015). PIP2 and PIP3 interact with N-terminus region of TRPM4 channel. In Biophys Chem, pp. 24-32.

Braun, A.P., and Sy, L. (2001). Contribution of potential EF hand motifs to the calcium-dependent gating of a mouse brain large conductance, calcium-sensitive K(+) channel. J Physiol *533*, 681-695.

Busin, M., Yau, C.W., Avni, I., and Kaufman, H.E. (1986). Comparison of K-Sol and M-K medium for cornea storage: results of penetrating keratoplasty in rabbits. Br J Ophthalmol *70*, 860-863.

Cai, R., Liu, X., Zhang, R., Hofmann, L., Zheng, W., Amin, M.R., Wang, L., Hu, Q., Peng, J.B., Michalak, M.*, et al.* (2020). Autoinhibition of TRPV6 Channel and Regulation by PIP2. iScience

23, 101444.

Cai, Y., Anyatonwu, G., Okuhara, D., Lee, K.B., Yu, Z., Onoe, T., Mei, C.L., Qian, Q., Geng, L., Wiztgall, R.*, et al.* (2004). Calcium dependence of polycystin-2 channel activity is modulated by phosphorylation at Ser812. J Biol Chem *279*, 19987-19995.

Cao, C., Zakharian, E., Borbiro, I., and Rohacs, T. (2013). Interplay between calmodulin and phosphatidylinositol 4,5-bisphosphate in Ca2+-induced inactivation of transient receptor potential vanilloid 6 channels. In J Biol Chem, pp. 5278-5290.

Caterina, M.J., Schumacher, M.A., Tominaga, M., Rosen, T.A., Levine, J.D., and Julius, D. (1997). The capsaicin receptor: a heat-activated ion channel in the pain pathway. Nature *389*, 816-824.

Cerella, C., Diederich, M., and Ghibelli, L. (2010). The dual role of calcium as messenger and stressor in cell damage, death, and survival. Int J Cell Biol *2010*, 546163.

Chen, X.Z., Vassilev, P.M., Basora, N., Peng, J.B., Nomura, H., Segal, Y., Brown, E.M., Reeders, S.T., Hediger, M.A., and Zhou, J. (1999). Polycystin-L is a calcium-regulated cation channel permeable to calcium ions. Nature *401*, 383-386.

Cheng, W., Sun, C., and Zheng, J. (2010). Heteromerization of TRP channel subunits: extending functional diversity. Protein Cell *1*, 802-810.

Chin, D., and Means, A.R. (2000). Calmodulin: a prototypical calcium sensor. Trends Cell Biol *10*, 322-328.

Christoph, T., Bahrenberg, G., De Vry, J., Englberger, W., Erdmann, V.A., Frech, M., Kögel, B., Röhl, T., Schiene, K., Schröder, W., et al. (2008). Investigation of TRPV1 loss-of-function phenotypes in transgenic shRNA expressing and knockout mice. Mol Cell Neurosci 37, 579-589.

Cornec-Le Gall, E., Alam, A., and Perrone, R.D. (2019). Autosomal dominant polycystic kidney

disease. Lancet *393*, 919-935.

Cosens, D.J., and Manning, A. (1969). Abnormal electroretinogram from a Drosophila mutant. Nature *224*, 285-287.

Dai, J., Cho, T.J., Unger, S., Lausch, E., Nishimura, G., Kim, O.H., Superti-Furga, A., and Ikegawa, S. (2010). TRPV4-pathy, a novel channelopathy affecting diverse systems. In J Hum Genet, pp. 400-402.

Dai, X.Q., Karpinski, E., and Chen, X.Z. (2006). Permeation and inhibition of polycystin-L channel by monovalent organic cations. Biochim Biophys Acta *1758*, 197-205.

Dai, X.Q., Ramji, A., Liu, Y., Li, Q., Karpinski, E., and Chen, X.Z. (2007). Inhibition of TRPP3 channel by amiloride and analogs. Mol Pharmacol *72*, 1576-1585.

Davis, J.B., Gray, J., Gunthorpe, M.J., Hatcher, J.P., Davey, P.T., Overend, P., Harries, M.H., Latcham, J., Clapham, C., Atkinson, K., et al. (2000). Vanilloid receptor-1 is essential for inflammatory thermal hyperalgesia. Nature 405, 183-187

DeCaen, P.G., Delling, M., Vien, T.N., and Clapham, D.E. (2013). Direct recording and molecular identification of the calcium channel of primary cilia. Nature *504*, 315-318.

DeCaen, P.G., Liu, X., Abiria, S., and Clapham, D.E. (2016). Atypical calcium regulation of the PKD2-L1 polycystin ion channel. Elife *5*.

Del Rosario, J.S., Gabrielle, M., Yudin, Y., and Rohacs, T. (2021). TMEM120A/TACAN inhibits mechanically activated Piezo2 channels. bioRxiv, 2021.2006.2030.450616.

Delling, M., DeCaen, P.G., Doerner, J.F., Febvay, S., and Clapham, D.E. (2013). Primary cilia are specialized calcium signalling organelles. Nature *504*, 311-314.

Delling, M., Indzhykulian, A.A., Liu, X., Li, Y., Xie, T., Corey, D.P., and Clapham, D.E. (2016). Primary cilia are not calcium-responsive mechanosensors. Nature *531*, 656-660.

DeMaria, C.D., Soong, T.W., Alseikhan, B.A., Alvania, R.S., and Yue, D.T. (2001). Calmodulin bifurcates the local Ca2+ signal that modulates P/Q-type Ca2+ channels. Nature *411*, 484-489.

Deng, Z., Paknejad, N., Maksaev, G., Sala-Rabanal, M., Nichols, C.G., Hite, R.K., and Yuan, P. (2018). Cryo-EM and X-ray structures of TRPV4 reveal insight into ion permeation and gating mechanisms. In Nat Struct Mol Biol, pp. 252-260.

Derler, I., Hofbauer, M., Kahr, H., Fritsch, R., Muik, M., Kepplinger, K., Hack, M.E., Moritz, S., Schindl, R., Groschner, K.*, et al.* (2006). Dynamic but not constitutive association of calmodulin with rat TRPV6 channels enables fine tuning of Ca2+-dependent inactivation. J Physiol *577*, 31-44.

Deschênes, I., Neyroud, N., DiSilvestre, D., Marbán, E., Yue, D.T., and Tomaselli, G.F. (2002). Isoform-specific modulation of voltage-gated Na(+) channels by calmodulin. Circ Res *90*, E49-57.

Deutsch, C. (2003). The birth of a channel. Neuron *40*, 265-276.

Diver, M.M., Cheng, Y., and Julius, D. (2019). Structural insights into TRPM8 inhibition and desensitization. Science *365*, 1434-1440.

Dong, X.P., Wang, X., and Xu, H. (2010). TRP channels of intracellular membranes. J Neurochem *113*, 313-328.

Dosemeci, A., and Jaffe, H. (2010). Regulation of phosphorylation at the postsynaptic density during different activity states of Ca2+/calmodulin-dependent protein kinase II. Biochem Biophys Res Commun *391*, 78-84.

Douguet, D., Patel, A., and Honoré, E. (2019). Structure and function of polycystins: insights into polycystic kidney disease. Nat Rev Nephrol *15*, 412-422.

Downing, G.J., Kim, S., Nakanishi, S., Catt, K.J., and Balla, T. (1996). Characterization of a

soluble adrenal phosphatidylinositol 4-kinase reveals wortmannin sensitivity of type III phosphatidylinositol kinases. In Biochemistry, pp. 3587-3594.

Duggan, A., García-Añoveros, J., and Corey, D.P. (2000). Insect mechanoreception: what a long, strange TRP it's been. Curr Biol *10*, R384-387.

Duncan, L.M., Deeds, J., Hunter, J., Shao, J., Holmgren, L.M., Woolf, E.A., Tepper, R.I., and Shyjan, A.W. (1998). Down-regulation of the novel gene melastatin correlates with potential for melanoma metastasis. Cancer Res *58*, 1515-1520.

Falcón, D., Galeano-Otero, I., Calderón-Sánchez, E., Del Toro, R., Martín-Bórnez, M., Rosado, J.A., Hmadcha, A., and Smani, T. (2019). TRP Channels: Current Perspectives in the Adverse Cardiac Remodeling. Front Physiol *10*, 159.

Fatehi, M., Carter, C.C., Youssef, N., and Light, P.E. (2017). The mechano-sensitivity of cardiac ATP-sensitive potassium channels is mediated by intrinsic MgATPase activity. J Mol Cell Cardiol *108*, 34-41.

Fecher-Trost, C., Wissenbach, U., Beck, A., Schalkowsky, P., Stoerger, C., Doerr, J., Dembek, A., Simon-Thomas, M., Weber, A., Wollenberg, P.*, et al.* (2013). The in vivo TRPV6 protein starts at a non-AUG triplet, decoded as methionine, upstream of canonical initiation at AUG. In J Biol Chem, pp. 16629-16644.

Forbes, S.A., Bhamra, G., Bamford, S., Dawson, E., Kok, C., Clements, J., Menzies, A., Teague, J.W., Futreal, P.A., and Stratton, M.R. (2008). The Catalogue of Somatic Mutations in Cancer (COSMIC). In Curr Protoc Hum Genet, pp. Unit.

Fu, S., Hirte, H., Welch, S., Ilenchuk, T.T., Lutes, T., Rice, C., Fields, N., Nemet, A., Dugourd, D., Piha-Paul, S.*, et al.* (2017). Erratum to: First-in-human phase I study of SOR-C13, a TRPV6 calcium channel inhibitor, in patients with advanced solid tumors. Invest New Drugs *35*, 397.

Gabelli, S.B., Yoder, J.B., Tomaselli, G.F., and Amzel, L.M. (2016). Calmodulin and Ca(2+) control of voltage gated Na(+) channels. Channels (Austin) *10*, 45-54.

Garcia-Elias, A., Berna-Erro, A., Rubio-Moscardo, F., Pardo-Pastor, C., Mrkonjic, S., Sepulveda, R.V., Vicente, R., Gonzalez-Nilo, F., and Valverde, M.A. (2015). Interaction between the Linker, Pre-S1, and TRP Domains Determines Folding, Assembly, and Trafficking of TRPV Channels. In Structure, pp. 1404-1413.

Gardill, B.R., Rivera-Acevedo, R.E., Tung, C.C., Okon, M., McIntosh, L.P., and Van Petegem, F. (2018). The voltage-gated sodium channel EF-hands form an interaction with the III-IV linker that is disturbed by disease-causing mutations. Sci Rep *8*, 4483.

Gees, M., Colsoul, B., and Nilius, B. (2010). The role of transient receptor potential cation channels in Ca2+ signaling. In Cold Spring Harb Perspect Biol, pp. a003962.

Giamarchi, A., Padilla, F., Coste, B., Raoux, M., Crest, M., Honoré, E., and Delmas, P. (2006). The versatile nature of the calcium-permeable cation channel TRPP2. EMBO Rep *7*, 787-793.

Goldin, E., Stahl, S., Cooney, A.M., Kaneski, C.R., Gupta, S., Brady, R.O., Ellis, J.R., and Schiffmann, R. (2004). Transfer of a mitochondrial DNA fragment to MCOLN1 causes an inherited case of mucolipidosis IV. In Hum Mutat, pp. 460-465.

Gordon-Shaag, A., Zagotta, W.N., and Gordon, S.E. (2008). Mechanism of Ca(2+)-dependent desensitization in TRP channels. Channels (Austin) *2*, 125-129.

Grieben, M., Pike, A.C., Shintre, C.A., Venturi, E., El-Ajouz, S., Tessitore, A., Shrestha, L., Mukhopadhyay, S., Mahajan, P., Chalk, R.*, et al.* (2017). Structure of the polycystic kidney disease TRP channel Polycystin-2 (PC2). Nat Struct Mol Biol *24*, 114-122.

Ha, K., Nobuhara, M., Wang, Q., Walker, R.V., Qian, F., Schartner, C., Cao, E., and Delling, M. (2020). The heteromeric PC-1/PC-2 polycystin complex is activated by the PC-1 N-terminus.

Elife *9*.

Hamilton, P.J., Belovich, A.N., Khelashvili, G., Saunders, C., Erreger, K., Javitch, J.A., Sitte, H.H., Weinstein, H., Matthies, H.J.G., and Galli, A. (2014). PIP2 regulates psychostimulant behaviors through its interaction with a membrane protein. In Nat Chem Biol, pp. 582-589.

Hanaoka, K., Qian, F., Boletta, A., Bhunia, A.K., Piontek, K., Tsiokas, L., Sukhatme, V.P., Guggino, W.B., and Germino, G.G. (2000). Co-assembly of polycystin-1 and -2 produces unique cation-permeable currents. Nature *408*, 990-994.

Hardie, R.C. (2004). Regulation of Drosophila TRP channels by lipid messengers. Novartis Found Symp *258*, 160-167; discussion 167-171, 263-166.

Harris, P.C. (1994). The polycystic kidney disease 1 gene encodes a 14 kb transcript and lies within a duplicated region on chromosome 16. The European Polycystic Kidney Disease Consortium. Cell *77*, 881-894.

Harris, P.C., and Torres, V.E. (2009). Polycystic kidney disease. Annu Rev Med *60*, 321-337.

Hasan, R., and Zhang, X. (2018). Ca(2+) Regulation of TRP Ion Channels. Int J Mol Sci *19*.

Himmel, N.J., Gray, T.R., and Cox, D.N. (2020). Phylogenetics Identifies Two Eumetazoan TRPM Clades and an Eighth TRP Family, TRP Soromelastatin (TRPS). Mol Biol Evol *37*, 2034-2044.

Hoenderop, J.G., Voets, T., Hoefs, S., Weidema, F., Prenen, J., Nilius, B., and Bindels, R.J. (2003). Homo- and heterotetrameric architecture of the epithelial Ca2+ channels TRPV5 and TRPV6. Embo j *22*, 776-785.

Hofherr, A., Wagner, C., Fedeles, S., Somlo, S., and Köttgen, M. (2014). N-glycosylation determines the abundance of the transient receptor potential channel TRPP2. J Biol Chem *289*, 14854-14867.

Hofmann, L., Wang, H., Beck, A., Wissenbach, U., and Flockerzi, V. (2017). A conserved gating element in TRPV6 channels. In Cell Calcium, pp. 24-28.

Horio, N., Yoshida, R., Yasumatsu, K., Yanagawa, Y., Ishimaru, Y., Matsunami, H., and Ninomiya, Y. (2011). Sour taste responses in mice lacking PKD channels. PLoS One *6*, e20007.

Huang, C.L., Feng, S., and Hilgemann, D.W. (1998). Direct activation of inward rectifier potassium channels by PIP2 and its stabilization by Gbetagamma. In Nature, pp. 803-806.

Huang, X., Pan, Q., Sun, D., Chen, W., Shen, A., Huang, M., Ding, J., and Geng, M. (2013). O-GlcNAcylation of cofilin promotes breast cancer cell invasion. In J Biol Chem, pp. 36418-36425.

Huang, Y., Winkler, P.A., Sun, W., Lü, W., and Du, J. (2018). Architecture of the TRPM2 channel and its activation mechanism by ADP-ribose and calcium. Nature *562*, 145-149.

Huber, S.M. (2013). Oncochannels. Cell Calcium *53*, 241-255.

Huffer, K.E., Aleksandrova, A.A., Jara-Oseguera, A., Forrest, L.R., and Swartz, K.J. (2020). Global alignment and assessment of TRP channel transmembrane domain structures to explore functional mechanisms. Elife *9*.

Hughes, T.E.T., Pumroy, R.A., Yazici, A.T., Kasimova, M.A., Fluck, E.C., Huynh, K.W., Samanta, A., Molugu, S.K., Zhou, Z.H., Carnevale, V.*, et al.* (2018). Structural insights on TRPV5 gating by endogenous modulators. Nat Commun *9*, 4198.

Hulse, R.E., Li, Z., Huang, R.K., Zhang, J., and Clapham, D.E. (2018). Cryo-EM structure of the polycystin 2-l1 ion channel. Elife *7*.

Huque, T., Cowart, B.J., Dankulich-Nagrudny, L., Pribitkin, E.A., Bayley, D.L., Spielman, A.I., Feldman, R.S., Mackler, S.A., and Brand, J.G. (2009). Sour ageusia in two individuals implicates ion channels of the ASIC and PKD families in human sour taste perception at the anterior

tongue. PLoS One *4*, e7347.

Hussein, S., Zheng, W., Dyte, C., Wang, Q., Yang, J., Zhang, F., Tang, J., Cao, Y., and Chen, X.Z. (2015). Acid-induced off-response of PKD2L1 channel in *Xenopus* oocytes and its regulation by Ca(2.). Sci Rep *5*, 15752.

Inada, H., Kawabata, F., Ishimaru, Y., Fushiki, T., Matsunami, H., and Tominaga, M. (2008). Off-response property of an acid-activated cation channel complex PKD1L3-PKD2L1. EMBO Rep *9*, 690-697.

Ishimaru, Y., Inada, H., Kubota, M., Zhuang, H., Tominaga, M., and Matsunami, H. (2006). Transient receptor potential family members PKD1L3 and PKD2L1 form a candidate sour taste receptor. Proc Natl Acad Sci U S A *103*, 12569-12574.

Iwamoto, N., Lu, R., Tanaka, N., Abe-Dohmae, S., and Yokoyama, S. (2010). Calmodulin interacts with ATP binding cassette transporter A1 to protect from calpain-mediated degradation and upregulates high-density lipoprotein generation. Arterioscler Thromb Vasc Biol *30*, 1446-1452.

Jaquemar, D., Schenker, T., and Trueb, B. (1999). An ankyrin-like protein with transmembrane domains is specifically lost after oncogenic transformation of human fibroblasts. J Biol Chem *274*, 7325-7333.

Jardín, I., López, J.J., Diez, R., Sánchez-Collado, J., Cantonero, C., Albarrán, L., Woodard, G.E., Redondo, P.C., Salido, G.M., Smani, T., et al. (2017). TRPs in Pain Sensation. Front Physiol 8, 392.

Jirku, M., Bumba, L., Bednarova, L., Kubala, M., Sulc, M., Franek, M., Vyklicky, L., Vondrasek, J., Teisinger, J., and Bousova, K. (2015). Characterization of the part of N-terminal PIP2 binding site of the TRPM1 channel. In Biophys Chem, pp. 135-142.

Joiner, W.J., Khanna, R., Schlichter, L.C., and Kaczmarek, L.K. (2001). Calmodulin regulates assembly and trafficking of SK4/IK1 Ca2+-activated K+ channels. J Biol Chem *276*, 37980-37985.

Kass, G.E., and Orrenius, S. (1999). Calcium signaling and cytotoxicity. Environ Health Perspect *107 Suppl 1*, 25-35.

Ke, M., Yu, Y., Zhao, C., Lai, S., Su, Q., Yuan, W., Yang, L., Deng, D., Wu, K., Zeng, W.*, et al.* (2021). Cryo-EM structures of human TMEM120A and TMEM120B. bioRxiv, 2021.2006.2027.450060.

Kefauver, J.M., Ward, A.B., and Patapoutian, A. (2020). Discoveries in structure and physiology of mechanically activated ion channels. Nature *587*, 567-576.

Kim, D.Y., and Park, J.H. (2016). Genetic Mechanisms of ADPKD. Adv Exp Med Biol *933*, 13-22.

Knowlton, W.M., Daniels, R.L., Palkar, R., McCoy, D.D., and McKemy, D.D. (2011). Pharmacological blockade of TRPM8 ion channels alters cold and cold pain responses in mice. PLoS One 6, e25894.

Kobori, T., Smith, G.D., Sandford, R., and Edwardson, J.M. (2009). The transient receptor potential channels TRPP2 and TRPC1 form a heterotetramer with a 2:2 stoichiometry and an alternating subunit arrangement. J Biol Chem *284*, 35507-35513.

Kobrinsky, E., Mirshahi, T., Zhang, H., Jin, T., and Logothetis, D.E. (2000). Receptor-mediated hydrolysis of plasma membrane messenger PIP2 leads to K+-current desensitization. Nat Cell Biol *2*, 507-514.

Köttgen, M., Buchholz, B., Garcia-Gonzalez, M.A., Kotsis, F., Fu, X., Doerken, M., Boehlke, C., Steffl, D., Tauber, R., Wegierski, T.*, et al.* (2008). TRPP2 and TRPV4 form a polymodal sensory

channel complex. J Cell Biol *182*, 437-447.

Kovalevskaya, N.V., Bokhovchuk, F.M., and Vuister, G.W. (2012). The TRPV5/6 calcium channels contain multiple calmodulin binding sites with differential binding properties. J Struct Funct Genomics *13*, 91-100.

Kremeyer, B., Lopera, F., Cox, J.J., Momin, A., Rugiero, F., Marsh, S., Woods, C.G., Jones, N.G., Paterson, K.J., Fricker, F.R.*, et al.* (2010). A gain-of-function mutation in TRPA1 causes familial episodic pain syndrome. Neuron *66*, 671-680.

Kuo, I.Y., Keeler, C., Corbin, R., Ćelić, A., Petri, E.T., Hodsdon, M.E., and Ehrlich, B.E. (2014). The number and location of EF hand motifs dictates the calcium dependence of polycystin-2 function. Faseb j *28*, 2332-2346.

Kwon, Y., Hofmann, T., and Montell, C. (2007). Integration of phosphoinositide- and calmodulin-mediated regulation of TRPC6. Mol Cell *25*, 491-503.

Landouré, G., Zdebik, A.A., Martinez, T.L., Burnett, B.G., Stanescu, H.C., Inada, H., Shi, Y., Taye, A.A., Kong, L., Munns, C.H.*, et al.* (2010). Mutations in TRPV4 cause Charcot-Marie-Tooth disease type 2C. Nat Genet *42*, 170-174.

Launay, P., Fleig, A., Perraud, A.L., Scharenberg, A.M., Penner, R., and Kinet, J.P. (2002). TRPM4 is a Ca2+-activated nonselective cation channel mediating cell membrane depolarization. Cell *109*, 397-407.

Lehen'kyi, V., Raphaël, M., and Prevarskaya, N. (2012). The role of the TRPV6 channel in cancer. J Physiol *590*, 1369-1376.

Li, Q., Dai, X.Q., Shen, P.Y., Wu, Y., Long, W., Chen, C.X., Hussain, Z., Wang, S., and Chen, X.Z. (2007). Direct binding of alpha-actinin enhances TRPP3 channel activity. J Neurochem *103*, 2391-2400.

Li, Q., Liu, Y., Shen, P.Y., Dai, X.Q., Wang, S., Smillie, L.B., Sandford, R., and Chen, X.Z. (2003). Troponin I binds polycystin-L and inhibits its calcium-induced channel activation. Biochemistry *42*, 7618-7625.

Li, Q., Liu, Y., Zhao, W., and Chen, X.Z. (2002). The calcium-binding EF-hand in polycystin-L is not a domain for channel activation and ensuing inactivation. FEBS Lett *516*, 270-278.

Liao, M., Cao, E., Julius, D., and Cheng, Y. (2013). Structure of the TRPV1 ion channel determined by electron cryo-microscopy. Nature *504*, 107-112.

Lieben, L., Benn, B.S., Ajibade, D., Stockmans, I., Moermans, K., Hediger, M.A., Peng, J.B., Christakos, S., Bouillon, R., and Carmeliet, G. (2010). Trpv6 mediates intestinal calcium absorption during calcium restriction and contributes to bone homeostasis. In Bone, pp. 301-308.

Liu, X., Vien, T., Duan, J., Sheu, S.H., DeCaen, P.G., and Clapham, D.E. (2018). Polycystin-2 is an essential ion channel subunit in the primary cilium of the renal collecting duct epithelium. Elife *7*.

Liu, Y., Li, Q., Tan, M., Zhang, Y.Y., Karpinski, E., Zhou, J., and Chen, X.Z. (2002). Modulation of the human polycystin-L channel by voltage and divalent cations. FEBS Lett *525*, 71-76.

Lopez-Romero, A.E., Hernandez-Araiza, I., Torres-Quiroz, F., Tovar, Y.R.L.B., Islas, L.D., and Rosenbaum, T. (2019). TRP ion channels: Proteins with conformational flexibility. Channels (Austin) *13*, 207-226.

Lu, Z., Cui, Y., Wei, X., Gao, P., Zhang, H., Wei, X., Li, Q., Sun, F., Yan, Z., Zheng, H.*, et al.* (2018). Deficiency of PKD2L1 (TRPP3) Exacerbates Pathological Cardiac Hypertrophy by Augmenting NCX1-Mediated Mitochondrial Calcium Overload. Cell Rep *24*, 1639-1652.

Lukacs, V., Thyagarajan, B., Varnai, P., Balla, A., Balla, T., and Rohacs, T. (2007). Dual regulation of TRPV1 by phosphoinositides. J Neurosci *27*, 7070-7080.

Luo, Y., Vassilev, P.M., Li, X., Kawanabe, Y., and Zhou, J. (2003). Native polycystin 2 functions as a plasma membrane Ca2+-permeable cation channel in renal epithelia. Mol Cell Biol *23*, 2600-2607.

Ma, R., Li, W.P., Rundle, D., Kong, J., Akbarali, H.I., and Tsiokas, L. (2005). PKD2 functions as an epidermal growth factor-activated plasma membrane channel. In Mol Cell Biol, pp. 8285-8298.

McGoldrick, L.L., Singh, A.K., Saotome, K., Yelshanskaya, M.V., Twomey, E.C., Grassucci, R.A., and Sobolevsky, A.I. (2018). Opening of the human epithelial calcium channel TRPV6. Nature *553*, 233-237.

Mercado, J., Gordon-Shaag, A., Zagotta, W.N., and Gordon, S.E. (2010). Ca2+-dependent desensitization of TRPV2 channels is mediated by hydrolysis of phosphatidylinositol 4,5-bisphosphate. J Neurosci *30*, 13338-13347.

Miura, S., Sato, K., Kato-Negishi, M., Teshima, T., and Takeuchi, S. (2015). Fluid shear triggers microvilli formation via mechanosensitive activation of TRPV6. Nature Communications *6*.

Mochizuki, T., Wu, G., Hayashi, T., Xenophontos, S.L., Veldhuisen, B., Saris, J.J., Reynolds, D.M., Cai, Y., Gabow, P.A., Pierides, A.*, et al.* (1996). PKD2, a gene for polycystic kidney disease that encodes an integral membrane protein. Science *272*, 1339-1342.

Nagata, K., Duggan, A., Kumar, G., and García-Añoveros, J. (2005). Nociceptor and hair cell transducer properties of TRPA1, a channel for pain and hearing. J Neurosci 25, 4052-4061.

Nauli, S.M., Alenghat, F.J., Luo, Y., Williams, E., Vassilev, P., Li, X., Elia, A.E., Lu, W., Brown, E.M., Quinn, S.J.*, et al.* (2003). Polycystins 1 and 2 mediate mechanosensation in the primary cilium of kidney cells. Nat Genet *33*, 129-137.

Negulescu, P.A., Shastri, N., and Cahalan, M.D. (1994). Intracellular calcium dependence of

gene expression in single T lymphocytes. Proc Natl Acad Sci U S A *91*, 2873-2877.

Nelson, T.M., Lopezjimenez, N.D., Tessarollo, L., Inoue, M., Bachmanov, A.A., and Sullivan, S.L. (2010). Taste function in mice with a targeted mutation of the pkd1l3 gene. Chem Senses *35*, 565-577.

Niemeyer, B.A., Bergs, C., Wissenbach, U., Flockerzi, V., and Trost, C. (2001). Competitive regulation of CaT-like-mediated Ca2+ entry by protein kinase C and calmodulin. Proc Natl Acad Sci U S A *98*, 3600-3605.

Nikolaev, Y.A., Cox, C.D., Ridone, P., Rohde, P.R., Cordero-Morales, J.F., Vasquez, V., Laver, D.R., and Martinac, B. (2019). Mammalian TRP ion channels are insensitive to membrane stretch. J Cell Sci *132*.

Nilius, B., and Owsianik, G. (2011). The transient receptor potential family of ion channels. Genome Biol *12*, 218.

Nilius, B., Owsianik, G., and Voets, T. (2008). Transient receptor potential channels meet phosphoinositides. Embo j *27*, 2809-2816.

Nilius, B., Prenen, J., Hoenderop, J.G., Vennekens, R., Hoefs, S., Weidema, A.F., Droogmans, G., and Bindels, R.J. (2002). Fast and slow inactivation kinetics of the Ca2+ channels ECaC1 and ECaC2 (TRPV5 and TRPV6). Role of the intracellular loop located between transmembrane segments 2 and 3. J Biol Chem *277*, 30852-30858.

Nilius, B., and Szallasi, A. (2014). Transient receptor potential channels as drug targets: from the science of basic research to the art of medicine. Pharmacol Rev *66*, 676-814.

Nilius, B., Vennekens, R., Prenen, J., Hoenderop, J.G., Bindels, R.J., and Droogmans, G. (2000). Whole-cell and single channel monovalent cation currents through the novel rabbit epithelial Ca2+ channel ECaC. J Physiol *527 Pt 2*, 239-248.

Niu, Y., Tao, X., Vaisey, G., Olinares, P.D.B., Alwaseem, H., Chait, B.T., and MacKinnon, R. (2021). Analysis of the Mechanosensor Channel Functionality of TACAN. bioRxiv, 2021.2006.2011.448078.

Nomura, H., Turco, A.E., Pei, Y., Kalaydjieva, L., Schiavello, T., Weremowicz, S., Ji, W., Morton, C.C., Meisler, M., Reeders, S.T.*, et al.* (1998). Identification of PKDL, a novel polycystic kidney disease 2-like gene whose murine homologue is deleted in mice with kidney and retinal defects. J Biol Chem *273*, 25967-25973.

Numata, T., Kiyonaka, S., Kato, K., Takahashi, N., and Mori, Y. (2011). Activation of TRP Channels in Mammalian Systems. In TRP Channels, M.X. Zhu, ed. (Boca Raton (FL)).

Numazaki, M., Tominaga, T., Takeuchi, K., Murayama, N., Toyooka, H., and Tominaga, M. (2003). Structural determinant of TRPV1 desensitization interacts with calmodulin. Proc Natl Acad Sci U S A *100*, 8002-8006.

Owsianik, G., Talavera, K., Voets, T., and Nilius, B. (2006). Permeation and selectivity of TRP channels. Annu Rev Physiol *68*, 685-717.

Park, E.Y.J., Baik, J.Y., Kwak, M., and So, I. (2019). The role of calmodulin in regulating calcium-permeable PKD2L1 channel activity. Korean J Physiol Pharmacol *23*, 219-227.

Park, E.Y.J., Kwak, M., Ha, K., and So, I. (2018). Identification of clustered phosphorylation sites in PKD2L1: how PKD2L1 channel activation is regulated by cyclic adenosine monophosphate signaling pathway. Pflugers Arch *470*, 505-516.

Parpaite, T., Brosse, L., Séjourné, N., Laur, A., Mechioukhi, Y., Delmas, P., and Coste, B. (2021). Patch-seq of mouse DRG neurons reveals candidate genes for specific mechanosensory functions. bioRxiv, 2021.2007.2007.451447.

Paulsen, C.E., Armache, J.P., Gao, Y., Cheng, Y., and Julius, D. (2015). Structure of the TRPA1

ion channel suggests regulatory mechanisms. In Nature, pp. 511-517.

Pei, Y. (2003). Molecular genetics of autosomal dominant polycystic kidney disease. Clin Invest Med *26*, 252-258.

Peng, J.B., Chen, X.Z., Berger, U.V., Vassilev, P.M., Tsukaguchi, H., Brown, E.M., and Hediger, M.A. (1999). Molecular cloning and characterization of a channel-like transporter mediating intestinal calcium absorption. J Biol Chem *274*, 22739-22746.

Peng, J.B., Chen, X.Z., Berger, U.V., Weremowicz, S., Morton, C.C., Vassilev, P.M., Brown, E.M., and Hediger, M.A. (2000). Human calcium transport protein CaT1. Biochem Biophys Res Commun *278*, 326-332.

Peng, J.B., Suzuki, Y., Gyimesi, G., and Hediger, M.A. (2018). TRPV5 and TRPV6 Calcium-Selective Channels. In Calcium Entry Channels in Non-Excitable Cells, J.A. Kozak, and J.W. Putney, Jr., eds. (Boca Raton (FL): CRC Press/Taylor & Francis
© 2017 by Taylor & Francis Group, LLC.), pp. 241-274.

Peng, J.B., Zhuang, L., Berger, U.V., Adam, R.M., Williams, B.J., Brown, E.M., Hediger, M.A., and Freeman, M.R. (2001). CaT1 expression correlates with tumor grade in prostate cancer. Biochem Biophys Res Commun *282*, 729-734.

Peters, A.A., Simpson, P.T., Bassett, J.J., Lee, J.M., Da Silva, L., Reid, L.E., Song, S., Parat, M.O., Lakhani, S.R., Kenny, P.A.*, et al.* (2012). Calcium channel TRPV6 as a potential therapeutic target in estrogen receptor-negative breast cancer. In Mol Cancer Ther, pp. 2158-2168.

Peterson, B.Z., DeMaria, C.D., Adelman, J.P., and Yue, D.T. (1999). Calmodulin is the Ca2+ sensor for Ca2+ -dependent inactivation of L-type calcium channels. Neuron *22*, 549-558.

Petri, E.T., Celic, A., Kennedy, S.D., Ehrlich, B.E., Boggon, T.J., and Hodsdon, M.E. (2010).

Structure of the EF-hand domain of polycystin-2 suggests a mechanism for Ca2+-dependent regulation of polycystin-2 channel activity. Proc Natl Acad Sci U S A *107*, 9176-9181.

Peyronnet, R., Martins, J.R., Duprat, F., Demolombe, S., Arhatte, M., Jodar, M., Tauc, M., Duranton, C., Paulais, M., Teulon, J.*, et al.* (2013). Piezo1-dependent stretch-activated channels are inhibited by Polycystin-2 in renal tubular epithelial cells. EMBO Rep *14*, 1143-1148.

Pinto, M.T., Malta, T.M., Rodrigues, E.S., Pinheiro, D.G., Panepucci, R.A., Malmegrim de Farias, K.C., Sousa Ade, P., Takayanagui, O.M., Tanaka, Y., Covas, D.T.*, et al.* (2014). Genes related to antiviral activity, cell migration, and lysis are differentially expressed in CD4(+) T cells in human t cell leukemia virus type 1-associated myelopathy/tropical spastic paraparesis patients. AIDS Res Hum Retroviruses *30*, 610-622.

Poblete, H., Oyarzún, I., Olivero, P., Comer, J., Zuñiga, M., Sepulveda, R.V., Báez-Nieto, D., González Leon, C., González-Nilo, F., and Latorre, R. (2015). Molecular determinants of phosphatidylinositol 4,5-bisphosphate (PI(4,5)P2) binding to transient receptor potential V1 (TRPV1) channels. J Biol Chem *290*, 2086-2098.

Prawitt, D., Monteilh-Zoller, M.K., Brixel, L., Spangenberg, C., Zabel, B., Fleig, A., and Penner, R. (2003). TRPM5 is a transient Ca2+-activated cation channel responding to rapid changes in [Ca2+]i. Proc Natl Acad Sci U S A *100*, 15166-15171.

Prescott, E.D., and Julius, D. (2003). A modular PIP2 binding site as a determinant of capsaicin receptor sensitivity. Science *300*, 1284-1288.

Pumroy, R.A., Samanta, A., Liu, Y., Hughes, T.E.T., Zhao, S., Yudin, Y., Rohacs, T., Han, S., and Moiseenkova-Bell, V.Y. (2019). Molecular mechanism of TRPV2 channel modulation by cannabidiol. eLife *8*.

Qian, F., Germino, F.J., Cai, Y., Zhang, X., Somlo, S., and Germino, G.G. (1997). PKD1 interacts

with PKD2 through a probable coiled-coil domain. Nat Genet *16*, 179-183.

Ranade, S.S., Syeda, R., and Patapoutian, A. (2015). Mechanically Activated Ion Channels. Neuron *87*, 1162-1179.

Rhoads, A.R., and Friedberg, F. (1997). Sequence motifs for calmodulin recognition. Faseb j *11*, 331-340.

Rohacs, T. (2014). Phosphoinositide regulation of TRP channels. Handb Exp Pharmacol *223*, 1143-1176.

Rong, Y., Jiang, J., Gao, Y., Guo, J., Song, D., Liu, W., Zhao, Y., Xiao, B., and Liu, Z. (2021). TMEM120A contains a specific coenzyme A-binding site and might not mediate poking- or stretch-induced channel activities in cells. bioRxiv, 2021.2006.2017.448797.

Rosenbaum, T., Gordon-Shaag, A., Munari, M., and Gordon, S.E. (2004). Ca2+/calmodulin modulates TRPV1 activation by capsaicin. J Gen Physiol *123*, 53-62.

Saimi, Y., and Kung, C. (2002). Calmodulin as an ion channel subunit. Annu Rev Physiol *64*, 289-311.

Samanta, A., Hughes, T.E.T., and Moiseenkova-Bell, V.Y. (2018). Transient Receptor Potential (TRP) Channels. Subcell Biochem *87*, 141-165.

Samtleben, S., Jaepel, J., Fecher, C., Andreska, T., Rehberg, M., and Blum, R. (2013). Direct imaging of ER calcium with targeted-esterase induced dye loading (TED). J Vis Exp, e50317.

Saotome, K., Singh, A.K., Yelshanskaya, M.V., and Sobolevsky, A.I. (2016). Crystal structure of the epithelial calcium channel TRPV6. Nature *534*, 506-511.

Schumacher, M.A., Rivard, A.F., Bächinger, H.P., and Adelman, J.P. (2001). Structure of the gating domain of a Ca2+-activated K+ channel complexed with Ca2+/calmodulin. Nature *410*, 1120-1124.

Shah, V.N., Chagot, B., and Chazin, W.J. (2006). Calcium-Dependent Regulation of Ion Channels. Calcium Bind Proteins *1*, 203-212.

Sharif-Naeini, R., Folgering, J.H., Bichet, D., Duprat, F., Lauritzen, I., Arhatte, M., Jodar, M., Dedman, A., Chatelain, F.C., Schulte, U.*, et al.* (2009). Polycystin-1 and -2 dosage regulates pressure sensing. Cell *139*, 587-596.

Shen, P.S., Yang, X., DeCaen, P.G., Liu, X., Bulkley, D., Clapham, D.E., and Cao, E. (2016). The Structure of the Polycystic Kidney Disease Channel PKD2 in Lipid Nanodiscs. Cell *167*, 763-773.e711.

Shimizu, T., Janssens, A., Voets, T., and Nilius, B. (2009). Regulation of the murine TRPP3 channel by voltage, pH, and changes in cell volume. Pflugers Arch *457*, 795-807.

Shoemaker, S.C., and Ando, N. (2018). X-rays in the Cryo-Electron Microscopy Era: Structural Biology's Dynamic Future. In Biochemistry, pp. 277-285.

Simon, H.U. (2003). Neutrophil apoptosis pathways and their modifications in inflammation. Immunol Rev *193*, 101-110.

Singh, A.K., McGoldrick, L.L., Twomey, E.C., and Sobolevsky, A.I. (2018a). Mechanism of calmodulin inactivation of the calcium-selective TRP channel TRPV6. Sci Adv *4*, eaau6088.

Singh, A.K., Saotome, K., McGoldrick, L.L., and Sobolevsky, A.I. (2018b). Structural bases of TRP channel TRPV6 allosteric modulation by 2-APB. Nat Commun *9*, 2465.

Songyang, Z., Lu, K.P., Kwon, Y.T., Tsai, L.H., Filhol, O., Cochet, C., Brickey, D.A., Soderling, T.R., Bartleson, C., Graves, D.J.*, et al.* (1996). A structural basis for substrate specificities of protein Ser/Thr kinases: primary sequence preference of casein kinases I and II, NIMA, phosphorylase kinase, calmodulin-dependent kinase II, CDK5, and Erk1. Mol Cell Biol *16*, 6486-6493.

Stallmeyer, B., Zumhagen, S., Denjoy, I., Duthoit, G., Hebert, J.L., Ferrer, X., Maugenre, S., Schmitz, W., Kirchhefer, U., Schulze-Bahr, E.*, et al.* (2012). Mutational spectrum in the Ca(2+)--activated cation channel gene TRPM4 in patients with cardiac conductance disturbances. In Hum Mutat, pp. 109-117.

Stefan, M.I., Edelstein, S.J., and Le Novère, N. (2008). An allosteric model of calmodulin explains differential activation of PP2B and CaMKII. Proc Natl Acad Sci U S A *105*, 10768-10773.

Stein, A.T., Ufret-Vincenty, C.A., Hua, L., Santana, L.F., and Gordon, S.E. (2006). Phosphoinositide 3-kinase binds to TRPV1 and mediates NGF-stimulated TRPV1 trafficking to the plasma membrane. J Gen Physiol *128*, 509-522.

Sternberg, J.R., Prendergast, A.E., Brosse, L., Cantaut-Belarif, Y., Thouvenin, O., Orts-Del'Immagine, A., Castillo, L., Djenoune, L., Kurisu, S., McDearmid, J.R.*, et al.* (2018). Pkd2l1 is required for mechanoception in cerebrospinal fluid-contacting neurons and maintenance of spine curvature. Nat Commun *9*, 3804.

Stewart, J.M. (2020). TRPV6 as A Target for Cancer Therapy. J Cancer *11*, 374-387.

Su, Q., Hu, F., Ge, X., Lei, J., Yu, S., Wang, T., Zhou, Q., Mei, C., and Shi, Y. (2018a). Structure of the human PKD1-PKD2 complex. Science *361*.

Su, Q., Hu, F., Liu, Y., Ge, X., Mei, C., Yu, S., Shen, A., Zhou, Q., Yan, C., Lei, J.*, et al.* (2018b). Cryo-EM structure of the polycystic kidney disease-like channel PKD2L1. Nat Commun *9*, 1192.

Sun, F., Xiao, L., Jang, X.X., Xiong, Y., Li, Q., Yue, X.J., Wei, Y.J., Wei, Y.X., Ma, Y.L., and Yu, Y.H. (2016). TRPV6 is a prognostic marker in early-stage cervical squamous cell carcinoma. Tumour Biol.

Sun, L., Hodeify, R., Haun, S., Charlesworth, A., MacNicol, A.M., Ponnappan, S., Ponnappan, U., Prigent, C., and Machaca, K. (2008). Ca2+ homeostasis regulates *Xenopus* oocyte maturation. Biol Reprod *78*, 726-735.

Suzuki, Y., Pasch, A., Bonny, O., Mohaupt, M.G., Hediger, M.A., and Frey, F.J. (2008). Gain-of-function haplotype in the epithelial calcium channel TRPV6 is a risk factor for renal calcium stone formation. In Hum Mol Genet, pp. 1613-1618.

Tan, L.L., Bornstein, J.C., and Anderson, C.R. (2008). Distinct chemical classes of medium-sized transient receptor potential channel vanilloid 1-immunoreactive dorsal root ganglion neurons innervate the adult mouse jejunum and colon. Neuroscience 156, 334-343.

Tan, L.L., Bornstein, J.C., and Anderson, C.R. (2009). Neurochemical and morphological phenotypes of vagal afferent neurons innervating the adult mouse jejunum. Neurogastroenterol Motil 21, 994-1001.

Tékus, V., Bölcskei, K., Kis-Varga, A., Dézsi, L., Szentirmay, E., Visegrády, A., Horváth, C., Szolcsányi, J., and Petho, G. (2010). Effect of transient receptor potential vanilloid 1 (TRPV1) receptor antagonist compounds SB705498, BCTC and AMG9810 in rat models of thermal hyperalgesia measured with an increasing-temperature water bath. Eur J Pharmacol 641, 135-141.

Teng, J., Loukin, S.H., Anishkin, A., and Kung, C. (2015). L596-W733 bond between the start of the S4-S5 linker and the TRP box stabilizes the closed state of TRPV4 channel. In Proc Natl Acad Sci U S A, pp. 3386-3391.

Thyagarajan, B., Benn, B.S., Christakos, S., and Rohacs, T. (2009). Phospholipase C-mediated regulation of transient receptor potential vanilloid 6 channels: implications in active intestinal Ca2+ transport. In Mol Pharmacol, pp. 608-616.

Thyagarajan, B., Lukacs, V., and Rohacs, T. (2008). Hydrolysis of phosphatidylinositol 4,5-bisphosphate mediates calcium-induced inactivation of TRPV6 channels. J Biol Chem *283*, 14980-14987.

Tobelaim, W.S., Dvir, M., Lebel, G., Cui, M., Buki, T., Peretz, A., Marom, M., Haitin, Y., Logothetis, D.E., Hirsch, J.A.*, et al.* (2017). Competition of calcified calmodulin N lobe and PIP2 to an LQT mutation site in Kv7.1 channel. Proc Natl Acad Sci U S A *114*, E869-e878.

Tominaga, M., Caterina, M.J., Malmberg, A.B., Rosen, T.A., Gilbert, H., Skinner, K., Raumann, B.E., Basbaum, A.I., and Julius, D. (1998). The cloned capsaicin receptor integrates multiple pain-producing stimuli. Neuron 21, 531-543.

Trudeau, M.C., and Zagotta, W.N. (2002). Mechanism of calcium/calmodulin inhibition of rod cyclic nucleotide-gated channels. Proc Natl Acad Sci U S A *99*, 8424-8429.

Trudeau, M.C., and Zagotta, W.N. (2003). Calcium/calmodulin modulation of olfactory and rod cyclic nucleotide-gated ion channels. J Biol Chem *278*, 18705-18708.

Tsiokas, L., Kim, E., Arnould, T., Sukhatme, V.P., and Walz, G. (1997). Homo- and heterodimeric interactions between the gene products of PKD1 and PKD2. Proc Natl Acad Sci U S A *94*, 6965-6970.

van Abel, M., Hoenderop, J.G., van der Kemp, A.W., van Leeuwen, J.P., and Bindels, R.J. (2003). Regulation of the epithelial Ca2+ channels in small intestine as studied by quantitative mRNA detection. In Am J Physiol Gastrointest Liver Physiol, pp. G78-G85.

van den Wijngaard, R.M., Welting, O., Bulmer, D.C., Wouters, M.M., Lee, K., de Jonge, W.J., and Boeckxstaens, G.E. (2009). Possible role for TRPV1 in neomycin-induced inhibition of visceral hypersensitivity in rat. Neurogastroenterol Motil 21, 863-e860.

van Goor, M.K.C., Hoenderop, J.G.J., and van der Wijst, J. (2017). TRP channels in calcium

homeostasis: from hormonal control to structure-function relationship of TRPV5 and TRPV6. In Biochim Biophys Acta, pp. 883-893.

Vangeel, L., and Voets, T. (2019). Transient Receptor Potential Channels and Calcium Signaling. Cold Spring Harb Perspect Biol *11*.

Vanhaesebroeck, B., Leevers, S.J., Ahmadi, K., Timms, J., Katso, R., Driscoll, P.C., Woscholski, R., Parker, P.J., and Waterfield, M.D. (2001). Synthesis and function of 3-phosphorylated inositol lipids. In Annu Rev Biochem, pp. 535-602.

Vanoevelen, J., Janssens, A., Huitema, L.F., Hammond, C.L., Metz, J.R., Flik, G., Voets, T., and Schulte-Merker, S. (2011). Trpv5/6 is vital for epithelial calcium uptake and bone formation. FASEB J *25*, 3197-3207.

Velisetty, P., Borbiro, I., Kasimova, M.A., Liu, L., Badheka, D., Carnevale, V., and Rohacs, T. (2016). A molecular determinant of phosphoinositide affinity in mammalian TRPV channels. Sci Rep *6*, 27652.

Vennekens, R., Hoenderop, J.G., Prenen, J., Stuiver, M., Willems, P.H., Droogmans, G., Nilius, B., and Bindels, R.J. (2000). Permeation and gating properties of the novel epithelial Ca(2+) channel. J Biol Chem *275*, 3963-3969.

Vien, T.N., Ng, L.C.T., Smith, J.M., Dong, K., Krappitz, M., Gainullin, V.G., Fedeles, S., Harris, P.C., Somlo, S., and DeCaen, P.G. (2020). Disrupting polycystin-2 EF hand Ca(2+) affinity does not alter channel function or contribute to polycystic kidney disease. J Cell Sci *133*.

Vinayagam, D., Quentin, D., Yu-Strzelczyk, J., Sitsel, O., Merino, F., Stabrin, M., Hofnagel, O., Yu, M., Ledeboer, M.W., Nagel, G.*, et al.* (2020). Structural basis of TRPC4 regulation by calmodulin and pharmacological agents. Elife *9*.

Voets, T., Owsianik, G., Janssens, A., Talavera, K., and Nilius, B. (2007). TRPM8 voltage sensor

mutants reveal a mechanism for integrating thermal and chemical stimuli. Nat Chem Biol *3*, 174-182.

Walker, M.B., and Kimmel, C.B. (2007). A two-color acid-free cartilage and bone stain for zebrafish larvae. Biotech Histochem *82*, 23-28.

Wang, J., Arbuzova, A., Hangyás-Mihályné, G., and McLaughlin, S. (2001). The effector domain of myristoylated alanine-rich C kinase substrate binds strongly to phosphatidylinositol 4,5-bisphosphate. J Biol Chem *276*, 5012-5019.

Wang, Q., Dai, X.Q., Li, Q., Wang, Z., Cantero Mdel, R., Li, S., Shen, J., Tu, J.C., Cantiello, H., and Chen, X.Z. (2012). Structural interaction and functional regulation of polycystin-2 by filamin. PLoS One *7*, e40448.

Wang, Z., Ng, C., Liu, X., Wang, Y., Li, B., Kashyap, P., Chaudhry, H.A., Castro, A., Kalontar, E.M., Ilyayev, L.*, et al.* (2019). The ion channel function of polycystin-1 in the polycystin-1/polycystin-2 complex. EMBO Rep *20*, e48336.

Wegierski, T., Steffl, D., Kopp, C., Tauber, R., Buchholz, B., Nitschke, R., Kuehn, E.W., Walz, G., and Köttgen, M. (2009). TRPP2 channels regulate apoptosis through the Ca2+ concentration in the endoplasmic reticulum. Embo j *28*, 490-499.

Weissgerber, P., Kriebs, U., Tsvilovskyy, V., Olausson, J., Kretz, O., Stoerger, C., Mannebach, S., Wissenbach, U., Vennekens, R., Middendorff, R.*, et al.* (2012). Excision of Trpv6 gene leads to severe defects in epididymal Ca2+ absorption and male fertility much like single D541A pore mutation. In J Biol Chem, pp. 17930-17941.

Weissgerber, P., Kriebs, U., Tsvilovskyy, V., Olausson, J., Kretz, O., Stoerger, C., Vennekens, R., Wissenbach, U., Middendorff, R., Flockerzi, V.*, et al.* (2011). Male fertility depends on Ca(2)+ absorption by TRPV6 in epididymal epithelia. In Sci Signal, pp. ra27.

Wen, H., and Levitan, I.B. (2002). Calmodulin is an auxiliary subunit of KCNQ2/3 potassium channels. J Neurosci *22*, 7991-8001.

Wes, P.D., Chevesich, J., Jeromin, A., Rosenberg, C., Stetten, G., and Montell, C. (1995). TRPC1, a human homolog of a Drosophila store-operated channel. Proc Natl Acad Sci U S A *92*, 9652-9656.

White, R.R., Kwon, Y.G., Taing, M., Lawrence, D.S., and Edelman, A.M. (1998). Definition of optimal substrate recognition motifs of Ca2+-calmodulin-dependent protein kinases IV and II reveals shared and distinctive features. J Biol Chem *273*, 3166-3172.

Wilkes, M., Madej, M.G., Kreuter, L., Rhinow, D., Heinz, V., De Sanctis, S., Ruppel, S., Richter, R.M., Joos, F., Grieben, M.*, et al.* (2017). Molecular insights into lipid-assisted Ca(2+) regulation of the TRP channel Polycystin-2. Nat Struct Mol Biol *24*, 123-130.

Wu, G., Hayashi, T., Park, J.H., Dixit, M., Reynolds, D.M., Li, L., Maeda, Y., Cai, Y., Coca-Prados, M., and Somlo, S. (1998). Identification of PKD2L, a human PKD2-related gene: tissue-specific expression and mapping to chromosome 10q25. Genomics *54*, 564-568.

Xiao, L., Cheng, J., Zhuang, Y., Qu, W., Muir, J., Liang, H., and Zhang, D. (2013). Botulinum toxin type A reduces hyperalgesia and TRPV1 expression in rats with neuropathic pain. Pain Med 14, 276-286.

Xue, J., Han, Y., Baniasadi, H., Zeng, W., Pei, J., Grishin, N., Wang, J., Tu, B.P., and Jiang, Y. (2021). TMEM120 is a coenzyme A-binding membrane protein with structural similarities to ELOVL fatty acid elongase. bioRxiv, 2021.2006.2013.448233.

Yang, F., Xiao, X., Cheng, W., Yang, W., Yu, P., Song, Z., Yarov-Yarovoy, V., and Zheng, J. (2015). Structural mechanism underlying capsaicin binding and activation of the TRPV1 ion channel. Nat Chem Biol *11*, 518-524.

Yang, J., Wang, Q., Zheng, W., Tuli, J., Li, Q., Wu, Y., Hussein, S., Dai, X.Q., Shafiei, S., Li, X.G.*, et al.* (2012). Receptor for activated C kinase 1 (RACK1) inhibits function of transient receptor potential (TRP)-type channel Pkd2L1 through physical interaction. J Biol Chem *287*, 6551-6561.

Yin, Y., Wu, M., Zubcevic, L., Borschel, W.F., Lander, G.C., and Lee, S.Y. (2018). Structure of the cold- and menthol-sensing ion channel TRPM8. In Science, pp. 237-241.

Yu, Y., Ulbrich, M.H., Li, M.H., Buraei, Z., Chen, X.Z., Ong, A.C., Tong, L., Isacoff, E.Y., and Yang, J. (2009). Structural and molecular basis of the assembly of the TRPP2/PKD1 complex. Proc Natl Acad Sci U S A *106*, 11558-11563.

Yue, L., Peng, J.B., Hediger, M.A., and Clapham, D.E. (2001). CaT1 manifests the pore properties of the calcium-release-activated calcium channel. Nature *410*, 705-709.

Zakharian, E., Cao, C., and Rohacs, T. (2011). Intracellular ATP supports TRPV6 activity via lipid kinases and the generation of PtdIns(4,5) P(2). In FASEB J, pp. 3915-3928.

Zhang, R., Varela, M., Vallentgoed, W., Forn-Cuni, G., van der Vaart, M., and Meijer, A.H. (2019). The selective autophagy receptors Optineurin and p62 are both required for zebrafish host resistance to mycobacterial infection. PLoS Pathog *15*, e1007329.

Zhang, S., Ehlers, M.D., Bernhardt, J.P., Su, C.T., and Huganir, R.L. (1998). Calmodulin mediates calcium-dependent inactivation of N-methyl-D-aspartate receptors. Neuron *21*, 443-453.

Zhang, X., Li, L., and McNaughton, P.A. (2008). Proinflammatory mediators modulate the heat-activated ion channel TRPV1 via the scaffolding protein AKAP79/150. Neuron 59, 450-461.

Zhao, J., Lin King, J.V., Paulsen, C.E., Cheng, Y., and Julius, D. (2020). Irritant-evoked activation and calcium modulation of the TRPA1 receptor. Nature *585*, 141-145.

Zheng, W., Cai, R., Hofmann, L., Nesin, V., Hu, Q., Long, W., Fatehi, M., Liu, X., Hussein, S., Kong, T.*, et al.* (2018a). Direct Binding between Pre-S1 and TRP-like Domains in TRPP Channels Mediates Gating and Functional Regulation by PIP2. Cell Rep *22*, 1560-1573.

Zheng, W., Hu, R., Cai, R., Hofmann, L., Hu, Q., Fatehi, M., Long, W., Kong, T., Tang, J., Light, P.*, et al.* (2018b). Identification and characterization of hydrophobic gate residues in TRP channels. Faseb j *32*, 639-653.

Zheng, W., Shen, F., Hu, R., Roy, B., Yang, J., Wang, Q., Zhang, F., King, J.C., Sergi, C., Liu, S.M.*, et al.* (2016a). Far Upstream Element-Binding Protein 1 Binds the 3' Untranslated Region of PKD2 and Suppresses Its Translation. J Am Soc Nephrol *27*, 2645-2657.

Zheng, W., Yang, J., Beauchamp, E., Cai, R., Hussein, S., Hofmann, L., Li, Q., Flockerzi, V., Berthiaume, L.G., Tang, J.*, et al.* (2016b). Regulation of TRPP3 Channel Function by N-terminal Domain Palmitoylation and Phosphorylation. J Biol Chem *291*, 25678-25691.

Zheng, W., Yang, X., Hu, R., Cai, R., Hofmann, L., Wang, Z., Hu, Q., Liu, X., Bulkley, D., Yu, Y.*, et al.* (2018c). Hydrophobic pore gates regulate ion permeation in polycystic kidney disease 2 and 2L1 channels. Nat Commun *9*, 2302.